Fundamental and Applied Studies Towards the Development of All-Solid-State Batteries Based on Sulfide-Based Alkali-Ion Conductors

Kumulative Dissertation

zur Erlangung des Grades eines
Doktor der Naturwissenschaften
(Dr. rer. nat.)

dem Fachbereich Chemie
der Philipps-Universität Marburg
vorgelegt von

Marc Duchardt, Master of Science
geboren in Kreuztal

Marburg an der Lahn, September 2020

Die vorliegende Dissertation wurde von März 2017 bis Oktober 2020 am Fachbereich Chemie der Philipps-Universität Marburg unter Leitung von Prof. Dr. Bernhard Roling und Prof. Dr. Stefanie Dehnen angefertigt. Es sei erwähnt, dass zwischen Mai 2018 und Februar 2019 ein Forschungsaufenthalt am Collège de France in Paris, Frankreich, unter der Leitung von Prof. Dr. Jean-Marie Tarascon, verbracht wurde. Die Arbeiten dort und ihre Ergebnisse sind allerdings nicht in diesem Manuskript enthalten.

Vom Fachbereich Chemie der Philipps-Universität Marburg als Dissertation angenommen am: Marburg, _____

Erstgutachter: Prof. Dr. Bernhard Roling
Zweitgutachter: Prof. Dr. Stefanie Dehnen
Tag der Disputation: _____.2020
Hochschulkennziffer: 1180

Erklärung

Ich erkläre, dass eine Promotion noch an keiner anderen Hochschule als der Philipps-Universität Marburg, Fachbereich Chemie, versucht wurde.

Hiermit versichere ich, dass ich die vorliegende Dissertation

Fundamental and Applied Studies Towards the Development of All-Solid State Batteries Based on Sulfide-Based Alkali-Ion Conductors

selbstständig, ohne unerlaubte Hilfe Dritter angefertigt und andere als die in der Dissertation angegebenen Hilfsmittel nicht benutzt habe. Alle Stellen, die wörtlich oder sinngemäß aus veröffentlichten oder unveröffentlichten Schriften entnommen sind, habe ich als solche kenntlich gemacht. Dritte waren an der inhaltlich-materiellen Erstellung der Dissertation nicht beteiligt; insbesondere habe ich hierfür nicht die Hilfe eines Promotionsberaters in Anspruch genommen. Kein Teil dieser Arbeit ist in einem anderen Promotions- oder Habilitationsverfahren verwendet worden. Mit dem Einsatz von Software zur Erkennung von Plagiaten bin ich einverstanden.

_____ _____

Ort/Datum Unterschrift (Vor- und Nachname)

Wissenschaftlicher Werdegang und Danksagung fehlen in dieser elektronischen Version der Dissertation

Preface

This dissertation summarizes the work that was carried out in the time between March 2017 and October 2020 at the Philipps-University Marburg under the supervision of Prof. Dr. Bernhard Roling and Prof. Dr. Stefanie Dehnen. It has to be noted that in the period between May 2018 and February 2019 a medium-term research period was spent at the Collège de France, Paris, France under the supervision of Prof. Dr. Jean-Marie Tarascon. However, the project dealt with there, is not included in this manuscript.

The results of the research have partially been published in the articles listed further below. This cumulative dissertation is thus mainly a shortened version of these articles with the fundamental results. The complete publications can be found in the annex. Nevertheless, where meaningful, additional results will be presented additionally to round out and add to the picture.

Articles published/prepared in the course of the doctoral research work and part of this cumulative dissertation:

[I] **Marc Duchardt**, Uwe Ruschewitz, Stefan Adams, Stefanie Dehnen and Bernhard Roling, Vacancy-Controlled Na-ion Superion Conduction in $Na_{11}Sn_2PS_{12}$, *Angewandte Chemie International Edition* **2018**, *57*, 1350–1355.

[II] **Marc Duchardt**, Sven Neuberger, Uwe Ruschewitz, Thorben Krauskopf, Wolfgang G. Zeier, Jörn Schmedt auf der Günne, Stefan Adams, Bernhard Roling and Stefanie Dehnen, Superion Conductor $Na_{11.1}Sn_{2.1}P_{0.9}Se_{12}$: Lowering the Activation Barrier of Na-ion Conduction in Quaternary 1−4−5−6 Electrolytes, *Chemistry of Materials* **2018**, *30*, 4134–4139.

[III] **Marc Duchardt,** Mirko Diels, Bernhard Roling, and Stefanie Dehnen, Flow-Oriented Synthesis of Li_2S and $Li_3PS_4 \cdot 3THF$: Opening Up a Completely Solvent-Based Solid Electrolyte Value Chain, *ACS Applied Energy Materials* **2020**, *3*, 6937–6945.

[IV] Moritz Kroll,[+] **Marc Duchardt**,[+] Sarah L. Karstens, Sabine Schlabach, Fabio Lange, Janika Hochstrasser, Bernhard Roling and Ulrich Tallarek, Kinetic Limitations in Sheet-Type All-Solid-State Battery Cathodes, submitted to *Advanced Energy Materials*.

[+] These authors contributed equally to this work.

Articles published in the course of the doctoral research work but <u>not</u> part of this cumulative dissertation:

[A] Saneyuki Ohno, Tim Bernges, Johannes Buchheim, **Marc Duchardt**, Anna-Katharina Hatz, Marvin A. Kraft, Hiram Kwak, Aggunda L. Santhosha , Zhantao Liu, Nicolò Minafra, Fumika Tsuji, Atsushi Sakuda. Roman Schlem, Shan Xiong, Zhenggang Zhang, Philipp Adelhelm, Hailong Chen, Akitoshi Hayashi, Yoon-Seok Jung, Bettina V. Lotsch, Bernhard Roling, Nella M. Vargas-Barbosa, Wolfgang G. Zeier: How Certain Are the Reported Ionic Conductivities of Thiophosphate-Based Solid Electrolytes? An Interlaboratory Study, *ACS Energy Lett.* **2020**, *5*, 910–915.

Abbreviations

(Li-)NCA	(**li**thium) **n**ickel **c**obalt **a**luminum oxide
(Li-)NMC	(**li**thium) **n**ickel **m**anganese **c**obalt oxide
ASS	**a**ll-**s**olid-**s**tate
ASSB	**a**ll-**s**olid-**s**tate battery
BTMS	**b**attery **t**hermal **m**anagement **s**ystem
CAM	**c**athode **a**ctive **m**aterial
CEI	**c**athode **e**lectrolyte **i**nterphase
CPE	**c**onstant **p**hase **e**lement
EV	**e**lectric **v**ehicle
FIB	**f**ocused **i**on **b**eam
H-NBR	**h**ydrogenated **n**itrile **b**utadiene **r**ubber
ICE	**i**nternal **c**ombustion **e**ngine
LCO	**l**ithium **c**obalt **o**xide
LE	**l**iquid **e**lectrolyte
LGPS	**L**i$_{10}$**G**e**P**$_2$**S**$_{12}$
LIB	lithium-**i**on **b**attery
LPSI	**L**i$_3$**PS**$_4$·Li**I**
NAP	**nap**hthalene
NaSnPS	**Na**$_{11}$**Sn**$_2$**PS**$_{12}$
NaSnPSe	**Na**$_{11.1}$**Sn**$_{2.1}$**P**$_{0.9}$**Se**$_{12}$
OEM	**o**riginal **e**quipment **m**anufacturer
PIB	**p**oly**i**so**b**utene
PT	**p**ellet-**t**ype
PXRD	**p**owder **X**-**r**ay **d**iffraction
PXRD	**p**owder **X**-**r**ay **d**iffraction
r.t.	**r**oom **t**emperature
SE	**s**olid **e**lectrolyte
SEI	**s**olid **e**lectrolyte **i**nterphase
SEM	**s**canning **e**lectron **mi**croscope
SEM	**s**econdary **e**lectron **mi**croscopy
SIB	**s**odium **i**on **b**attery

SOC	**s**tate **o**f **c**harge
SOH	state **o**f **h**ealth
ST	**s**heet-**t**ype
TEM	**t**ransmission **e**lectron **m**icroscopy
THF	**t**etra**h**ydro**f**urane
TM	**t**ransition **m**etal
TMO	**t**ransition **m**etal **o**xide
XRD	**X**-**r**ay **d**iffraction
β-LPS	β-**L**i_3**PS**$_4$

Table of Contents

Table of Figures

1 Introduction and Motivation

Crises are polymorphous. Some are short but destructive, others are more prolonged but do not demand the same amount of sacrifices. Nevertheless, be it an economic recession or a pandemic such as the recent global outbreak of Covid-19 – provided political volition – humanity usually has the means to fight the causes. Because a crisis – by its definition – is something non-perpetual, it will pass. Moreover, most often, crises are rather locally limited.

Global warming is different. Admittedly, the amounts of greenhouse gases emitted by different countries vary greatly – and, quite unfairly – so do, but rather inversely, the direct repercussions of it: droughts, desertification and floods. However, these are only the most salient consequences. Indirect consequences will affect each country on this planet. In contrast to a conventional crisis, instead of climate crisis, we should speak of climate catastrophe. Global warming is not something that will stop anytime soon. The concentration of greenhouse gases in the air, most importantly CO_2 (**Figure 1**), knows just one direction – particularly during the past 40 years: upwards. The only thing we can do is slow down the process. We cannot halt it and, most certainly, we will not be able to reverse it in the near future because whereas important greenhouse gases, like methane and nitrous oxide, have a rather short half-life due to chemical degradation of 12 and 114 years, respectively, CO_2 is thermodynamically stable and will not disappear in the human time horizon.[1] Geochemical alterations of the CO_2 concentration – based on erosion and weathering of rocks – cover large time spans of several thousands of years.[2] Quite rapidly, though, a large fraction of the anthropogenic CO_2 is continuously absorbed by the oceans. Although this reduces the atmospheric content of CO_2 this is highly problematic as it is a major contributor to the devastating effect of coral bleaching. Owing to the decreased pH value of the carbonic acid-enriched seawater, the equilibrium $H_3O^+ + CO_3^{2-} \rightleftharpoons H_2O + HCO_3^-$ is shifted toward HCO_3^- being inaccessible to marine calcifiers such as corals.[3] Other than oceans, swamps and wetlands are considered as powerful carbon sinks. Furthermore, thanks to its high heat capacity the water in virgin or well-managed wetland landscapes can effectively attenuate large temperature variations *e.g.* between day and night.[4]

However, the destruction of these – both from a perspective of climate and biodiversity – precious habitats happens just as quickly as the incline of global CO_2 emissions.[5,6] Nature's material flows are a delicate web of loops and cycles. Humankind, though, continuously ruptures these cycles with a general focus on short-term productivity gains fundamentally linked to the depletion of natural resources rather than attempting a genuinely sustainable use thereof. Even today, in the 21st century, humankind still predominantly behaves like what biologist would call an r-strategist: rapid growth of a population during easy access to resources. For centuries, we made exploitive use of nature's ample and seemingly inexhaustible natural resources but in the meantime, we have reached the ecological limitations of our planet. Consequently, we ought to adapt to this new situation by shifting our handling of natural resources to a one of much more pronounced circular economy in every aspect of our everyday life. The high living standard of modern society – a product of a long history of division of labor and specialization – is inextricably linked to the constant availability of energy to power our machines and tools. Thus, if we want to preserve our living standard with the vast amount of amenities we have gathered, it is high time that we drastically change the way we produce, store and consume energy.

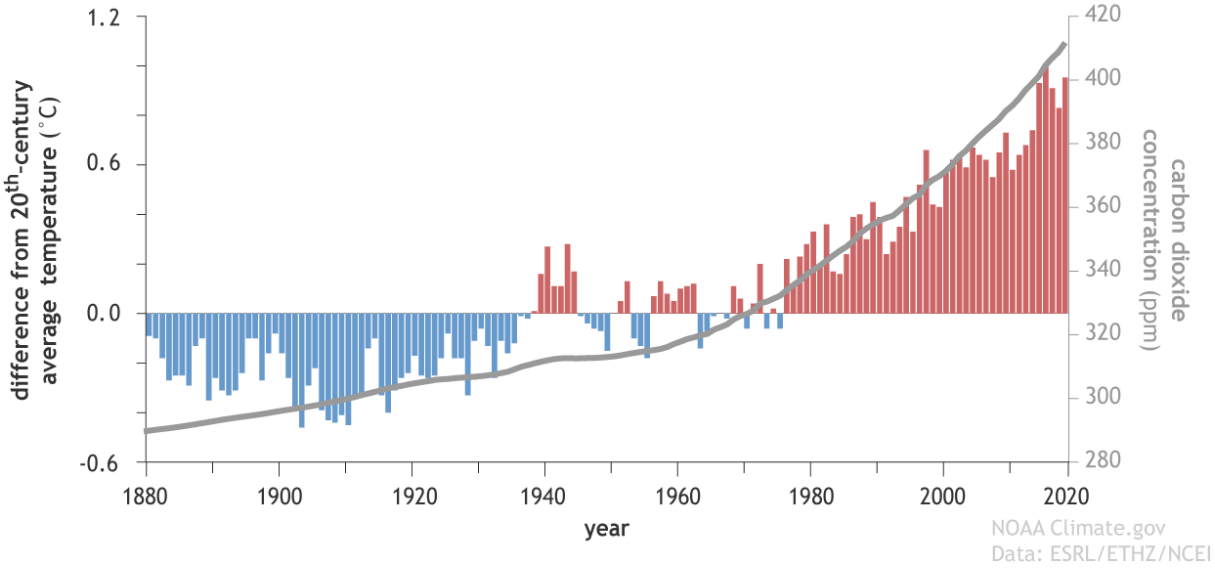

Figure 1: Atmospheric carbon dioxide concentration and absolute yearly averaged difference (1880 – 2020) from the average temperature of the 20th century. Carbon dioxide levels (grey line, right-hand axis) are given in parts per million, temperature differences (left-hand axis) in degrees Celsius.[7]

Fortunately, already today, due to a continuous development of the underlying technologies and typical scaling effects, the production costs of renewable energies, like wind or solar,

have become competitive with those of fossil fuels.[8] In many places, though, the costs as primary counterargument have been superseded by fears and health concerns of individuals and local communities predominantly linked to the emission of infrasonic, which, however, cannot at all be backed scientifically.[9,10] After all, the main reasons causing annoyance might be very subjective including aesthetic reservations, social acceptance, benefits and attitudes, the local situation and the conditions of planning.[11] The erection of a wind plant has indeed a large visual impact on the landscape and, especially in touristic areas, can have a considerable economic impact too.[12] The velocity of the further expansion of renewable energy plants will thus be highly dependent on whether policymakers, companies and land owners will find the right means to render those plants more – financially – attractive to those immediately affected by their construction.[13,14] Nevertheless, due to a lack of alternatives – "*electricity does not simply come from the socket, indeed"* – it is most likely that commonsense will finally prevail and we will see a substantial rise in renewable energy production in the upcoming decades.[15–17]

However, this creates a big and predominantly unsolved problem: Naturally, wind and solar energy are not continuously supplied. How can we store large amounts of energy for times of lower production but higher demand? A permanent and controllable generation of energy is a convenient myth of the fossil era that we have become just too accustomed to over the last century. Sustainable energy generation is just as dynamic as life itself. Fortunately, though, humankind can come up with ways to emulate what nature provided us with for so many years. We can create our own systems to effectively store large amounts of energy. Endeavors to balance the seasonal differences in the supply of renewable energies will crucially depend on the coupled generation of hydrogen from electrolysis of water.[15] Excess hydrogen might find extensive use as fuel in the transport sector. However, storage and utilization of H_2 are linked to certain risks, as H_2 is known for its tendency to form explosive mixtures with oxygen. Moreover, storage of H_2 is not an easy task and demands for complicated and bulky storage systems. Hence, for special applications like planes, where safety and lightweight construction are of paramount importance, another solution might play out handier. The hydrogen generated together with CO_2 could be used as feedstock for the large-scale synthesis of hydrocarbon-based sustainable fuels.[18] However, as the production of H_2 and even more so of the more easy-to-handle hydrocarbons consumes a considerable fraction of the energy itself, these are only sought for in long-distance and heavy-duty transport.

For (comparably) lightweight transport as cars, it is batteries that are key for an effective and efficient exploitation of renewable energy in the transport sector. Additionally, batteries will play a key role in the clean storage of surplus energy in the grid when short-term – *i.e.* daily

to weekly – differences have to be balanced. Generally, Li-ion batteries (LIBs) find widespread applications in many different fields today. Their combination of extremely appealing characteristics – high energy densities, longevity – and a continuously decreasing price[8] have led to the replacement of many former – and now inferior – battery technologies that dominated the market for a long time (ellipsoids in the lower left corner in **Figure 2**). Those less sophisticated battery technologies are nowadays only used in certain applications where the price is the decisive criterion. Nickel metal hydride (Ni-MH) batteries for instance – having earlier superseded Ni-Cd batteries – for their part have been almost completely replaced in consumer electronics by LIBs today. Lead-acid (PbA) batteries, on the other hand, motivated by their cheap price, are one of the few systems that are still produced in large volumes besides LIBs. They have found their predominant application in automotive starter batteries for cars and other vehicles making use of an internal combustion engine (ICE). In the long run, though, the days of ICE cars are numbered and so are those of the PbA battery. Prices for LIBs on the cell-level have currently reached a price of approximately 170 $/kg which astonishingly beats the predicted price – already anticipated by experts and analysts to dwindle considerably only 5 years ago – by almost a factor of 2.[19,20] Moreover, a large leap forward has been achieved from the early days of LIBs until today also in terms of specific as well as volumetric energy density.[21] However, whereas a significant further reduction of cell prices is projected to continue in the upcoming years, the attainable energy densities of the current cell-chemistries are reaching their limits within the current paradigm.[22] Therefore, innovative new battery systems are needed and hence frenetically researched like for example Na/K ion or Li-S to name just a few.

As can be seen from **Figure 2**, Li-ion technology currently makes use of liquid electrolytes (LE) and predominantly graphite as anode material (pinkly encircled ellipsoid). Currently, a partial substitution of graphite by silicon is underway. However, the potential is limited as will be shown in more detail in section **2.1.2.3**. A considerable further increase in volumetric energy density, being decisive for the widespread adoption of electric vehicles (EVs), can most likely be expected from a further development of Li-ion chemistry – rather than from completely different cell chemistries as Na-ion or Li-S. The most promising concept is the one of the so-called all-solid-state battery (ASSB). In an ASSB, the LE is substituted by a solid electrolyte (SE). In the case of Li, this might possibly enable the long-cherished dream of battery researchers: usage of elementary Li on the anode side boosting the attainable energy densities significantly.[23] In a LE-based cell, this is hardly possible as will be explained in section **2.1.2.3**. Only recently, a successful prototype of an ASS-LIB was reported by Samsung that retained roughly 90% of its original capacity over an unprecedented number of 1000 cycles, making

quite some waves in the community.[24] Long-hold skepticism towards the ASSB-technology gradually gives way to more optimistic opinions on the future of ASSB with key researchers and companies considering the rollout of ASSBs only as a matter of time.[22,25–27]

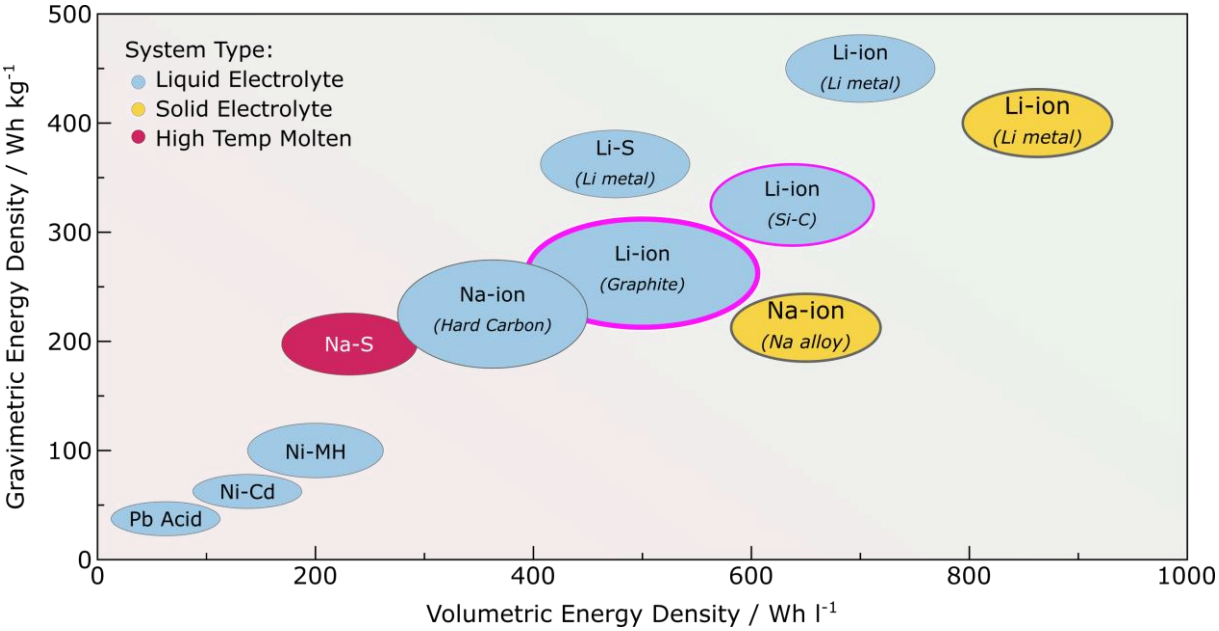

Figure 2: Different battery technologies plotted with regard to their gravimetric and volumetric energy densities at cell level. Approximate performance parameters for different applications are shown as supplementary information. Adapted from reference [28].

However, priorities might lie on other aspects when looking at different applications. Given that no Na-ion battery (SIB) cells have been commercialized, yet, their thorough evaluation, let alone predictions with regard to their future importance are difficult. Still, their current performance already compares to that of commercial Li-ion cells in their early days.[29] A variety of studies have shown their feasibility and proven long-term capacity retention.[30–32] With sodium being a bit heavier and having a slightly higher redox potential than Li, the attainable energy densities will be lower. Nevertheless, sodium's abundance and worldwide availability coupled with the prospect of cheap and benign cathode materials[30] might give rise to a powerful alternative energy storage technology. Its scope would be particularly in the field of grid-scale energy storage[33] because here the price is the decisive criterion and the relevance of high energy densities is rather low.

Inspired by the prospect of ASS-LIBs, much research has also been carried out on all-solid state Na-ion batteries (ASS-SIBs). Given that not even their liquid counterparts have been commercialized yet, research regarding them is still entirely fundamental. Nevertheless, with differences between solid state-based LIBs and SIBs being essentially the same ones as for their liquid counterparts, the development of ASS-SIBs is carried out in parallel with LE-based ones.

However, especially in grid storage applications, safety and longevity become decisive criterions.[28] Typical LEs are organic carbonates, which pose a safety risk due to their volatility and flammability.[34] Packed together to form large-scale grid storage fires could have devastating consequences. SEs, with their intrinsic non-volatility and inflammability, promise to mend these problems. Thus, SIB technology is particularly attractive for grid storage when linked to the usage of SEs.[28] In contrast to ASS-LIBs, though, usage of the elementary alkali metal will most likely not be possible. Na has a very low melting point of 98 °C, which – together with its higher reactivity compared to Li – would pose a safety risk.

With the world becoming ever more complex "one-size-fits-all" approaches seem less and less appropriate. It will be rather a couple of different chemistries with each of them being further discriminated into small variations that fulfill slightly different requirements and demands. Research during my PhD studies was shared between Na-ion and Li-ion solid-state ionics and so will be the following thesis. I will give a short introduction on conventional LIBs and then cover the developments of both Na-ion and Li-ion solid-state ionics, respectively. Afterwards, the current state of ASS-LIBs and ASS-SIBs will be discussed separately followed by the cumulative section presenting my original work on the subjects, respectively. Finally, I will conclude with some final remarks and my opinion on where to expand future research efforts to building upon my results.

2 Theoretical Background and State of Research

2.1 The Standard Li-Ion battery

2.1.1 Operating Principle of a Standard Li-Ion Battery

Conventional Li-ion batteries (LIBs) contain a porous anode (negative electrode) and a porous cathode (positive electrode) as 'active' storage components (**Figure 3**), coated on thin copper and aluminum foils, respectively. These metals serve as current collectors. The initially developed version of the LIB deployed $LiCoO_2$ (LCO) as electrochemically active material on the cathode side. On the anode side – due to its very low potential in the lithiated state being almost as low as for elementary lithium – graphite is used; separated from the cathode by means of an electrolyte-filled ceramic separator.[35] In addition to both active materials, both electrodes generally contain binders (polymers) for mechanical stabilization and an electronically conductive additive such as active carbon, respectively. The combination of LCO with graphite as active materials leads to a cell voltage of approximately 3.8 V. Since this value by far exceeds the electrochemical stability window of water, non-aqueous electrolytes have to be utilized. The most commonly applied systems consist of lithium hexafluorophosphate in a mixture of organic carbonates, like for instance ethylene carbonate and dimethyl carbonate. A thin separator (grey band in **Figure 3**) is placed between the much thicker electrodes (each about 100 µm thick). The liquid electrolyte infiltrates the porous electrode and separator assembly, providing fast ion transfer between the electrodes and preventing electronic short-circuiting. The operating principle of such a LIB is based on the transfer of Li ions and electrons between both electrodes upon the charge/discharge cycles with both species going back and forth. This led to the description via the so-called "rocking-chair model".[36]

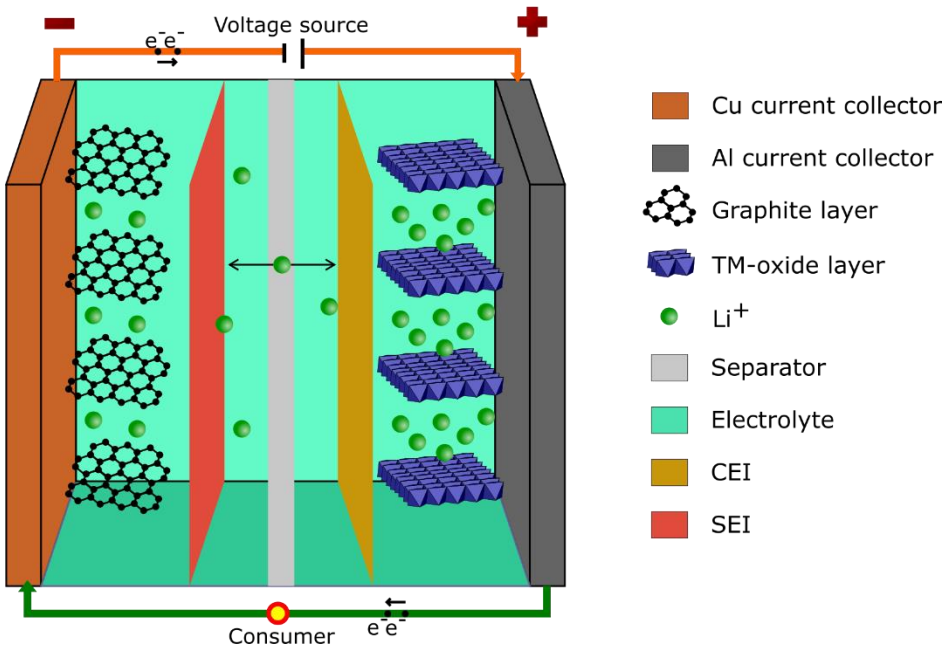

Figure 3: Schematic drawing of a liquid electrolyte-based Li-ion battery. Comparably heavy copper current collectors are necessary on the anode side since Li is known to be able to alloy with the lighter Al. CEI: cathode electrolyte interphase, SEI: solid electrolyte interphase, TM: Transition metal.

In the initially discharged state of a LIB, the transition metal oxide (TMO) is fully lithiated. Upon charging, Li ions (green spheres in **Figure 3**) is transported through the electrolyte and the separator towards the graphite and are subsequently intercalated into the carbon host. The electrons are concomitantly transferred to the same destination via the external circuit.

$$\begin{aligned} C_n + x \cdot Li^+ + x \cdot e^- &\rightarrow Li_x C_n \\ Li_1 CoO_2 &\rightarrow Li_{1-x} CoO_2 + x \cdot Li^+ + x \cdot e^- \end{aligned} \tag{1}$$

Upon the following discharge, the Li ions return and are reintercalated into the TMO host. The electrons, again, have to take the external circuit enabling them to perform work at an intermediary consumer. This discharge reaction is eponymous for terming the TMO the cathode and the other – usually consisting of graphite as active material – the anode material inside a LIB:

$$\begin{aligned} Li_n C_n &\rightarrow x \cdot Li^+ + C_n + x \cdot e^- \\ Li_{1-x} CoO_2 + x \cdot Li^+ + x \cdot e^- &\rightarrow LiCoO_2 \end{aligned} \tag{2}$$

The vast application of LE-based LIBs in modern consumer electronics easily distracts from the fact that the chemistry behind these batteries is far from straightforward. These batter-

ies only work because the common electrode materials are able to form electronically passivating interlayers that prevent the continuous decomposition of the respective electrode material and its adjacent current collector upon parasitic reactions with the electrolyte. Much research has been devoted towards a better understanding of these processes, especially on the anode side. However, a clear and comprehensive picture of the exact nature of these protecting layers has still not been established.[37–39] Undoubtedly, their vast complexity justifies calling the LIB a fortunate coincidence.[40,41]

2.1.2 Limitations of Current Cells

Considerable progress has been made over the past almost 30 years of commercial LIBs on several levels: on the (**1**) battery level, (**2**) cell level and (**3**) the materials level. Whereas, for consumer electronics – albeit the understandable and widespread wish of consumers for even longer battery runtimes – the performance parameters allow for an appropriate utilization of the respective devices: laptops, smartphones, smart watches and electric tools to name only a few. For more demanding applications both in terms of energy and power density, like electric vehicles, the current state of technology still leaves much to be desired. Several contradicting goals have to be minded: Primarily, the energy density has to be considerably enlarged in order to allow for comparable ranges as the habitual ones from internal combustion engines (ICEs). Secondly, and hardly less importantly, the time needed to recharge the batteries must be drastically reduced in order to offer clients roughly the same comfortable experience of refueling as the one they are used to.[42] Thirdly, the previously mentioned aims have to be reached concomitantly with a further decrease in prices in order to render EV batteries cost-competitive with combustion engines.

2.1.2.1 Battery Level

A LIB for EVs consists of multiple individual (modules of) cells which are packed together to form the actual battery (pack). On the battery level, the individual constituting cells are monitored with respect to important parameters, like for instance the state of charge (SOC) or the state of health (SOH) both being crucial for efficient battery management.[43] The overarching goal for a high-performing LIB is to reach a suitable compromise between the two competing main requirements: on the one hand energy and power density and on the other hand longevity. Both prerequisites generally contradict each other, comparable to the common

tradeoff between rolling friction and wet grip in the tire industry. Commonly, in order to reach higher energy densities, industrial cell manufacturers continuously try to increase the electrode thickness, but reduce the thickness and thus the weight of the current collectors (especially that of the heavier Cu on the anode side – cf. **Figure 3**) and use less electrochemically inactive materials *e.g.* for casing. However, these manipulations most often result in increased resistances inside the cell leading to more pronounced Joule heating and thus to more serious aging of the battery.[42] This is further exacerbated by the dense packing of the individual cells in order to reach the necessary volumetric energy densities for EVs.[44] In order to improve longevity, an efficient battery thermal management system (BTMS) is thus of paramount importance. It keeps the temperature constantly not only below a temperature of 80 °C – above which thermal runaway becomes possible – but also below a temperature of approximately 35 °C, above which ageing phenomena become much more pronounced.[45,46]

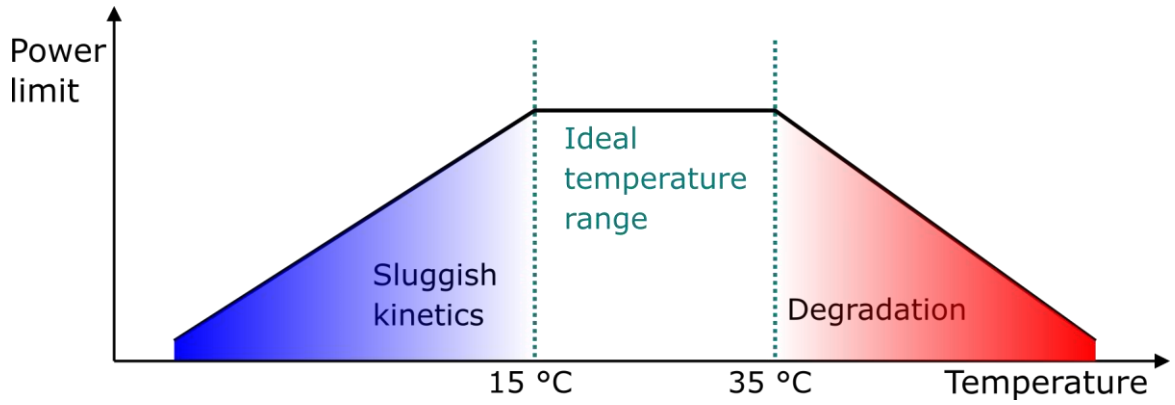

Figure 4: Schematic of the power limit of a commercial Li-ion battery depending on the respective temperature. Temperature values for upper and lower limit of optimal operation range according to reference [44].

BTMSs can generally be divided into air- and liquid-based ones. Initially, the simpler air-cooling was predominantly used, but for example the early EV Nissan Leaf showed increased battery degradation when operated in the hot climate of Arizona.[42] With the construction of more and more energy-dense batteries, this issue becomes even more problematic, facilitating the shift towards more complex liquid-based BTMS, which can cool the batteries much more effectively. To this end, a coolant (usually consisting of a mixture of glycol and water) is used. It can dissipate the energy either passively (using the airstream of the driving car) or make additional use of the vehicle's air conditioning system thus enlarging the chilling effect. Moreover, solely by using a liquid-based BTMS, the battery can also be warmed with an integrated heating element rendering the car operable at temperatures < 10 °C when the kinetics of commercial Li-ion batteries become much more sluggish. This technology is used for example in

the soon to be released Volkswagen ID.3, the company's first "real" electric car based on its newly-developed e-mobility platform.[47]

2.1.2.2 Cell Level

On the cell level, engineering successes have continuously increased the performance of LIBs, *i.e.* increased their energy density and simultaneously lowered their prices. The most typical cell format of a Li-ion cell is the so-called 18650 one. One of the most powerful of these standard 18650-cells available today (manufactured by LG Chem)[48] delivers a 3500 mAh charge capacity at a mean voltage of 3.65 V corresponding to a gravimetric energy density w_{grav} of roughly 265 Wh·kg^{-1} at the cell level. This represents an overall increase by almost a factor of 4 in terms of energy density compared to the first commercial cells from Sony in 1990 (**Figure 10**A), which is partially due to improvement of the cell-design. A handful of these cylindrical cells make up common laptop-batteries. Tesla, the currently largest manufacturer of EVs, uses these cylindrical cells– manufactured in a collaboration with Panasonic – also for their traction batteries (**Figure 6A**). A total of 7104 individual 18650-cells make up the battery that drives the Tesla Model-S.[49] A change that happened only recently is the transition from these cells to their larger relatives: the bigger 21700-cells (**Figure 6B**) offering roughly 50% more capacity per cell.[50,51]

Figure 5: **A**: Size comparison of a commercial 18650-cell with the well-known standard alkaline cell formats AA, taken from reference [52]. **B**: Battery module of Tesla Model-S being composed of an array of 18650-cells, top view, taken from reference [49].

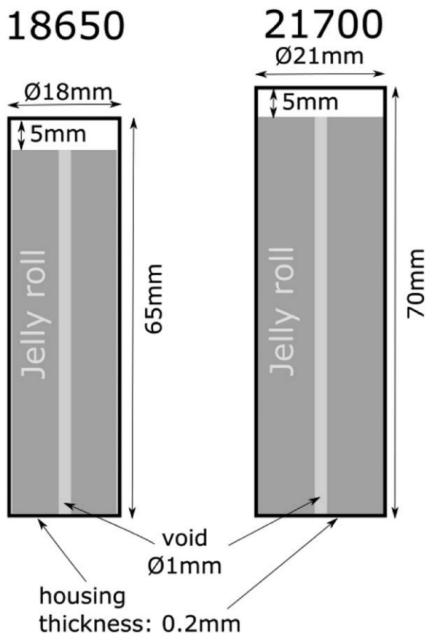

Figure 6: Size comparison of the standard 18650-type cell and the upcoming new default cell type 21700. The naming is according to the following logic: The first two digits describe the width in mm and the subsequent two digits indicate the length in mm followed by an additional "0". Taken from reference [50].

The anticipated improvements in terms of gravimetric and volumetric energy density rely mostly on the reduced number of housings necessary to reach the same overall capacity and, as a result, fewer processing steps per kWh. This reduces the cost, but a considerable impact on the overall energy density is not expected;[50] it will remain in the low single-digit percentage area.[50,51] The general disadvantage of these cylindrical cells – be it 18650, 21700, or even larger future formats like 25700 or 30700 – is their comparably high weight per kWh because of the many individual aluminum housings. Due to the typical cost reductions stemming from economies of scale their prices have gone down considerably in the past decade.[53,54] However, only little space is left for further improvements of the energy density in terms of cell design which is why most original equipment manufacturers (OEMs) like Volkswagen – in conjunction with cell-suppliers like LG Chem, Samsung SDI or Northvolt – draw on prismatic cells to power their electric cars, be it hard-case ones our pouch cells (**Figure 7**). Those cell types possess larger potentials for future improvements.[27,47]

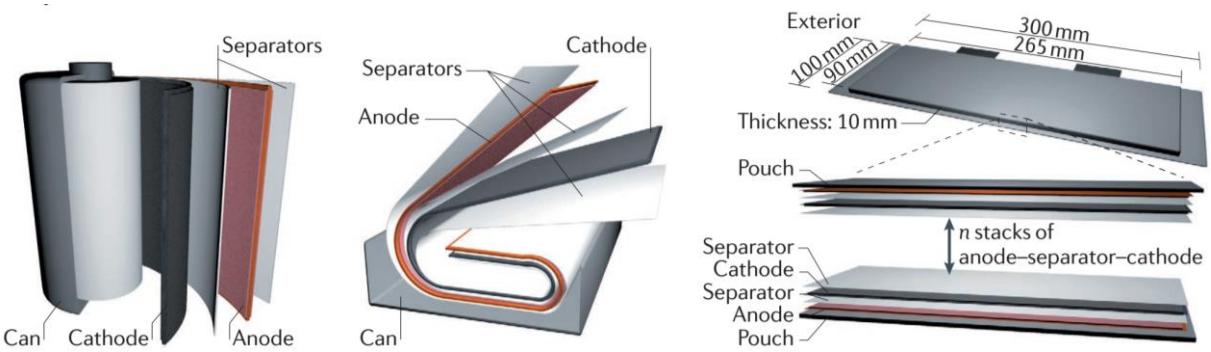

Figure 7: Overview of different cell formats for Li-ion Batteries. From left to right: a cylindrical, prismatic hard case and a pouch cell. Taken from reference [55]. Copyright© 2016, with permission from Springer Nature.

2.1.2.3 Materials Level

Major advancements on the materials level consist for instance in the deployment of one of several alternative cathode materials. The most widely used ones today are the so-called NMC and NCA materials both being formal derivatives of LCO. They have in common that a considerable fraction of the **c**obalt in LCO is replaced with **n**ickel, which has several advantages. Firstly, cobalt is much more expensive than nickel.[56,57] Secondly, cobalt is mined, to a large extent, under very critical circumstances in the Democratic Republic of Congo.[57] Thirdly, substitution of nickel for cobalt considerably enlarges the capacity.[58] Higher nickel contents increase the share of Li that can be deintercalated from the transition metal (TM) host material compared to LCO where the maximum delithiation corresponds to a chemical formula of $Li_{0.5}CoO_2$. A certain amount of cobalt, though, is needed as helps to limit the capacity loss during prolonged cycling.[58] Furthermore, a small amount of **m**anganese in the case of **NMC** or **a**luminum in the case of **NCA** is added as the high nickel content of the materials would otherwise lead to a drastic decrease in their structural stability. The reason lies in the similar ionic radii of Li-ion and Ni^{2+}[59–62] which may result in cation mixing during the synthesis if the parameters are not carefully optimized.[58] In addition, Mn increases the thermal stability of NMC materials. As for the possibility to vary the exact amounts of the constituting metallic elements, NCA materials behave much more rigid. The typical composition for commercial applications is $LiNi_{0.8}Co_{0.15}Al_{0.05}O_2$. NMC materials on the other hand – boasting a general formula of $LiNi_xMn_{1-x}Co_{1-x-y}O_2$ – offer the possibility to extensively vary their stoichiometry regarding the transition metals. Therefore, NMC materials are widely denoted with a postposed three-digit number indicating the respective share of each element in the TM-layer: *e.g.* NMC-111 being composed of 1/3 of each constituting TM-element. Further substitutions of Co lead to NMC-523 or -622 and finally NMC-811 which is at the verge of being utilized in next-

generation batteries.[26] Currently, even higher shares of Ni are researched further driving the energy densities.[20] However, the notoriously unstable $LiNiO_2$ represents the soon to be reached theoretic maximum.[63] Another possibility for driving the energy density on the cathode side rather than enlarging the share of Ni is partially substituting the TMs in NMC-based materials by Li giving rise to so-called Li-rich NMC materials able to perform anionic redox.[64–67] The participation of oxygen in the redox processes in addition to the TMs enables markedly larger capacities compared to the previously discussed "Ni-rich" NMCs. However, these come at the cost of many hitherto unsolved problems: large irreversible capacities, sluggish kinetics and low Coulomb efficiencies.[64] Thus, for a commercialization of these materials, significant further advances are necessary.

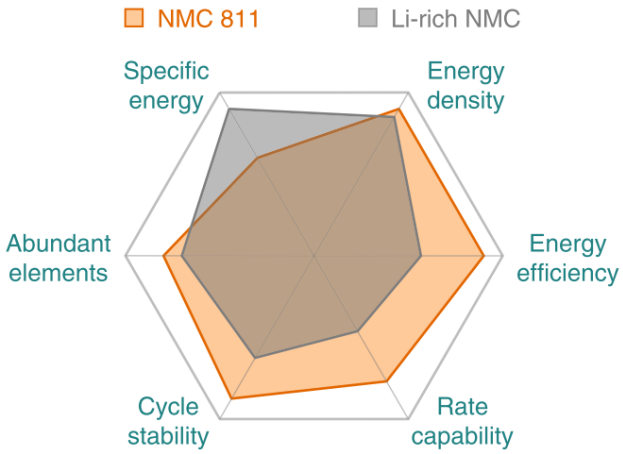

Figure 8: Benchmarking Li-rich NMC against conventional (Ni-rich) NMC materials. Comparison of NMC-811 and Li-rich NMC electrode materials according to six key figures of merit, taken from reference [64].

After exhausting short-term possibilities on the cathode side, the next possible enlargement will most likely stem from the utilization of certain amounts of silicon complementary to graphite on the anode side as recently announced by Volkswagen and Contemporary Amperex Technology (CATL)[68] – the currently largest manufacturer of Li-ion cells worldwide (**Figure 9**) – independently from each other. However, this strategy – having been subject to extensive research since the discovery of the excellent capacity of Si upon alloying with Li[69,70] – will only be applicable to a very limited extent (approximately 20% of silicon).[27] This is due to the long-known issue of serious, associated volume expansion which leads to fracture and ultimately to the electrical isolation of the majority of the silicon particles.[71,72] The same holds for other elements like Ge and P which are likewise known for their large Li-ion capacities but behave very similarly when it comes to volume expansion.[73]

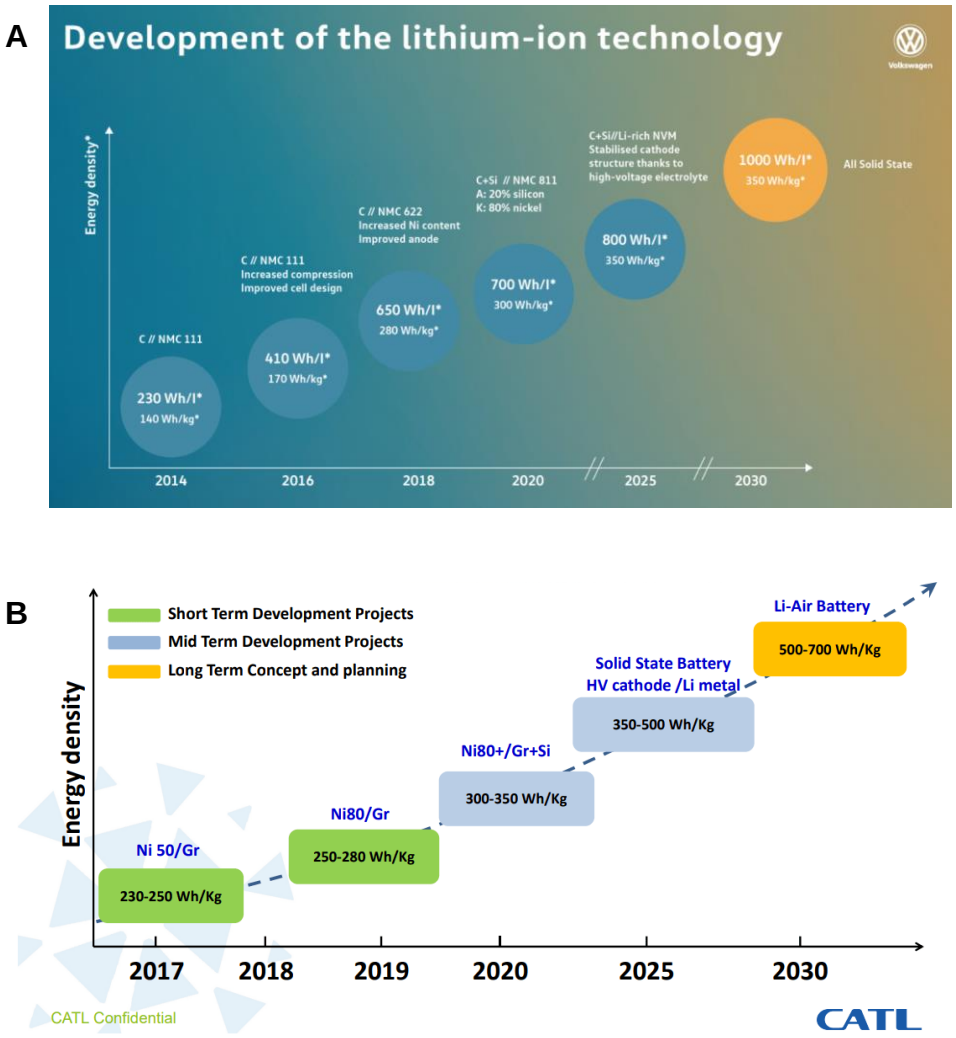

Figure 9: Roadmaps of **A**: Volkswagen and of **B**: China-based Contemporary Amperex Technology (CATL) – the currently largest manufacturer of Li-ion cells worldwide – for the development of energy densities of Li-ion batteries from today until beyond 2030.[27,68]

The "holy grail" of Li-ion battery research is, without a doubt, the safe implementation of elementary lithium as renouncing a graphitic host material would considerably boost attainable energy densities.[74] However, its utilization inside LE-based LIBs is not easily feasible, since the massive changes upon plating and stripping of Li render the SEI rather unstable. The continuous consumption of the liquid electrolyte and lithium shorten the cell life. Furthermore, the formation of so-called lithium metal dendrites or filaments is rampant. Firstly, these continuously growing structures can pierce through the separator, subsequently reach the cathode side and thus cause cell shorting and even explosion. Secondly, they induce the so-called "dead Li".[75] Under certain circumstances, upon plating, the SEI at the root of the Li dendrite may become thinner than the SEIs on the tip. When the current direction is subsequently reversed and Li metal is stripped, the impedance at the root is lower, and so it might shrink faster than the tip. This eventually results in a hollow SEI stem at the root electrically disconnecting the

branches of the dendrite from the current collector. Already a small degree of convection in the electrolyte suffices to break off the root leading to small lithium flotsam.[76]

2.1.2.4 Summary and Roadmap

In summary, both engineering and materials advances have continuously driven the energy densities of LIBs. Currently, an even higher Ni-content corresponding to NMC-90|05|05 as cathode material is researched.[77] On the anode side, cell manufacturers will continuously exhaust the possibility to replace graphite with alloying materials like silicon, but the limits are tight. Both strategies will only slightly increase the energy density of the current cells. Thus, in the current paradigm, state-of-the-art Li-ion batteries are reaching their physicochemical limitations (**Figure 10**).[48]

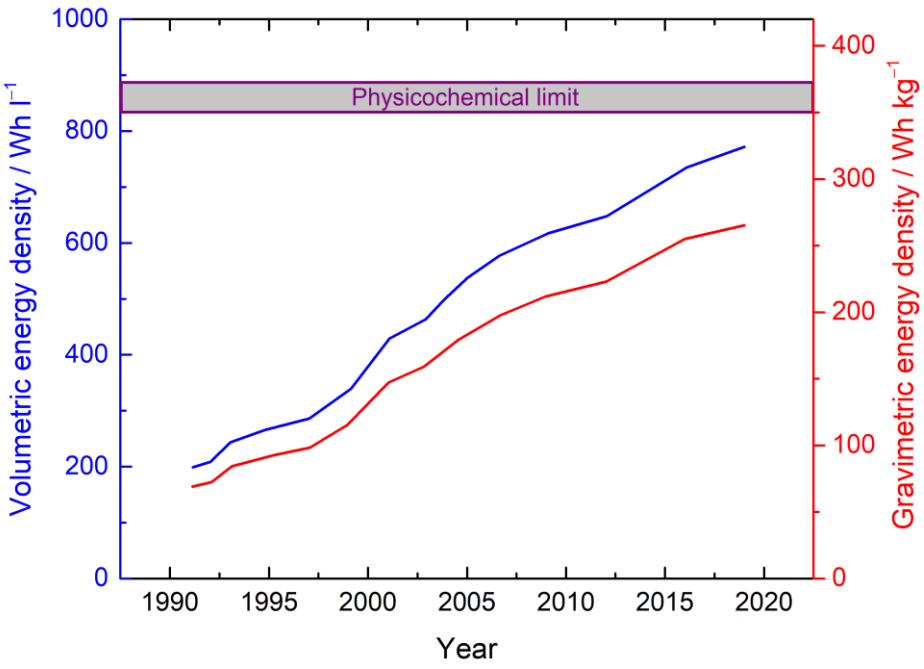

Figure 10: **A**: Adapted from reference [22]. Evolution of volumetric and gravimetric energy densities of standard cylindrical 18650-cells since the beginning of their commercialization in 1990. A value for a current cell with one of the highest energy densities available on the market today (manufactured by LG Chem) is taken from reference [48]. The energy density of commercial LIB cells may soon reach a limit (represented by a bar that refers to their volumetric energy density assuming no unforeseen developments in materials technology. The exact value of the limit is influenced by how the cell is designed and processed.[78]

If no complete change on the materials level will occur, the maximum attainable energy density is limited to a volumetric value of slightly above 800 mAh/l (**Figure 10**) depending on the exact materials used and on the cell design.[22] With regard to the gravimetric energy density, this corresponds to a value of 350 mAh/g (cf. **Figure 9A** and **B**). Therefore, in order to reach

significant gains in both energy and power density, fundamental changes in cell chemistry are needed.

The so-called all-solid state battery (ASSB) is currently the likeliest candidate to enable this urgently needed step forward. According to both cell manufacturers and EV producers (**Figure 9**) the ASSB will be next big issue in battery science possibly substantially boosting both energy and power densities of LIBs finally enabling the widespread introduction of EVs into the market.

2.2 The All-Solid-State Battery

2.2.1 Development of Solid State Ionics

The advent of research in ASSBs is inextricably linked to the discovery of its most crucial and fundamental component: the SE. After the ground laying works of scientific giants like, among others, *Michael Faraday* and *Walther Nernst*, the properties of the archetype of ionic conductors was discovered in 1914: the high-temperature α-phase of AgI.[79] At its phase transition from the β- to the α-phase at 147 °C, the conductivity increases by three orders of magnitude to 1.3 S/cm.[80] The reason for this behavior lies in the peculiar change of its crystal structure involving two key aspects. Firstly, the number of neighboring vacancies of every Ag ion by far exceeds the number of Ag ions, which is oftentimes termed as structural disorder. Secondly, the anions form an array, which provides the cationic sublattice with flat potentials along interconnecting pathways. These two prerequisites can basically be transferred to all high-performance ionic conductors.[81]

The α-phase of AgI served in the following as an inspiration for the investigation of more sophisticated Ag-ion conductors with similar features. This led, among others, to the discovery of Ag_3SI and Ag_3SBr in 1964 with similar conductivities at elevated temperatures[82] but higher melting temperatures than α-AgI which assumes the liquid state at 550 °C. Also, and more importantly, these two compounds showed a decent ionic conductivity already at r.t., 0.01 S/cm, prompting researchers to construct silver-based cells. The first one was an $Ag|Ag_3SI|I_2$ cell[83] which already boasted current densities in the mA/cm² range surpassing all hitherto existing battery concepts which only allowed current densities in the µA/cm² range.[84] Subsequently, an even higher Ag-ion conductivity at RT was attained in the case of $RbAg_4I_5$ (firstly discovered in 1965)[85,86] exhibiting an RT ionic conductivity of 0.27 S/cm in its polycrystalline form.[87] This value comes close to the record holder of RT solid state ionic conductor materials that are known up to the present time: the Cu^+ conductor $Rb_4Cu_{16}I_7Cl_{13}$ with a specific conductivity of 0.34 S/cm at 25 °C.[88]

Obviously, in the early days of solid state ionics, high conductivities were only known for the 1st and 2nd row coinage metals: thus Ag and Cu. Consequently, as one of the very first examples for ASSBs, the Ag-based SEs were used to construct batteries with elementary silver as the anode and iodine as cathode material.[89]

However, Ag – and by extension Cu as well – are noble metals. As such, they display rather high redox potentials leading to comparably low cell potentials attainable when employed

as anode material. Therefore, in order to design competitive ASSBs, solid-state ionic conductors that employ cationic elements with a more favorable (thus lower) redox potential were needed. In this regard, it seems reasonable to resort to the alkali or even alkaline-earth metals. In fact, in a next step on the road to improved ASSBs – far before the commercialization of LE-based Li-ion cells by Sony in 1990[90] – the first Li-based cell was developed: a primary Li|LiI|I_2 cell with *in situ* generated LiI aimed at the utilization in pacemaker devices.[91] To this end, the battery was well-suited because it combined the two most important prerequisites: longevity and a high energy density achieved by the – in contrast to the Ag-based cells – significantly increased cell voltage of roughly 2.8 to 2.4 V over the course of the discharge. Additionally, it exhibits several further advantages sought for in ASSBs: high energy density, impossibility to leak and robustness. Hence, these batteries – with small modifications – are still used today in the initial scope.

But while the low conductivity of LiI (10^{-7} S/cm)[92] did not prevent the triumph of these cells in low energy medical gadgets, it is by far not enough for devices like smartphones, laptops or even electric vehicles. These have much larger requirements regarding the power density. For this purpose, more conductive electrolytes are needed. After the commercialization of the Li|LiI|I_2 cell, only a few further articles were published on the matter of Li-ion batteries until one of the pivotal points of battery-based energy storage research: the introduction of rechargeable liquid Li-ion cells by Sony in 1990 (cf. **Figure 11**).[90,93] Afterwards, in the past decades, an intensive investigation of suitable materials for ASS-LIBs has begun. Whereas the interest seemed too abate in the first decade of this millennium it has regained momentum around 2011 which could be explained by – among other things – the discovery of promising Li-ion solid electrolytes, such as $Li_{10}GeP_2S_{12}$ (LGPS) in 2011[94] and the anomalously well-conductive β-LPS in 2013.[95] The conductivities of LGPS and some other SEs are high enough in order to steadily advance from the level where the electrolyte is necessarily the limiting factor for the operation of these devices to the current paradigm where ASS-LIBs are predominantly limited by the appropriate design of the respective interfaces inside the battery.

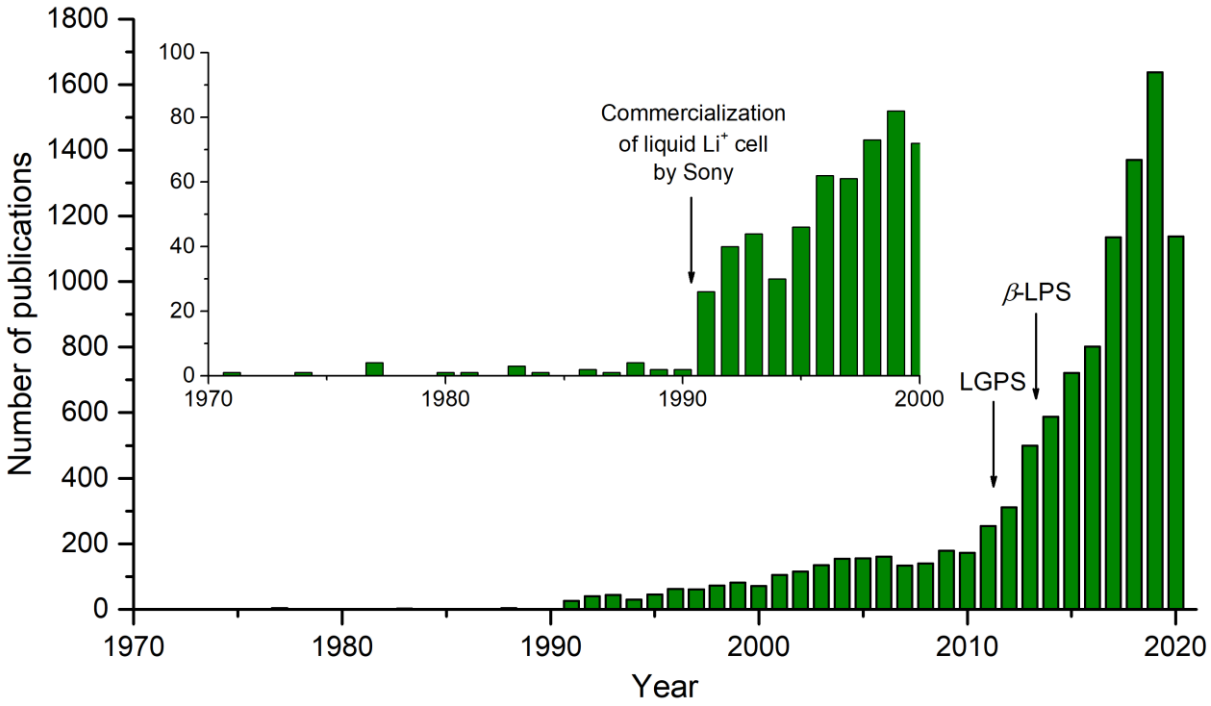

Figure 11: Overview of the number of publications per year from 1970 until 2020 when searching for "Li solid electrolyte" in the Web of Science database, date accessed: 31th July 2020.[93]

For all-solid-state Na-ion batteries (ASS-NIBs) on the other hand, research is still at a considerably earlier stage where great progress is still made in the mere discovery of new and promising materials. Interestingly, highly conductive Na-ion electrolytes have been discovered significantly earlier than respective Li-ion conductors. The stellar material in the domain of solid state Na-ion electrolytes was already discovered in the 1930s:[96] β- or β''-alumina ($NaAl_{11}O_{17}$). Its high conductivity was described much later in 1967.[97] As a single crystalline material, its conductivity amounts to 0.035 S/cm at r.t. As a polycrystalline, however, the overall conductivity with 0.0012 S/cm at r.t. is much lower due to large grain boundary resistivities but upon heating, the Na-ion conductivity rises to roughly 0.25 S/cm at 300 °C. [98–100] Only at this elevated temperature, the material is conductive enough to allow for the operation of two interesting battery concepts that have already been commercialized: the sodium-sulfur battery and the ZEBRA battery both boasting liquid sodium as the anode material. This is separated from liquid sulfur or $NiCl_2$ as cathode material, respectively, by a thin layer of the β''-alumina ceramic. The firstly devised sodium-sulfur battery was pioneered already in the late 1960s by the Ford Motor Company.[101] In the following years, this concept was further developed and experimental applications were intensively tested. Unfortunately, a considerable breakthrough was never achieved in the field of electro-mobility. However, since 2002, the system is manufactured commercially by the Japan-based company NGK Insulators Ltd. and used for grid-scale energy storage.[102]

2.2.2 The All-Solid-State Li-Ion Battery (ASS-LIB)

Whether or not ASS-LIBs will finally reach the state of commercialization is very much contingent on whether the hitherto most urgent problems on the materials and interfaces level will be solved in the upcoming years:

1. Simple and cheap large-scale synthesis of SEs.[103,104]
2. Development of stable and cost-effective coating layers for the cathode materials mitigating interfacial decomposition reactions between cathode material and SE due to the low thermodynamic stability of the SE.[105,106]
3. Morphological fine-tuning of the SE and thus the cathode composites in order to enable effective properties for both electronic and ionic transport.[103,107]
4. Identification of well-suited binders for efficient slurry casting of both SE and cathode composite film without hampering the electrochemical properties.[106,108]
5. Development of effective strategies for the safe and dendrite-free implementation of elementary Li anodes.[109,110]
6. Eliminating the current necessity of utilizing high pressures for long-term cycling of ASSBs.[111,112]

2.2.2.1 The Solid Electrolyte (SE)

The SE is the critical component that differentiates the ASS-LIB from the currently employed LE-LIBs. It is thus inarguably the most important component of an ASS-LIB. Today, mainly three different classes of SE exist: polymer-, oxide- and sulfide-based ones, the latter two of which can be crystalline, glassy or glass-ceramic in nature. Furthermore, composites of the three classes exist, being mostly composed of both oxides and polymers.[113] Polymer-based SEs are very ductile enabling good contacting of the active materials. Their major disadvantage, however, are their hitherto low conductivities making them operable only at elevated temperatures.[22] Oxide-based SEs, on the other hand, can exhibit suitable ionic conductivities surpassing the commonly stated threshold value for high power density batteries: 10^{-3} S/cm. They are also relatively stable at high potentials. Unfortunately, though, they have considerable downsides too. They generally show large grain boundary resistances necessitating high sintering temperatures. In addition, due to their high shear modulus and brittleness, creation of effectively packed cathode composites and mechanically stable separator layers, respectively, are almost impossible to achieve. Lastly, sulfide-based SEs offer high conductivities of over 10^{-3} S/cm as in the case of LGPS and Li_6PS_5Cl linked to a low shear modulus facilitating dense packing of

CAM and SE inside the composite cathode. Especially Li_6PS_5Cl has evolved in the last 2–3 years as the stellar material. It complements its suitable conductivity with a good compatibility (kinetic stability) toward elementary Li and a low price due to the absence of any expensive starting materials as for example Ge as in the case of LGPS.

The most widely applied synthesis methods for SEs on the laboratory scale are either mechanical ball-milling (mechanical alloying) or high-temperature (HT) syntheses carried out in a quartz glass ampule or a combination of the two techniques (**Figure 12**).

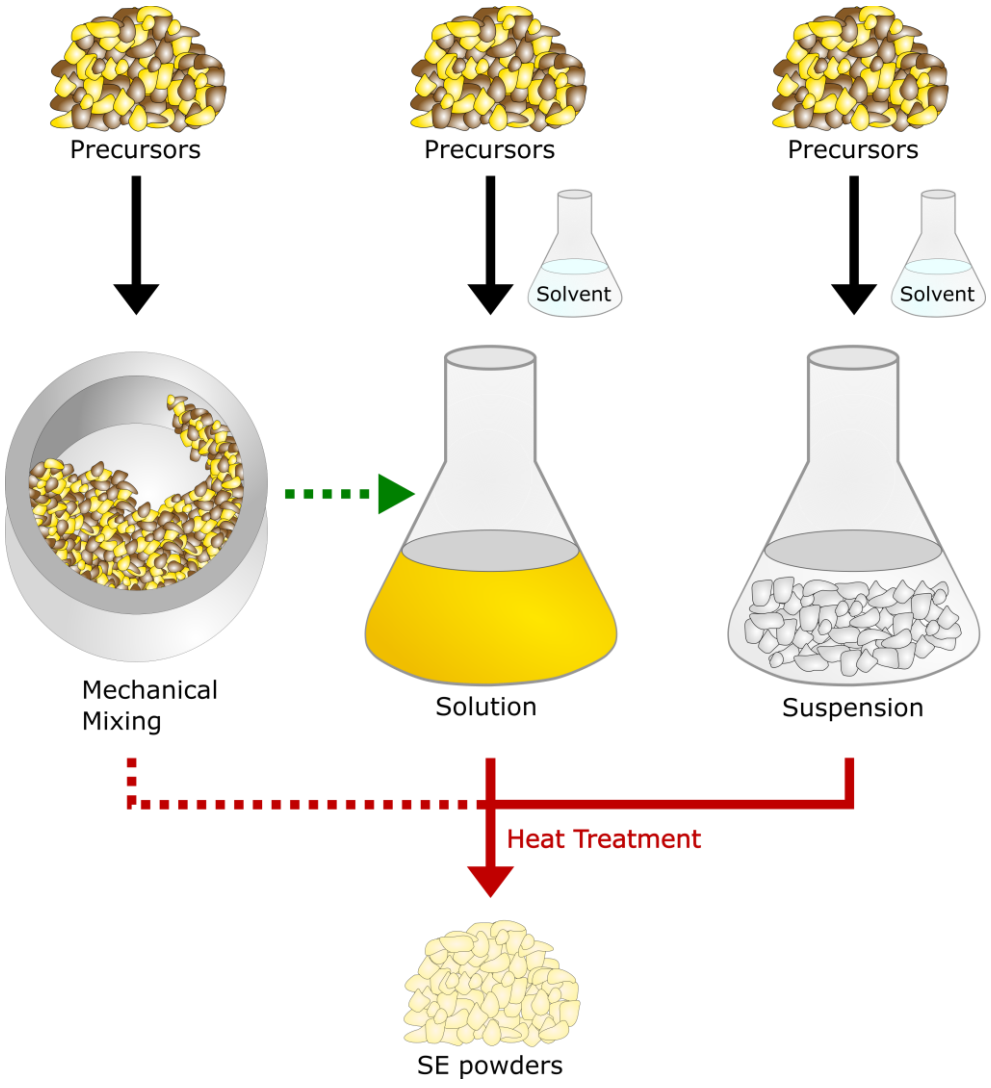

Figure 12: Schematic diagram illustrating the different synthesis protocols for the preparation of sulfide-based SE materials. Left: mechanical milling, middle: solution-based synthesis, right: suspension-based synthesis. Subsequent heat treatment for obtaining the final product is mandatory for solvent-based syntheses but optional for the ball milling procedure. Inspired by reference [114].

However, mechanical ball-milling is a process that is very difficult to scale up as many parameters have to be adjusted and optimized, whereas HT syntheses require a lot of energy in

form of heat. Therefore, a lot of effort has been invested in the development of synthesis strategies for SEs involving solvents – be it solution- or suspension-based ones (**Figure 12**) – which promise to improve scalability and cost-effectiveness.[103,104]

One of the very first examples arousing a great interest was the discovery of β-Li_3PS_4 (β-LPS) derived from a solvent-mediated synthesis in THF exhibiting an unexpectedly high ionic conductivity as mentioned in section **2.2.1**. The synthesis proceeds via the suspension route illustrated on the right hand side in **Figure 12**. Li_2S and P_2S_5 are added to THF as solvent forming the THF-adduct $Li_3PS_4 \cdot 3THF$.[95] Subsequent heat treatment at 140 °C yields β-LPS showing an ionic conductivity of more than 10^{-4} S/cm. When derived from a classical solid state synthesis (denoted bulk Li_3PS_4 in **Figure 13**) , however, the conductivity – when extrapolating its Arrhenius plot to r.t. – amounts to a value of only approximately 10^{-6} S/cm. This value is similarly low as the value reported for γ-Li_3PS_4 which is the stable modification at r.t. (**Figure 13**).[95,115]

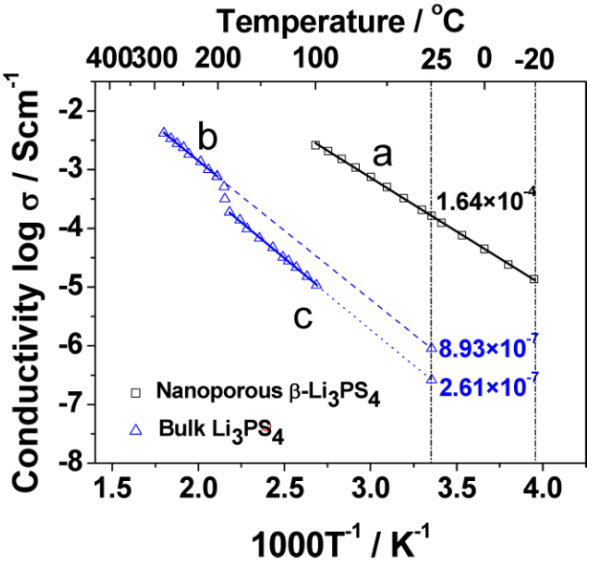

Figure 13: Arrhenius plots of conductivities of a) nano-sized β-LPS, b) high-temperature (HT) β-LPS (extrapolated to r.t., denoted bulk Li_3PS_4) and c) γ-Li_3PS_4, taken from references [95,115]. Copyright© 2013, with permission from the American Chemical Society.

The high temperature β-modification of Li_3PS_4 had previously been known to be stable only above 195 °C.[95,116] When synthesized from THF, though, β-LPS becomes metastable at RT. Along with the higher conductivity comes a peculiar mesoporous structure brought about by the evaporation of THF during heat treatment. The violent release of THF breaks the initially

µm-sized and rod-shaped single crystals of $Li_3PS_4 \cdot 3THF$ and – upon conservation of their former crystal habitus – transforms them into a skeleton of nanoparticles highly pervaded by mesopores. This is a very unique feature differentiating it from any other SE known today synthesized either from ball-milling or high temperature solid state reactions. Those electrolytes consist invariably of large secondary particles whose primary particles are much more densely packed.[107,117,118] The consequences of the peculiar morphology of β-LPS are the subject of the publication discussed in section **3.4**.

Many other solvents as for instance acetonitrile or ethyl acetate have subsequently been found to enable the same reaction leading to comparable conductivities of the obtained β-LPS phases.[119,120] Nevertheless, it should be noted that – using the same stoichiometry – conductivities of solution-derived SE products do not necessarily emulate or even surpass those of ball-milling-derived ones. In the case of Li_3PS_4, the amorphous state brings about a conductivity of roughly $2.0 \cdot 10^{-4}$ S/cm, which is similarly high as the conductivity reported for solvent-derived β-LPS.[95,121] Owing to its straightforward synthesis, β-LPS is a well-established SE in basic ASS-LIB research today.[110] Its conductivity of slightly more than 10^{-4} S/cm is not enough for high-power-density applications such as EVs but for less demanding applications, it might still play a future role. Other SE systems have equally been explored in solvent-based syntheses: mainly $Li_7P_3S_{11}$ and Li_6PS_5Cl.[122,123] Whereas the synthesis of $Li_7P_3S_{11}$ proceeds equally via the suspension route, Li_6PS_5Cl is prepared as a solution in ethanol if preformed Li_3PS_4 is used as precursor. In both cases, the sheer removal of solvent does not suffice. The SEs have to be heated to 270 and 550 °C, respectively, in order to reach their typically high conductivities of more than 10^{-3} S/cm. This subsequent treatment generally leads to rather large particles and particle agglomerates, respectively, which has considerable downsides when it comes to interfacial properties with cathode materials.[107] It is also important to note that EtOH-derived Li_6PS_5Cl reproducibly shows a small share of Li_3PO_4 as by-phase slightly lowering the ionic conductivity compared to Li_6PS_5Cl obtained without any involvement of EtOH.[124,125]

Usage of solvents is, of course, a source of additional cost. Nevertheless, replacing any complex ball milling steps during the course of the synthesis might be worth the extra cost. Chemical interactions of solvents with precursors or intermediates opens up completely new possibilities of reaction control. Ultimately, with more in-depth understanding of the underlying reaction mechanisms, fine-tuning of, for instance, reaction pathways, the local structure and the morphology of SEs might become possible.[103] Furthermore, if the solvent can be recycled and the different steps toward the final SE product are combined, synergies might arise that render the solvent-mediated synthesis the pathway of choice for SEs. A novel and innovative strategy

to this end is presented in section **3.3**. Moreover, the solvent might not be the most expensive expenditure for a SE manufacturer. In fact, Li_2S, the most crucial component for the synthesis of Li-ion SEs, is much more costly as will likewise be shown in section **3.3**.

2.2.2.2 The Interfacial Challenge – The Cathode

Although being the most promising enabler for ASSBs, sulfide-based SEs have significant shortcomings, too. Their stability range is generally very limited.[126,127] Reactions occur both in contact with the anode as well as in contact with the cathode material (**Figure 14**).

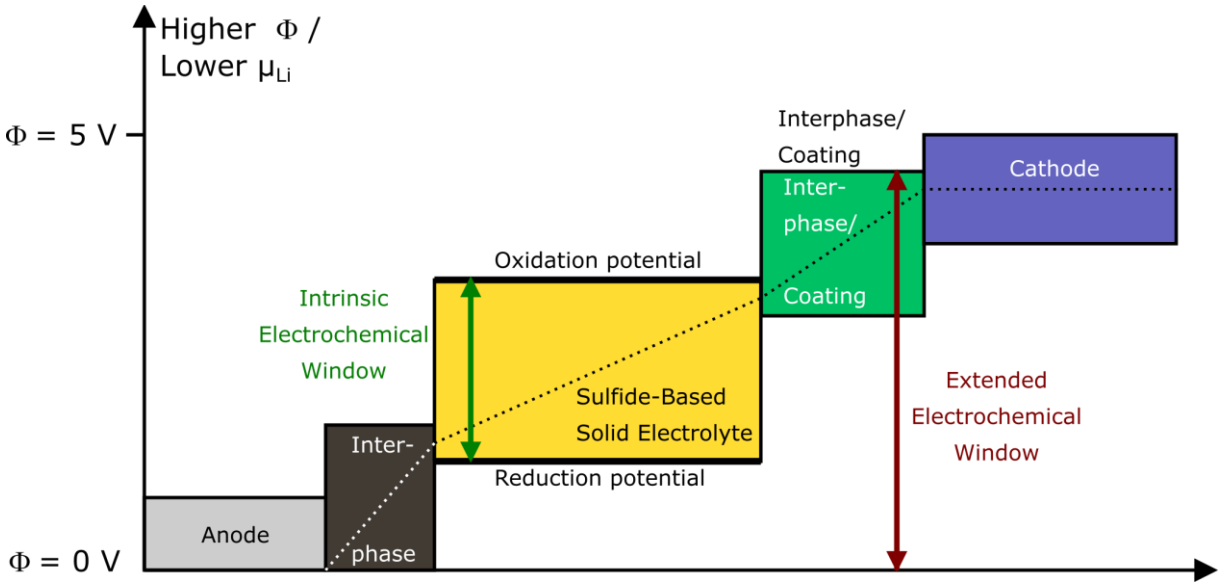

Figure 14: Schematic diagram illustrating the electrochemical (stability) window and the Li chemical potential profile (black dotted line) in an ASS-LIB. The profile of the chemical potential should be seen as schematic and may not be linear in a real world example. The high μ_{Li} in the anode (light grey) and low μ_{Li} in the cathode (blue) are beyond the stability window of the SE (yellow). The interphases (dark grey and green) account for the gap of μ_{Li} between SE and the electrodes across the interfaces, respectively. The observed intrinsic (nominal) electrochemical window is considerably smaller than the extended one owing to the passivating character of the interphases/coatings on both electrode sides. Adapted according to reference [128].

Sulfide ions can easily be oxidized forming polysulfides and finally even possibly elemental sulfur when exposed to delithiated cathode materials. Hence, (electro)chemical stability becomes a decisive criterion for their utilization and the operation of LIBs (SIBs). In order to mend the instability of thiophosphates towards the oxidized TMOs in the charged state, specific coatings are utilized. These coatings are applied as very thin films in the range of only several nm acting as Li-ion conducting buffer layers that prevent direct contact between cathode and electrolyte material and thus a degradation reaction by the highly oxidative character of the TMO in the delithiated state.[129,130] A whole set of materials has already been explored that

show the desired effect, *inter alia* $LiNbO_3$, $LiTaO_3$, solid solutions thereof: $LiNb_xTa_{1-x}O_3$, $Li_4Ti_5O_{12}$, ZrO_2.[131–134] Until now, not much is known about the way these materials work their magic. Investigations are rather difficult due to the thin nature of the coatings and the rather low statistical significance when examined by means of transmission electron microscopy (TEM) probing only small segments of individual particles. Phenomenologically, however, it has undoubtedly been proven that the overpotentials upon cycling are considerably lowered and long-term cycling improved. Therefore, in the study presented in section **3.4**, one of the above-mentioned materials – $LiNbO_3$ – was employed in order to enhance the cycling performance of the constructed ASS-LIBs.

Another serious issue to tackle is the generally insufficient contact area between SE and cathode active material (CAM). A liquid electrolyte (LE) – despite its usually rather high viscosity – is still able to penetrate almost every void in both the porous anode and cathode of a LE-based LIB leading to a high coverage of the theoretic surface area of the active materials. The SE inside a ASSB, on the other hand, is very much limited when it comes to its homogenous distribution inside the composite cathode. It could be shown that the reduction of the particles size of the CAM has a positive impact on the practical capacities reached with regard to the theoretically expected values.[135] Laboratory-scale mixing of CAM and SE involves in the simplest case only thorough mixing inside an agate mortar.[136,137] However, manual grinding does not necessarily lead to efficient mixing if large electrolyte particles are used. A closer look on the effects of the particle size of the electrolyte on the battery performance is taken in section **3.4**Fehler! Verweisquelle konnte nicht gefunden werden.

2.2.2.3 The Interfacial Challenge – The Anode

The ASSB as a concept promises to increase the available energy density and power density – both volumetric and gravimetric. However, this will only hold true if elementary lithium will be implemented (**Figure 15**), which possesses a very high theoretical capacity of 3860 mAh/g.[138] Therefore, research on ASSB is inextricably linked to the facilitation of Li as anode material, but elementary Li is not an easily-employed anode material. Lithium has the lowest redox potential of all elements, and thus easily reduces almost any SE. Indeed, some oxide-based SEs exist such as garnets that are stable in contact with elementary lithium.[139] In the realm of sulfide-based SEs, however, no electrolyte is thermodynamically stable against Li (**Figure 14**). The positively charged phosphorous atoms in thiophosphates can readily be reduced in contact with Li metal, forming Li_3P.[140,141] In the worst case, the SE contains transition

metals or metalloids that form intermetallic alloys upon their reduction by Li, rendering the composite formed by the decomposition products partially electronically conductive. Thus, nothing stands in the way of a further reduction of the SE.[142–144] For the long-term stability of a Li|SE interface, a situation like the one found for the LiC_6|LE interface in LE cells has to be created, where a passivating SEI is formed (cf. **Figure 3** and section **2.1.1**). Be it beforehand or during the initial cycles: an electronically insulating, but ionically conducting, interlayer has to be formed to passivate the anode from further decomposition reactions. Metal-/metalloid-free SEs, like for instance β-LPS or Li_6PS_5Cl, have been reported to be unexpectedly stable in contact with elementary Li due to the formation of passivating interphases.[127] Another possibility to facilitate chemical compatibility is an artificial buffer layer as for the cathode material. To this end, Li-ion conducting polymers are intensively tested.[145]

Electrochemical stability of the interface is not the only issue stemming from an Li anode. Li is an extremely soft and malleable material and the high pressures generally necessary for the compaction of an ASSB[146] can easily lead to Li flowing through the pore space inside the SE separator and thus short-circuiting the battery.[147] Intuitively, one might think that due to the more rigid nature of SEs, Li dendrites could not penetrate the separator as easily as in the case of a LE. Extensive evidence, though, has been presented in the past decade disproving this theory.[110] Lithium can penetrate the SE both mechanically and electrochemically, the latter of which through plating and stripping. Plated lithium can even lead to fracture of oxide-based SE grains despite their great hardness and Young's modulus.[148]

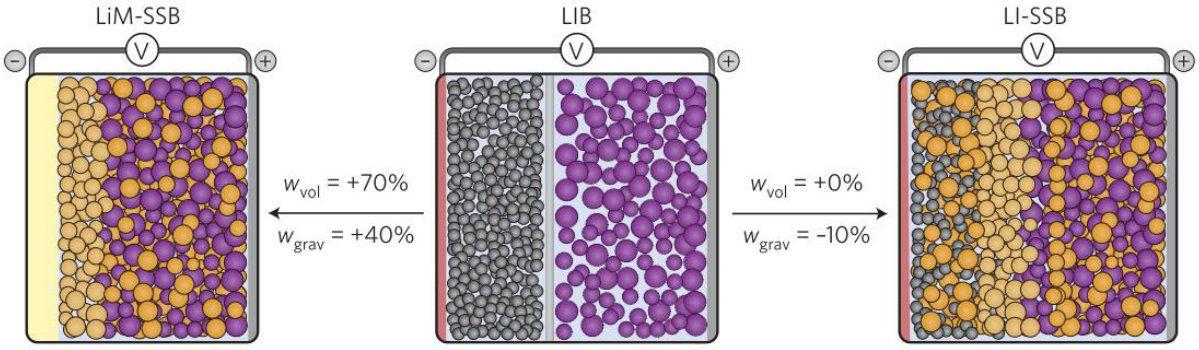

Figure 15: Typical battery architectures for conventional LE-based LIBs (middle), ASS-LIBs based on a graphite-SE composite as anode (right), or Li metal as anode (left). The volumetric and gravimetric energy densities are represented by w_{vol} and w_{grav}, respectively. Only with a lithium-metal anode (light yellow) that has a theoretical energy density of 3,700 mA g^{-1} a significant gain in energy density can be achieved. Changes in energy density are estimated based on the density increase from liquid to solid, taking into account the high specific capacity of lithium metal (left, LiM-SSB) and complete replacement of the graphite and the anolyte (electrolyte utilized in the anode compartment), taken from reference [22]. Copyright© 2016, with permission from Springer Nature.

2.2.2.4 Scale-Up of All-Solid-State Li-Ion Batteries

Research on ASS-LIBs started out by investigating dry-pressed pellet cells. In this setup, the batteries are assembled by merely pressing the different sheets of a battery: cathode composite|electrolyte|anode (composite). Sulfide-based SEs might be less brittle than oxide-based ones; however, their eventual commercialization will not be possible without mechanically stabilizing the respective layers of an ASS-LIB stack. Otherwise, development of ASS-LIBs will not evolve from the laboratory stage where predominantly dry-pressed pellet cells are constructed for the sake of materials' testing. Polymeric binders are already used in today's LE-LIBs for exactly the same purpose as one out of three main components: the CAM, a conductive additive (usually soot), and the binder. They enable roll-to-roll processing and thus a quick and cost-competitive manufacturing.[149] A similar strategy can be devised for ASS-LIBs, too leading to so-called sheet-type ASS-LIBs (ST-ASS-LIBs).

However, extremely polar solvents like *N*-methyl-2-pyrrolidone – extensively used in the slurry casting of cathodes for LE-LIBs – cannot be transferred to the manufacturing of cathodes for ASSBs involving sulfide-based SEs, as they are very prone to decomposition when brought into contact with highly polar solvents.[150] Hence, completely different combinations of solvents and binders have to be found. Polymers like (hydrogenated) nitrile butadiene rubber – (H)-NBR, polyisobutene (PIB) or styrene-butadiene-styrene copolymer (SES) have been tested most intensively. Solvents used are mostly simply functionalized benzene derivatives as toluene, p-xylene or anisole which do not show any negative side reactions with the sulfide-based SEs due to their low polarity.[149–155]

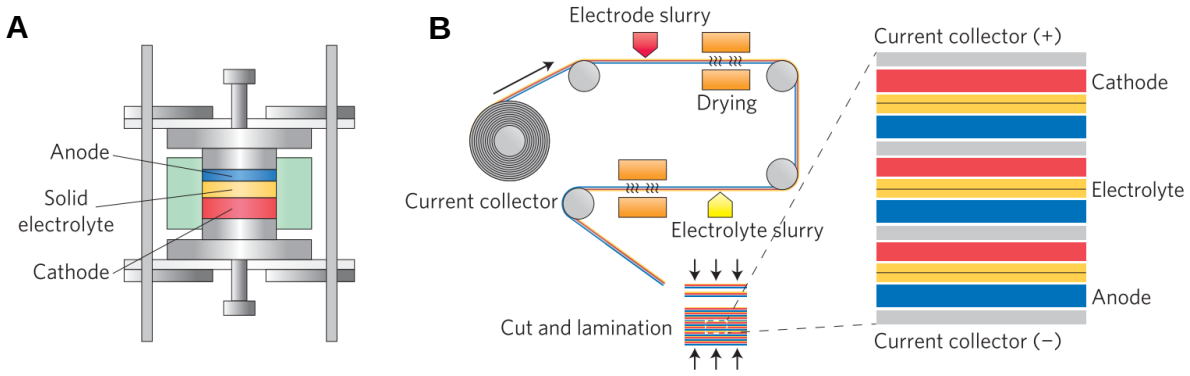

Figure 16: Two fundamentally different preparation procedures of ASS-LIBs. **A**: Typical laboratory scale ASS-LIB preparation via dry pressing of the respective powders. **B**: Possibly future large-scale manufacturing of ASS-LIBs via roll-to-roll processing – considering a composite anode instead of elementary Li using for instance the zero strain material $Li_4Ti_5O_{12}$.[156,157] An electrode slurry is coated on the current collector, then dried and subsequently the SE slurry is casted on top of it. The resulting double-layer sheets - together with the complementary anode (not depicted here) – are cut and laminated together to manufacture the all-solid state batteries. Note: Using elementary Li as anode material the process would be different. Adapted from reference [158]. Copyright© 2016, with permission from Springer Nature.

A typical procedure for the preparation of a composite cathode film on the laboratory scale is depicted in **Figure 17**. Firstly, the polymer is dissolved in the respective solvent giving rise to a viscous polymer solution. Afterwards, premixed SE and CAM are added to the solution inside a mortar and thoroughly suspended therein. Then, by means of doctor-blading, the resulting slurry is casted onto a substrate, usually either aluminum or a polyester foil, dried and then calendared between a hot rolling press. Afterwards, suitable pieces can be punched out. This approach was used in the publication discussed in section **3.4**.

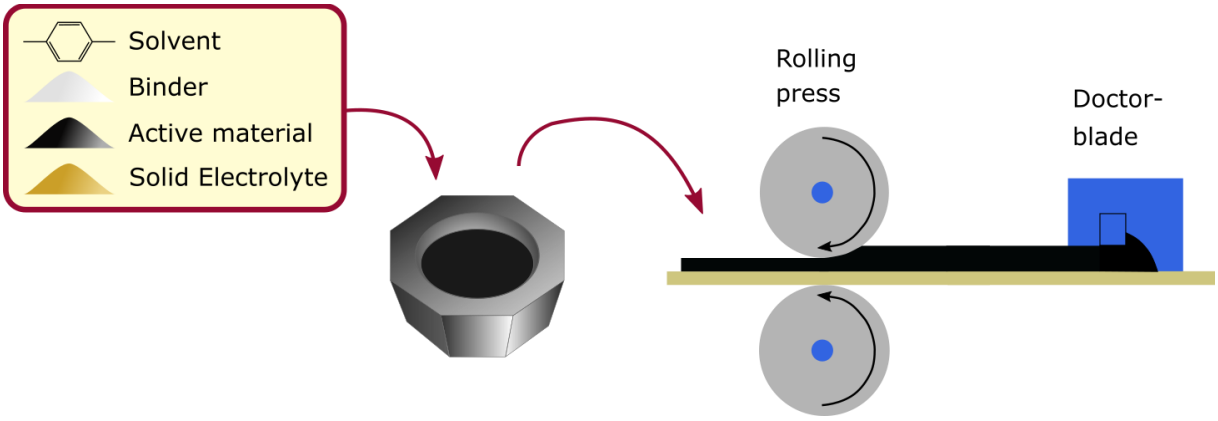

Figure 17: Strategy for the lab-scale manufacturing of a cathode composite sheet.

2.2.3 The All-Solid-State Na-Ion Battery (ASS-SIB)

The working principle of a SIB, be it a LE-based or ASS-SIB, corresponds exactly to the way a respective LIB works as schematically introduced in section **2.1.1**. Research on SIBs is largely inspired by the known similarities between the chemistries of Li and Na. Cathode materials for SIBs are predominantly either TM layered oxides according to the general formula AMO_2 (M = Cr, Mn, Fe, Co, Ni and mixtures thereof),[159–163] like for LIBs or fluorophosphates, particularly some compounds that contain vanadium.[164] On the anode side, a very fundamental difference exists towards LIBs: graphite cannot be utilized as anode material as it is unable to accommodate Na in a large extent due to very weak Na–C interactions. Only low sodiation states of roughly NaC_{64} can be obtained, which are insufficient in order to reach reasonable energy densities.[165,166] Instead, highly disordered pyrolytic carbon is most often used. It is characterized by a very large number of defects, facilitating capacities of up to 300 mAh/g

which comes close to the ones observed for LiC_6.[167,168] Liquid electrolytes employed are generally the same ones as for LIBs: organic carbonates with conducting salts, such as $NaPF_6$ or the like, but with differences regarding the ideal mixtures of organic carbonates for stable SEIs that enable long-term cycling.[164]

Due to the very favorable characteristics of LIBs that led to the progressive replacement of many former battery technologies (**Figure 2**), renewed interest for SIBs developed only quite recently. Simultaneous with the renewed attention for ASS-LIBs around 2010, research on ASS-SIBs picked up pace, too (**Figure 18**). The underlying motivation is mainly governed by the idea that the available, exploitable resources of Li are not sufficient to meet the future demand for electric gadgets, EVs, as well as intermediate grid energy storage.[169] However, due to enormous and largely successful efforts exploring new lithium deposits, this can be debated. More critically, instead, seems the conflict-ridden procurement of sufficient cobalt for the state-of-the-art cathode materials in LIBs. Nevertheless, bearing in mind that the content of cobalt in NMC is constantly decreasing, this problem constantly diminishes. Thus, a serious bottleneck for the manufacturing of ASS-LIBs in terms of precursor supply is not expected. In the end, the major advantage of potential ASS-SIBs would be their lower price. Because not only is sodium much more abundant in the earth's crust but also offers the opportunity to manufacture cathode materials constituting more available TMs: for instance Mn and Fe or V.[170–172]

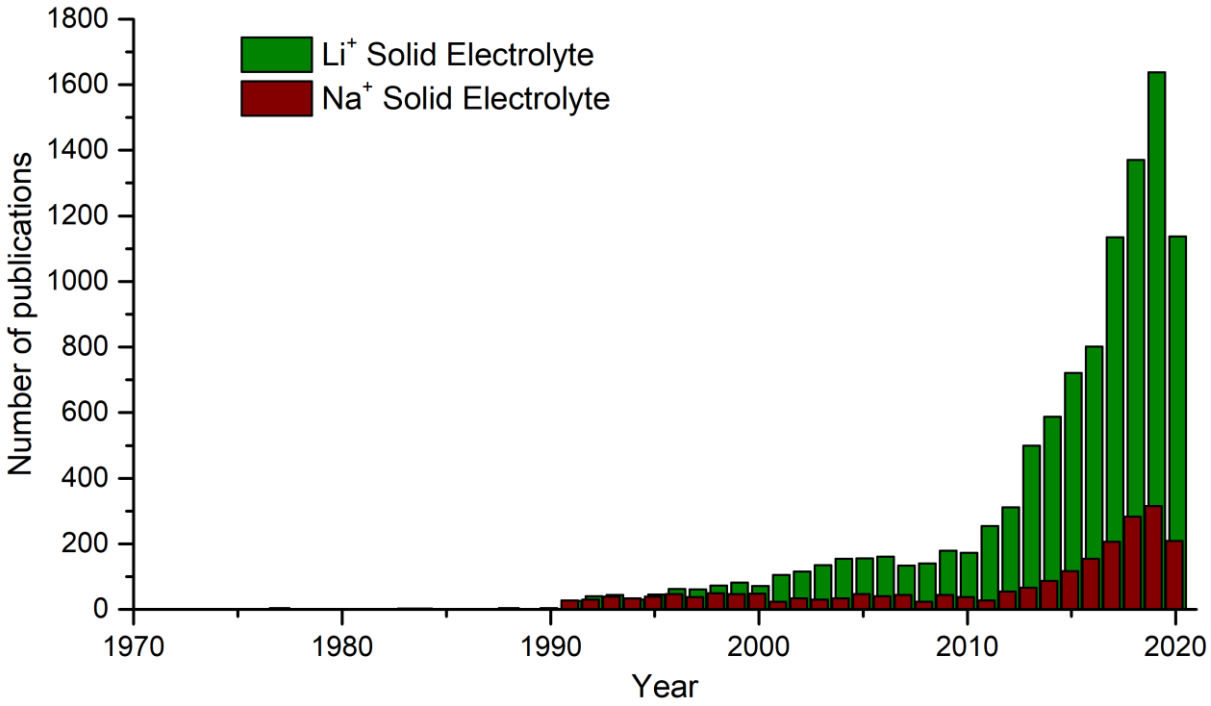

Figure 18: Overview of the number of publications per year from 1970 until 2020 when searching for either "Li solid electrolyte" or "Na solid electrolyte" in the Web of Science database, date accessed: 31th July 2020.[93]

Moreover, these TMs are much more environmentally benign. These advantages could prompt the usage of ASS-SIBs as stationary energy storage systems for the grid where overly high energy densities are not of paramount importance, but rather a low price, longevity and safety. Concerning the latter, with elementary Na having a lower melting temperature and being even more malleable than Li, the implementation of an Na anode could be even harder to master. However, until now, this is only speculation and will be shown in upcoming years. Regardless of the possible downsides, the sheer abundance of Na and the high similarity with Li make it an interesting research topic worth exploring.

Just as for ASS-LIBs, the SE is the most crucial and basic component of an ASS-SIB. Similarly to ASS-LIBs, possible SEs for ASS-SIBs can be categorized into the very same groups (section **2.2.2.1**): polymer-, oxide-, and sulfide-based ones with their advantages and disadvantages being virtually the same.[173] Research in SEs for ASS-SIBs has largely been governed by the successes that had previously been achieved for Li-ion SEs. Shortly after the discovery of LGPS in 2011 arousing renewed interest in ASS-LIBs, an important discovery for the field of sulfide-based Na-ion SEs was made. The group of *Tatsumisago* reported the hitherto unknown cubic modification of Na_3PS_4 (c-Na_3PS_4).[174] Tetragonal Na_3PS_4 (t-Na_3PS_4) had previously been described, however, it exhibited only a comparably low conductivity of less than 10^{-6} S/cm.[175] The new compound was prepared by means of ball-milling, resulting in a glass-ceramic compound. It exhibited a conductivity of more than 10^{-4} mS/cm, which rendered it the record holder for sulfide-based Na-ion SEs until then. Further improvements by means of isovalent substitution of either the pnictogen or the chalcogen led to Na_3SbS_4 and Na_3PSe_4, both showing conductivities surpassing the common threshold value of 10^{-3} S/cm: $3 \cdot 10^{-3}$ and $1.2 \cdot 10^{-3}$ S/cm, respectively.[176,177] Replacing P with Sb brought about the additional advantage of an increased stability towards oxygen and water, which enabled the processing of water-soluble Na_3SbS_4 in aqueous solutions.

Building upon those findings for ternary sulfide-based Na-ion SEs, researchers tried to predict the Na-ion analogue of LGPS and both its lighter and heavier tetrel analogues: $Na_{10}GeP_2S_{12}$, $Na_{10}SiP_2S_{12}$ and $Na_{10}SnP_2S_{12}$.[178,179] Synthesis attempts on $Na_{10}SnP_2S_{12}$ indeed resulted in the evolution of a new compound that could be observed in the PXRD pattern, yet with considerable fractions of the starting materials Na_2S and P_2S_5 as by-phases. This prompted my research on these quaternary sulfide-based Na-ion conductors, the results of which are shared in sections **3.1** and **3.2**. Further work has been published subsequently by other groups and will be included in further discussion in both the summary and the outlook sections **4** and **0**.

3 Cumulative Section

The cumulative section of this dissertation, as the scientific body of this document, comprises only those publications listed in the preface, to which I contributed as main researcher (see the list below). Every article is summarized with its key results. The own share in the shown works is declared. The intellectual property rights belong to the respective journal. However, permissions have been granted for all publications contained. All figures and tables shown in the following have been left unchanged from the original version unless otherwise stated. A complete copy of the original publications together with a preceding license agreement, respectively, can be found in the appendix at the very end of this document.

[I] **Marc Duchardt**, Uwe Ruschewitz, Stefan Adams, Stefanie Dehnen, Bernhard Roling, Vacancy-Controlled Na-ion Superion Conduction in $Na_{11}Sn_2PS_{12}$, *Angewandte Chemie International Edition* **2018**, *57*, 1350–1355.

[II] **Marc Duchardt**, Sven Neuberger, Uwe Ruschewitz, Thorben Krauskopf, Wolfgang G. Zeier, Jörn Schmedt auf der Günne, Stefan Adams, Bernhard Roling, Stefanie Dehnen, Superion Conductor $Na_{11.1}Sn_{2.1}P_{0.9}Se_{12}$, Lowering the Activation Barrier of Na-ion Conduction in Quaternary 1−4−5−6 Electrolytes, *Chemistry of Materials* **2018**, *30*, 4134–4139.

[III] **Marc Duchardt**, Mirko Diels, Bernhard Roling, and Stefanie Dehnen, Flow-Oriented Synthesis of Li_2S and $Li_3PS_4 \cdot 3THF$: Opening Up a Completely Solvent-Based Solid Electrolyte Value Chain, *ACS Applied Energy Materials* **2020**, *3*, 6937–6945.

[IV] Moritz Kroll,[+] **Marc Duchardt**,[+] Sarah L. Karstens, Sabine Schlabach, Fabio Lange, Janika Hochstrasser, Bernhard Roling and Ulrich Tallarek, Kinetic Limitations in Sheet-Type All-Solid-State Battery Cathodes, submitted to *Advanced Energy Materials*.

[+] These authors contributed equally to this work.

3.1 Vacancy-Controlled Na-Ion Superion Conduction in $Na_{11}Sn_2PS_{12}$

[I]

Marc Duchardt, Uwe Ruschewitz, Stefan Adams, Stefanie Dehnen, Bernhard Roling

Angewandte Chemie Internation Edition **2018**, 57, 1350–1355.

In this publication, the new Na-ion conductor $Na_{11}Sn_2PS_{12}$, with a hitherto unprecedented structure motif, was reported with the highest conductivity (3 mS/cm) of sulfide-based Na-ion conductors until then. Inspired by the highly conductive $Li_{10}TtP_2S_{12}$ with Tt = Ge, Sn,[94,118,180] first theoretical publications[178,179] had earlier suggested that the analogous quaternary sodium compounds "$Na_{10}TtP_2S_{12}$" (Tt = Ge, Sn) would also be thermodynamically stable. However, the experimental synthesis of "$Na_{10}SnP_2S_{12}$" had already proven difficult.[178] Beside a whole new set of unassignable peaks, the powder diffraction pattern showed large amounts of Na_3PS_4 and the binary starting materials Li_2S and P_2S_5. This led to the assumption that the actual composition of a quaternary Na-Sn-P-S compound could deviate with a higher content of Sn than anticipated. Therefore, a study was designed to systematically vary the ratio of the formally ternary constituents Na_4SnS_4 and Na_3PS_4 in order to examine the exact stoichiometry of the targeted Na-Sn-P-S compound (**Figure 19**).

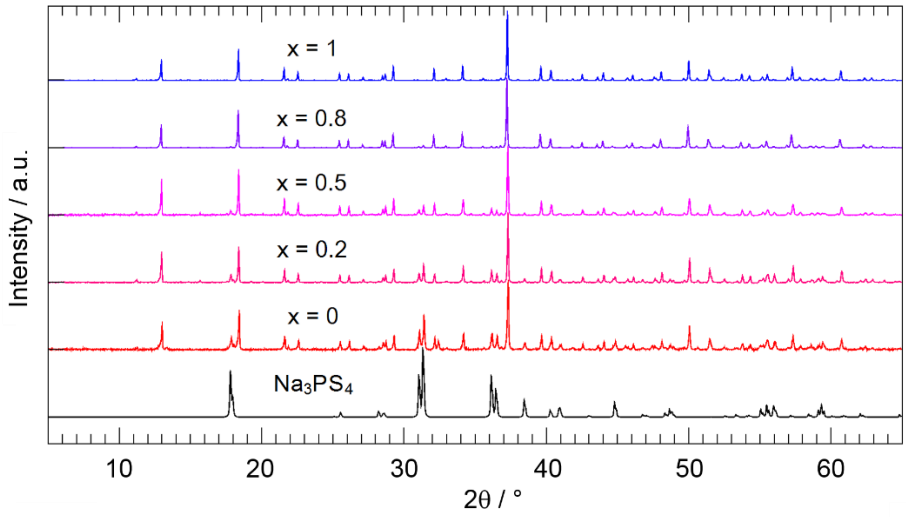

Figure 19: Normalized, stacked powder X-ray diffraction (PXRD) patterns of the solid phases summarized as $Na_{10+x}Sn_{1+x}P_{2-x}S_{12}$ (x = 0, 0.2, 0.5, 0.8, 1), which are actually mixtures of 0.5+0.5x $Na_{11}Sn_2PS_{12}$ with 1.5–1.5x Na_3PS_4. The lowermost diagram represents, for comparison, a simulated pattern of tetragonal Na_3PS_4.[175]

Previously prepared ternary precursors Na_3PS_4 and Na_4SnS_4 were used instead of the respective binary reagents in order to limit the by-phases to Na_3PS_4, and thus facilitate the quantification of by-phase vs. targeted phase. This led to the discovery of $Na_{11}Sn_2PS_{12}$ as the actual composition of the quaternary Na-Sn-P-S compound. Consequently, the ratio of P:Sn is exactly the opposite of the one found for the quaternary Li-ion conductors $Li_{10}TtP_2S_{12}$ with Tt = Ge, Sn.

The PXRD signature of $Na_{11}Sn_2PS_{12}$ (NaSnPS) did not suggest any close relation between the newly found structural motif and the one of $Li_{10}SnP_2S_{12}$, but the structure is similar to the one of tetragonal Na_3PS_4 (**Figure 20b**). Unfortunately, all endeavors at obtaining single crystals of the compound failed. Therefore, an attempt was made to solve the structure from high-resolution synchrotron powder diffraction data. This, in fact, proved successful, establishing the first structural model of NaSnPS in the tetragonal space group $I4_1/acd$.

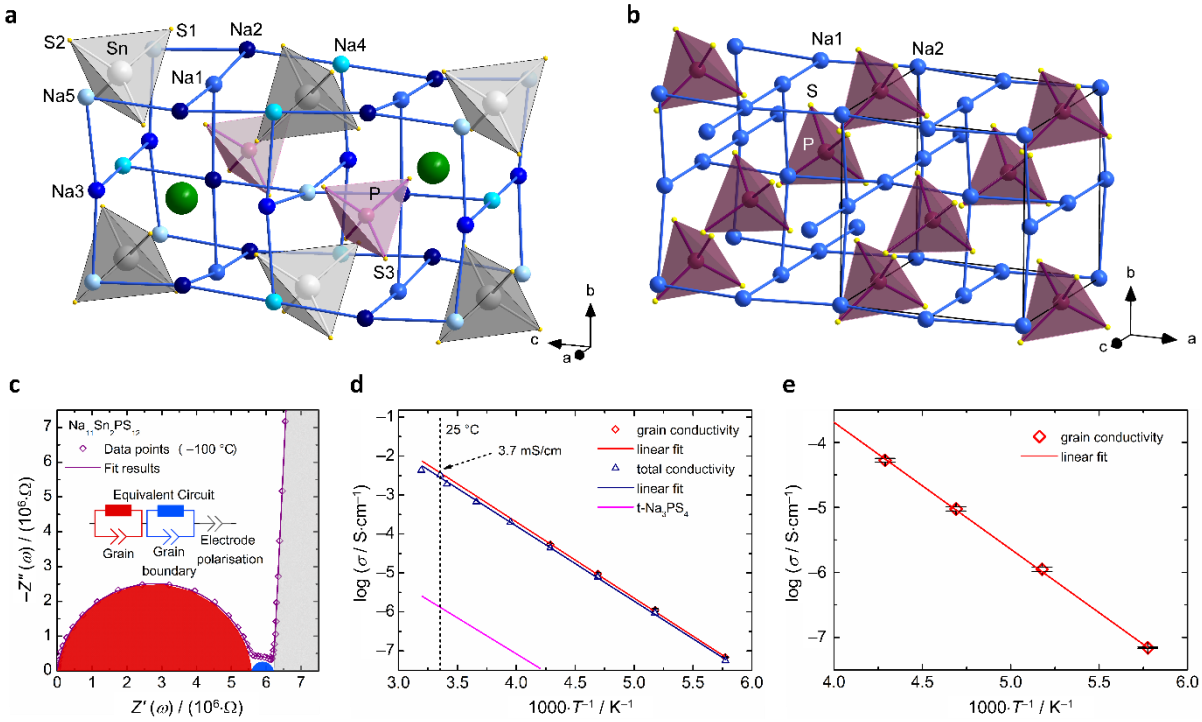

Figure 20. Structural and impedance data of $Na_{11}Sn_2PS_{12}$ in comparison to Na_3PS_4. a) Illustration of Na···Na interatomic contacts in the crystal structure of $Na_{11}Sn_2PS_{12}$. Large green spheres mark unoccupied vacancies in the NbO-type structure formed by the Na-ion cations (for details, see text). b) Illustration of Na···Na interatomic contacts in the crystal structure of Na_3PS_4 for comparison (shown here as 2×1×1 supercell for easier comparison).[27] $[PS_4]^{3-}$ tetrahedra are drawn in dark purple and all Na-ion cations in blue. c) Nyquist impedance plots of $Na_{11}Sn_2PS_{12}$ after annealing together with the equivalent circuit utilized for fitting the spectra. The different contributions to the total impedance, obtained from the fits, are highlighted in different colors. d) Arrhenius plot of the grain and total conductivity of $Na_{11}Sn_2PS_{12}$, obtained from the mean values of three measurements on annealed $Na_{11}Sn_2PS_{12}$ pellets; for comparison, conductivity data of tetragonal Na_3PS_4 is included.[175] e) magnified view of the Arrhenius plot of the grain conductivity of $Na_{11}Sn_2PS_{12}$ with error bars indicating the standard deviation of the mean values.

The structure is significantly more complex than the one of the lithium counterparts. Eight formula units make up the unit cell ($Z = 8$), in contrast to only 2 in the case of LGPS. The five main Na sites of NaSnPS (Na1–Na5, **Figure 20**) are each surrounded by four other Na atoms in a nearly square-planar fashion, which gives rise to Na-ion channels along all three crystallographic axes. The structure can be seen as a deficient NaCl-type structure, with ¼ of its sites being vacancies – and of those vacancies, ¾ are filled with either $[SnS_4]^{4-}$ or $[PS_4]^{3-}$ tetrahedra. The remaining vacancies (¼ of ¼ of the positions in the *pseudo* NaCl-type structure amounting to a total of 8, indicated as green spheres in **Figure 20a**) are partially occupied by Na ions. Therefore, the overall number of crystallographic Na positions equals six. Apart from its special location inside the crystal structure, Na6 is furthermore only occupied to a very low extent of roughly 20%. This leads to the question of whether or not this peculiar position Na6 significantly contributes to the long-range overall conductivity of NaSnPS by interconnecting different pathways. More light on this question will be shed in the subsequent publication (see section **3.2**).

The impedance spectrum of phase-pure NaSnPS shows two processes (**Figure 20c**): mainly the grain contribution and a rather negligible grain boundary contribution. The grain conductivity of NaSnPS amounts to 3.7 mS/cm (**Figure 20d** and **e**), which was the highest conductivity measured for a sulfide-based Na-ion conductor until the date of publication. ^{23}Na-NMR measurements showed only one signal. This corroborates that all Na ions take part in the conduction mechanism, proving it truly 3D. Strikingly, however, the activation energy E_A of NaSnPS was unexpectedly high: 0.39 eV compared to 0.24 eV reported for the lithium counterpart $Li_{10}SnP_2S_{12}$. The reason for this behavior might be found in the peculiar Na position Na6. Backed up by bond-valence simulations, the low occupation factor suggests the potential energy of this position to be by a few k_BT higher than the potential energy of the other positions. Consequently, the involvement of Na6 leads to an overall higher E_A. Concomitantly, conceiving this vacancy position to be similar to typical Frenkel defects, the entropy of activation should also be larger giving rise to the untypically large preexponential factor compensating the high E_A.

Even though the chemical stability of NaSnPS toward Li is equally low as for $Li_{10}TtP_2S_{12}$ (Tt = Ge, Sn), the compound represents a promising electrolyte which – if used with protected/coated electrodes – could enable r.t. high-power-density Na-ion ASSBs.

As research on solid electrolytes and ASSBs, be it Na-ion-based or Li-ion-based ones, is a fast-paced field, simultaneous research efforts on similar subjects and topics in different research groups are quite likely. Indeed, the results shared in this article were published simultaneously by the group of *Linda Nazar*, and a littler later also by the *Wang* group.[181,182] Although the reported models of the crystal structure and the measured conductivities were quite similar, different results were obtained with respect to the role, which the peculiar Na6 atom plays in the conduction mechanism.

Own Share of work

I conceived the laboratory PXRD and impedance experiments and discussed their outcome with *Stefanie Dehnen* and *Bernhard Roling*. Apart from the synchrotron PXRD measurement and the bond valence simulations, I carried out all other experiments. *Uwe Ruschewitz* performed the synchrotron P-XRD measurement during beam time of his co-worker *Melanie Werker*, and he came up subsequently with the structural model of $Na_{11}Sn_2PS_{12}$. *Stefan Adams* carried out the bond valence simulations and designed the respective figures. I wrote the first draft of the manuscript. In the following, *Stefanie Dehnen*, *Bernhard Roling* and I further elaborated on it. All authors contributed to the final version. It should be noted that the essentially phase-pure synthesis of $Na_{11}Sn_2PS_{12}$ and preliminary impedance results were already included in my Master thesis.

3.2 Superion Conductor $Na_{11.1}Sn_{2.1}P_{0.9}Se_{12}$: Lowering the Activation Barrier of Na-ion Conduction in Quaternary 1−4−5−6 Electrolytes

[II]

Marc Duchardt, Sven Neuberger, Uwe Ruschewitz, Thorben Krauskopf, Wolfgang G. Zeier, Jörn Schmedt auf der Günne, Stefan Adams, Bernhard Roling, Stefanie Dehnen

Chemistry of Materials **2018**, 30, 4134–4139.

An oftentimes observed trend for ionic conductors is that the softer the lattice, the lower the activation energy E_A and thus the higher the ionic conductivity at r.t.[183] The substitution of selenium for sulfur had been discussed for $Li_{10}TtP_2S_{12}$ with Tt = Si, Ge, Sn shortly after the discovery of $Li_{10}GeP_2S_{12}$.[183] However, a complete substitution was never accomplished experimentally, only minor subsitutions proved possible.[184] Na^+ with its larger ionic radius, on the other hand, might be able to stabilize a potential $Na_{11}Sn_2PSe_{12}$. Thus, following the previous publication, it was attempted to transfer the newly found stoichiometry of $Na_{11}Sn_2PS_{12}$ (NaSnPS) to the respective selenide: $Na_{11}Sn_2PSe_{12}$ (NaSnPSe).

After optimizing the temperature protocol (extremely slow cooling after the solid-state reaction: 2 K/h), it was finally possible to obtain single crystals of both the previously published NaSnPS and NaSnPSe. This allowed for a more in-depth analysis of their structural characteristics compared to the previous publication, where the structural investigation was solely based on powder X-ray data. Significant differences between both compounds were found. First, strongly deviating occupational factors for the six crystallographic sodium positions Na1–Na6 were unveiled. Second, upon several synthesis attempts, the stoichiometry of NaSnPSe was constantly deviating from the expected one, which proved to correspond to a sum formula of $Na_{11.1}Sn_{2.1}P_{0.9}Se_{12}$ instead of $Na_{11}Sn_2PSe_{12}$. Third, concomitantly to this variation of the Sn:P-ratio, the compound exhibits a rotational disorder of the $[PS_4]^{3-}$ tetrahedra (see **Figure 21**) in a 9:1 ratio. However, since the $[PS_4]^{3-}$ tetrahedra show exactly the same (P/Sn)–S bond lengths – independent of their orientation – the occupational disorder appears to be completely independent from the rotational one. The partial substitution of P by Sn at the P position should formally lead to a P-containing by-phase. However, the amount is small, and the PXRD pattern (**Figure 21c**) did not show any sign of a crystalline by-phase.

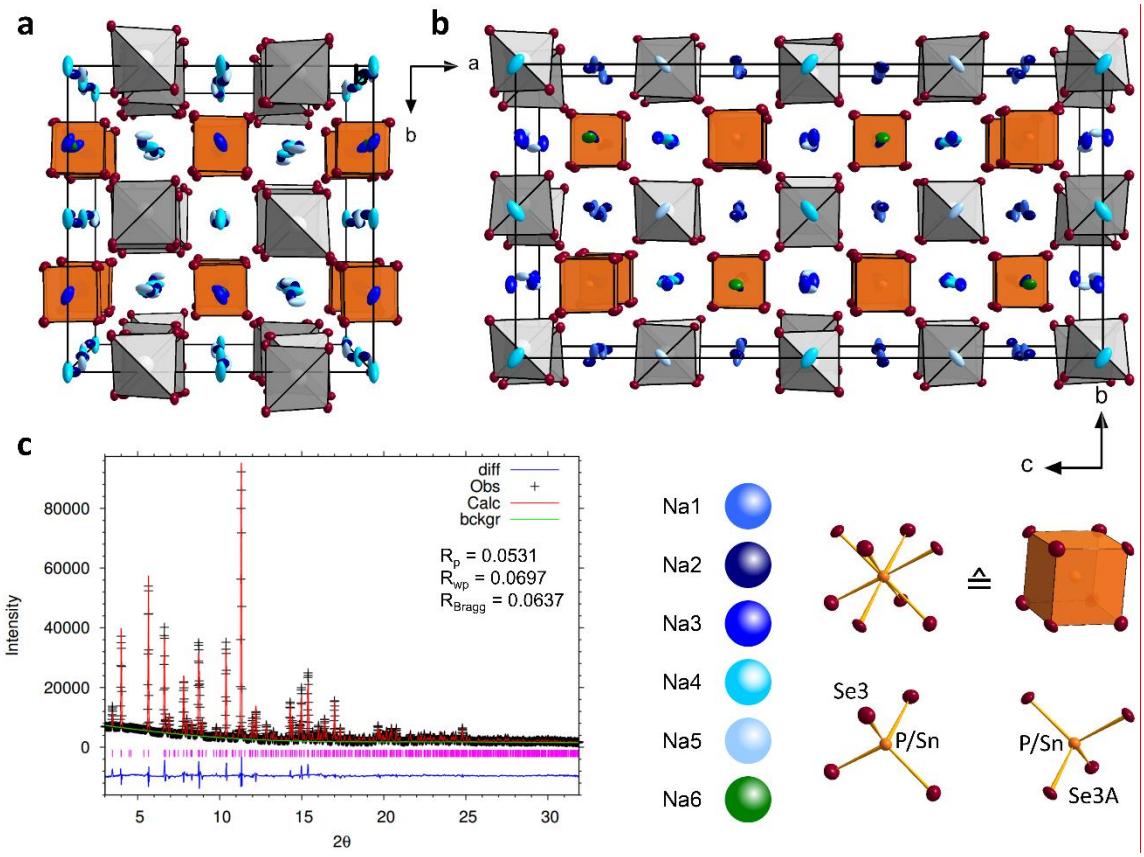

Figure 21. Cut-off from the crystal structure of NaSnPSe, viewed along [001] (a) and [100] (b). Sn atoms and $[SnSe_4]^{4-}$ tetrahedra are drawn in grey, P atoms and $[PSe_4]^{3-}$ tetrahedra in orange, Se atoms in dark red, and Na-ion cations in different shades of blue in order to differentiate between the six crystallographically distinct sites. For a comprehensive visualization of the $[PS_4]^{3-}$ tetrahedra, both possible orientations are shown. Their superimposition leads to the appearance as a cube. c: Rietveld refinement of a diffraction pattern collected at beamline BL9 of the DELTA synchrotron radiation facility, Dortmund/Germany (λ = 0.49594 Å; T = 295 K). The refinement residuals are given in the inset.

NaSnPSe exhibits a similar impedance behavior as NaSnPS exhibiting small grain boundary contributions. The activation energy E_A of 0.30 eV is considerably lower than the one of NaSnPS (0.39 eV), which is well in line with the value observed for similar systems, like $Na_3PS_xSe_{4-x}$ or $Na_3SbS_xSe_{4-x}$, and also for Li_6PS_5X (X = Cl, Br).[185–188] However, the lowered activation energy does not entail a higher r.t. ionic conductivity. NaSnPSe exhibits a slightly lower conductivity compared to NaSnPS. This is surprising, as intuitively one would expect a decrease in E_A to be accompanied by an increase in the r.t. conductivity. This indicates that a softer lattice is not necessarily advantageous for a higher conductivity. A general explanation is that – apart from lowering the activation energy – a broadening of the potential of the jump oscillators also leads to an altered, thus lowered, attempt frequency overcompensating the gain of a higher probability of successful jumps.[188] However, when explicitly comparing NaSnPS and NaSnPSe, careful consideration should also be devoted to the occupational pattern of the six Na positions. Both compounds exhibit a peculiar interstitial position i1, which, according to

bond-valence-simulation (BVS) calculations, plays a crucial role in long-range ionic motion (**Figure 22**): The 3D network of pathways in both compounds can be regarded as being composed of two interpenetrating 3D networks comprising either Na1, Na4, Na5 and i1, or Na2, Na3, Na6 and i1. Position Na6 in the crystal structure can be regarded as a crossroads for both subnetworks. In NaSnPSe, this position is, on the one hand, completely filled (no vacancies) and, on the other hand, its potential energy is considerably reduced compared to NaSnPS. This presumably engenders a reduced contribution of the higher energy Na2-Na6-Na3-i1 pathway branches.

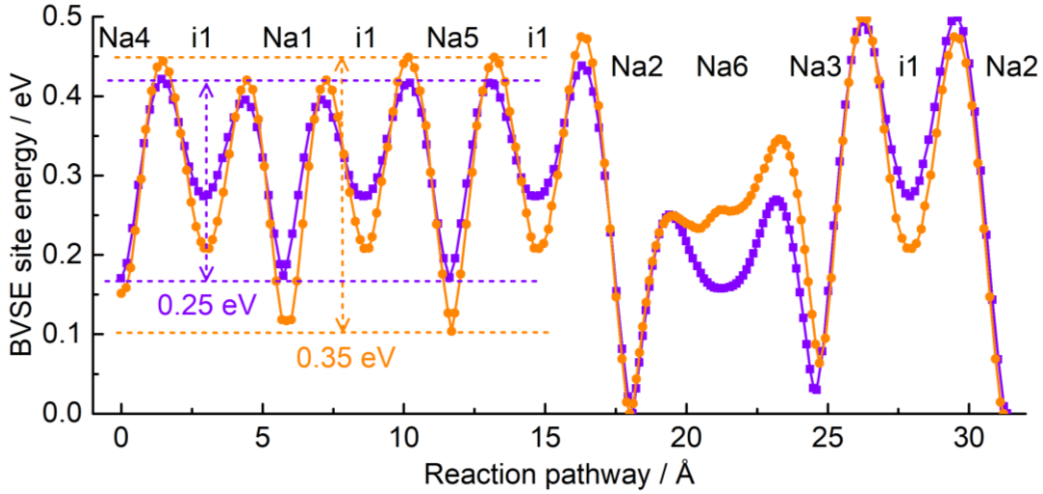

Figure 22: Comparison of BVSE energy landscapes for the Na-ion motion in $Na_{11.1}Sn_{2.1}P_{0.9}Se_{12}$ (violet squares, relaxed local structure model using $PSe(3)_4$ positions) and $Na_{11}Sn_2PS_{12}$ (orange circles – based on the single crystal structure data in this work). Besides the generally somewhat lower migration barriers for the selenide, significant differences include the higher site energy for the interstitial site ***i***1 and the more regular local energy minimum corresponding to Na(6), while the same region in the sulfide contains several extremely shallow local minima.

Through this study, an in-depth insight into the conduction mechanism at play in NaSnP(S/Se) could be gained. Due to the lower activation energy, NaSnPSe is better suitable for low temperature applications, and is also worth being considered for an application in batteries following the concept of Na-Se batteries.[189–192]

Own Share of work

I synthesized the compounds and measured both the impedance data and the single crystal XRD data. I solved and refined the crystal structures of both NaSnPS and NaSnPSe. The results were discussed with *Bernhard Roling* and *Stefanie Dehnen*. *Thorben Krauskopf* and *Wolfgang G. Zeier* contributed speed-of-sound measurements for both compounds. *Uwe Ruschewitz* acquired a synchrotron PXRD of NaSnPSe at Delta synchrotron and performed the Rietveld refinement. *Stefan Adams* contributed BVS calculations for both NaSnPS and NaSnPSe. *Sven*

Neuberger and *Jörn Schmedt auf der Günne* carried out ^{23}Na-, ^{77}Se-, ^{119}Sn- and ^{31}P-NMR measurements. I mainly wrote the manuscript in close consultation with *Bernhard Roling* and *Stefanie Dehnen*, but all authors contributed to the final version.

3.3 Flow-Oriented Synthesis of Li_2S and $Li_3PS_4 \cdot 3THF$: Opening Up a Completely Solvent-Based Solid Electrolyte Value Chain

[III]

Marc Duchardt, Mirko Diels, Bernhard Roling, Stefanie Dehnen

ACS Applied Energy Materials **2020**, 3, 6937–6945.

For a potential commercialization of ASSBs, not only the materials themselves are important, but also time and cost-effective ways to synthesize them. As part of the two previous publications, the syntheses of SEs hitherto predominantly resort to classical solid-state syntheses. However, in order to synthesize large amounts of SEs in a reproducible and scalable fashion, it will be necessary to develop optimized methods to access those electrolytes in scale.

Naturally, the most important precursor for the synthesis of sulfide-based Li-ion SEs is Li_2S, but it is not an easily accessible chemical. Its conventional synthesis involves carbothermic reduction at temperatures around 1000 °C (**Scheme 1 (1)**) where Li_2SO_4 – the precursor – is liquid: $T_m(Li_2SO_4)$ = 845 °C. Thus, the process is extremely energy-intensive and, furthermore, produces large amounts of CO_2. In the laboratory, Li_2S can be easily synthesized by reacting Li with S in liquid ammonia (**Schema 1 (2)**); however, this process completely lacks large-scale feasibility. Another alternative is the acid-base reaction of Li_2CO_3 or LiOH with inexpensive H_2S (**Scheme 1 (3)**). Temperatures needed are lower compared to those applied in the contemporary process (**1**), but still considerably higher than r.t. Another disadvantage of this pathway is the high toxicity of H_2S gas, which poses a serious safety hazard. Moreover, the concomitant formation of $Li_xS_yO_z$ species requires subsequent washing of the crude product, which is very cumbersome.

Scheme 1: Reaction schemes (1) – (3) corresponding to the synthesis processes of Li_2S detailed in the text.

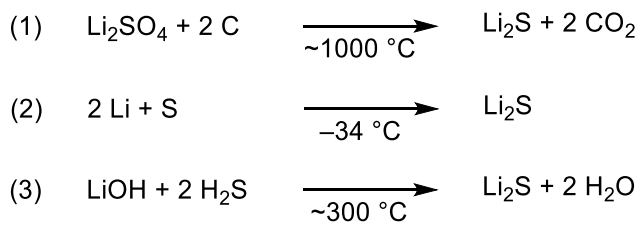

Hence, in this paper, we showed an alternative strategy for the synthesis of Li_2S with the aim to develop a process that links the manufacture of Li_2S with the subsequent formation of sulfide-based SEs (**Figure 23**), which might become the major secondary product of Li_2S upon the potential commercialization of sulfide-based Li-ion ASSBs. Li, S, and naphthalene (NAP) are mixed in THF as solvent. NAP functions as electron transfer agent. It is reduced by elementary lithium to form the corresponding radical anion. Subsequently, the spare electron is transferred to the respective sulfur species, reducing it down to S^{2-}. In order to reach a reasonable reaction time, the reaction mixture is heated to 90 °C. Using 50 mol% NAP (with reference to the amount of Li) the reaction time can be pushed below 8 h. Following the first step, according to **Figure 23**, two slightly different approaches are conceivable.

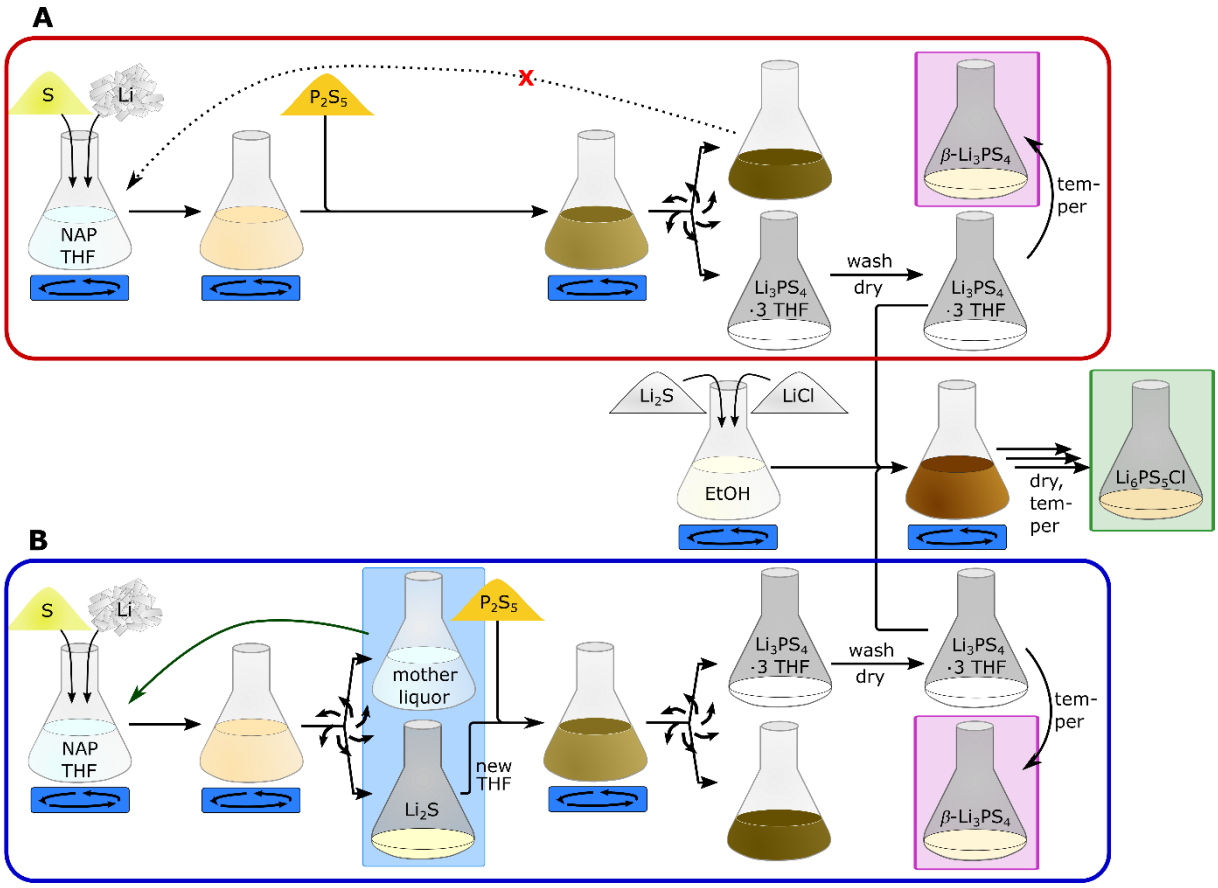

Figure 23: Schematic illustration of the two different preparation procedures of $Li_3PS_4 \cdot 3THF$ starting out from elementary lithium and sulfur, with the possibility to proceed by either synthesizing β-LPS (purple boxes), or Li_6PS_5Cl (as example for the argyrodite-type Li_6PS_5X series; X = Cl, Br, I) in an ethanolic solution with Li_2S and LiCl (green box). Approach **A**: After the synthesis of Li_2S, P_2S_5 is added to the same flask without any intermediate work-up step. Approach **B**: After the synthesis of Li_2S, the reaction mixture is centrifuged (or filtered). The supernatant can be reused in a further Li_2S synthesis batch, while the Li_2S precipitate is reacted with P_2S_5 in fresh THF.

Firstly, one can use the resulting mixture of Li_2S in THF plus the remaining NAP and directly add P_2S_5 in order to synthesize $Li_3PS_4 \cdot 3THF$. Secondly, and slightly more sophisticatedly, one can separate the solid fraction from the solution of NAP in THF. The solution, on the one hand,

can be reutilized in another batch synthesis of Li_2S. The solid fraction, on the other hand, is mixed with fresh THF, after which P_2S_5 is added in order to synthesize $Li_3PS_4 \cdot 3THF$.

At first sight, the energy-intensive reduction of elementary lithium might not appear as a sensible and competitive alternative to the strategies discussed in **Scheme 1**. However, all processes in **Scheme 1** suffer from tremendous disadvantages themselves, as they either resort to cheap starting materials, but harsh and nonselective synthesis conditions (**(1)** and **(3)**), or they draw on mild reaction conditions, yet utilizing very hazardous starting materials (**(2)**). Furthermore, none of the approaches mentioned is designed specifically for the subsequent fabrication of SEs.

Drawing on comparably low purity (99%) elementary starting materials – which does not lead to lower conductivities compared with syntheses from purer starting materials – the calculated prices seem very competitive (**Table 1**).

Table 1: Prices of relevant chemicals in order to roughly estimate the costs for the synthesis of Li_2S via the suggested approach (prices from https://www.sigmaaldrich.com, retrieved on June, 2nd 2020, 16:15 pm).

Compound	**Purity / %**	**Quantity / g**	**Price / €**	**Price / €/kg**
Li_2S	99.98	50	652	13040
Li	99	100	195	1950
S	99	1000	127	127
P_2S_5	99	100	27	265
Naphthalene	99	5000	125	25
THF (anhydrous)	99.9	1 l	157	157 €/l
"Li_2S" (2 $Li_{99\%}$ + $S_{99\%}$) + $THF_{anh.}$	~99	N.A.	N.A.	1885

According to **Table 1** – deliberately not considering the process costs, as they are almost impossible to estimate – the specific raw material costs for the synthesis of Li_2S based on the approach revealed in this paper amount to 1885 €/kg being more than 5 times lower than the specific costs for commercial Li_2S. Minding the additional synergies that might arise from the reutilization of the solvent, a further rise in profitability seems likely. Subsequently, independent of the synthesis pathway chosen (**A** or **B**), phase-pure $Li_3PS_4 \cdot 3THF$ is obtained, which can be converted to β-LPS or Li_6PS_5Cl.

Samples of β-LPS obtained from previous Li_2S syntheses with different amounts of NAP showed virtually no difference in their impedance behavior. Furthermore, the material allowed for the construction of ASSBs with indium as anode and $LiCoO_2$ (coated with 1 wt% of $LiNbO_3$)

as cathode materials, which exhibited no disadvantage towards cells utilizing conventionally-synthesized β-LPS from commercial Li_2S and P_2S_5 in THF (**Figure 24**).

Samples of highly topical Li_6PS_5Cl – hitherto being the most promising SE candidate material for an eventual commercialization of ASSBs – could also be synthesized. Those samples contained considerable amounts of impurity phases like Li_2S, LiCl and Li_3PO_4 (**Figure 25A**) which had a rather small but non-negligible effect on their conductivity (**Figure 25B** and **C)**. However, their concentration and obstructive effects were well in line with those observed in earlier studies on solvent-based syntheses of argyrodite materials of the general formula Li_6PS_5X (X = Cl, Br).[193,194]

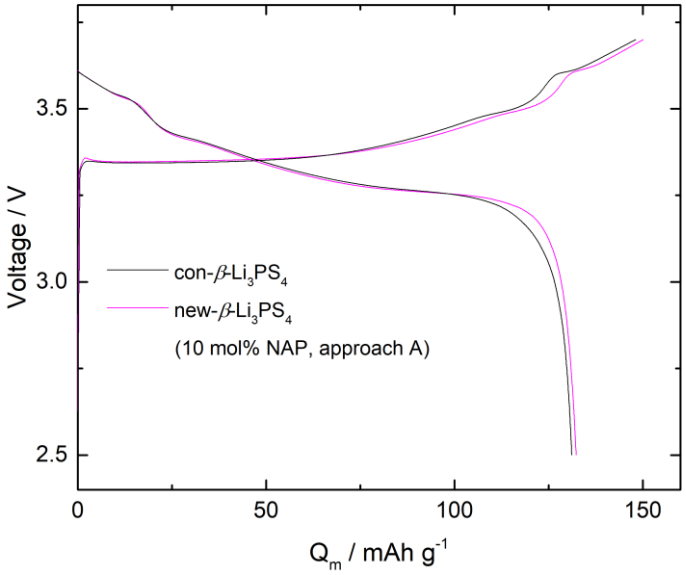

Figure 24: Comparison of voltage profiles (voltage E vs. specific capacity Q_m) of first charge and discharge cycle of ASSBs utilizing new-β-LPS synthesized according to approach A with 10 mol%(Li) of NAP (magenta curve), in comparison with con-β-LPS (black curve).

Even though the reduction of Li^+ to elementary lithium is naturally very energy-intensive, the proposed approach poses an interesting alternative to the commercial fabrication method (**Scheme 1 (1)**) that is very energy-intensive itself and additionally produces large amounts of CO_2. Combined with the subsequent synthesis of versatile $Li_3PS_4 \cdot 3THF$ it represents the first realization of a concept that combines the synthesis of Li_2S with its most important secondary product class: SEs. This linkage might act as a crucial factor for cutting down the costs of SE synthesis down to a competitive level.

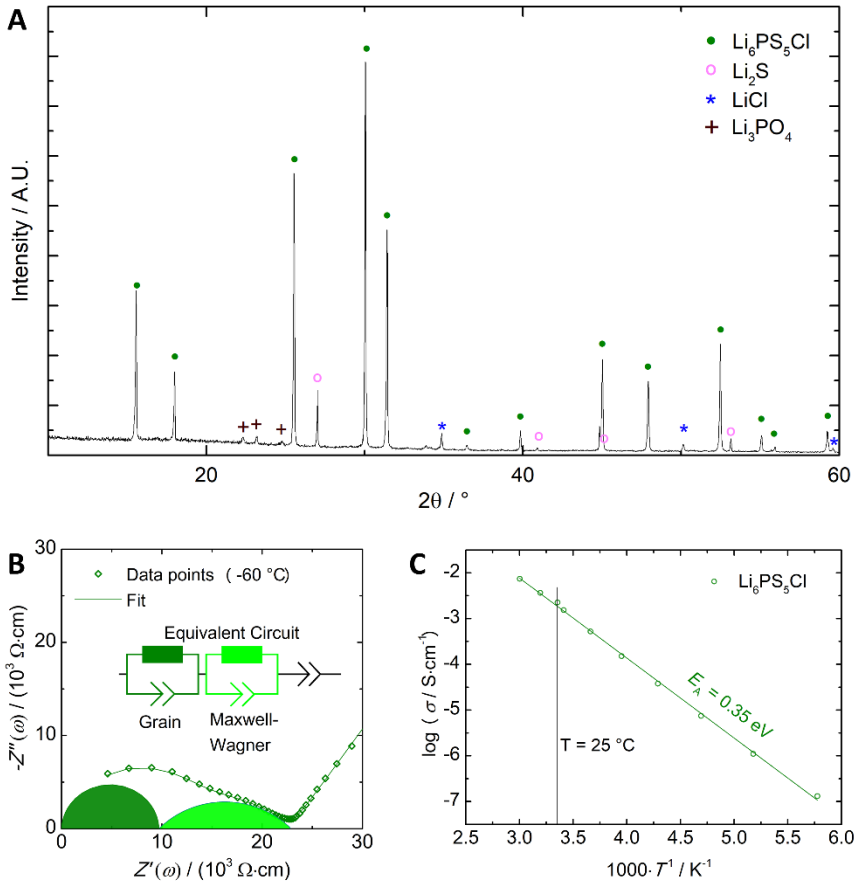

Figure 25: A: PXRD diagram of Li_6PS_5Cl after sintering at 550 °C for 5 h. The diagram indicates the presence of small amounts of the reactants, as well as traces of Li_3PO_4, which is similar to the observation made by *Zhou et al.*[194] Green filled circles: target compound Li_6PS_5Cl, blue asterisks: LiCl, lilac hollow circles: Li_2S, brown plus signs: Li_3PO_4. B: Nyquist plot of Li_6PS_5Cl from measured at –60 °C (olive data points). Fit to the data: olive line. The spectrum exhibits two R-CPE contributions, which are attributed to the grain, and a Maxwell-Wagner effect, respectively, the latter of which is caused by the impurity phases of Li_2S, LiCl and Li_3PO_4. C: Arrhenius-plot of the total conductivity of Li_6PS_5Cl. Olive line: linear fit of the data. As both semicircles in **Fig. 4B** are not clearly separated, **Fig. 4C** only shows the total conductivity.

Own Share of work

I conceived the experiments and discussed their outcome with *Stefanie Dehnen* and *Bernhard Roling*. I carried out the vast majority of experiments. *Mirko Diels* investigated the influence of the amount of naphthalene on the reaction rate of the formation of Li_2S. Furthermore, I supervised him conducting impedance measurements on *β*-LPS samples. I mainly wrote the manuscript in close consultation with *Stefanie Dehnen*. All authors gave their consent to the final version of the manuscript.

3.4 Kinetic Limitations in Sheet-Type All-Solid-State Battery Cathodes

[IV]

Moritz Kroll,[+] **Marc Duchardt**,[+] Sarah L. Karstens, Sabine Schlabach, Fabio Lange, Janika Hochstrasser, Bernhard Roling and Ulrich Tallarek

Submitted to *Advanced Energy Materials*

[+] These authors contributed equally to this work.

Despite the favorable plastic properties of sulfide-based solid electrolytes (S-based SEs), their mixing with CAM inside the cathode composite usually leads to a large fraction of imbedded void space. These voids reduce the contact area between SE and CAM and increase the tortuosity of the Li^+ transport within the SE component of the cathode composite. Therefore, void space tends to increase both the charge transfer resistivity as well as the transport resistivity of Li ions inside the cathode composite.

However, not much is known about how different S-based SEs influence the morphology of cathode composites and thus the batteries' performance. Therefore, in this paper, two model cathodes are introduced, each based on NMC-85|05|10 as CAM with a small average particle size of 3.5 µm. The first contains β-LPS as SE (σ = 0.2 mS/cm) and the second Li_3PS_4·LiI (LPSI, σ = 0.8 mS/cm) which is synthesized by means of ball-milling.[117] Whereas β-LPS has a peculiar microporous morphology as has been described in the previous section **3.3** (cf. **Figure 26a**, **c**), the latter shows the typical morphology of a conventionally synthesized S-based SE, being composed of rather large junks (**Figure 26b**, **d**). Both model cathodes were manufactured incorporating polyisobutene as binder, according to the sheet-type (ST) strategy introduced in section **2.2.2.4**, in order to create an application-oriented perspective. Afterwards, they were galvanostatically cycled and physically reconstructed using focused ion beam secondary electron microscopy (FIB-SEM) tomography. As can be seen from the complete reconstructions of both samples in **Figure 27**, three phases (CAM, SE, and voids) could be well segmented. The binder, however, could not be resolved, because it does not possess a distinct morphology but rather builds a thin cover over available interfaces. Whereas the cathode based on β-LPS seems to show virtually no void space at all (**Figure 27a**), the LPSI-based one (**Figure 27b**) exhibits almost 10% void space (**Table 2**).

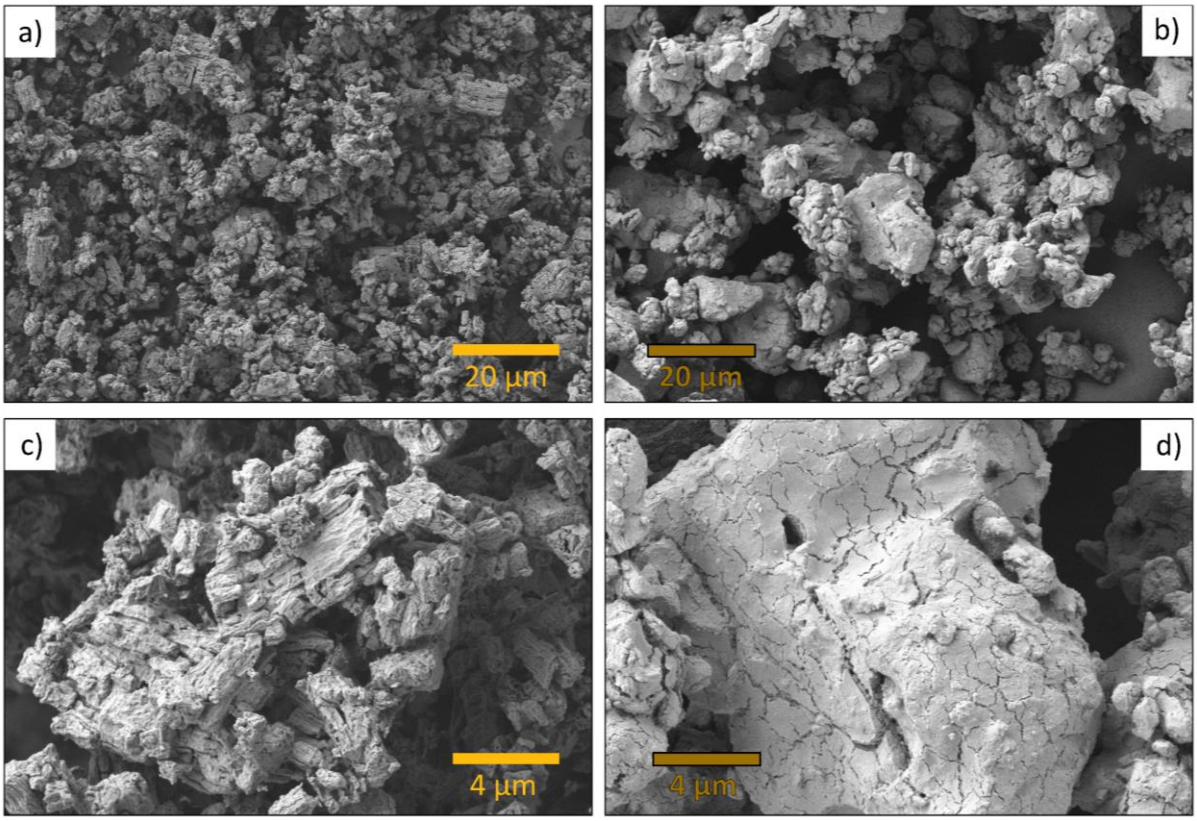

Figure 26: Morphology of as-prepared solid electrolyte powders. Left: *β*-LPS particles, right: LPSI particles.

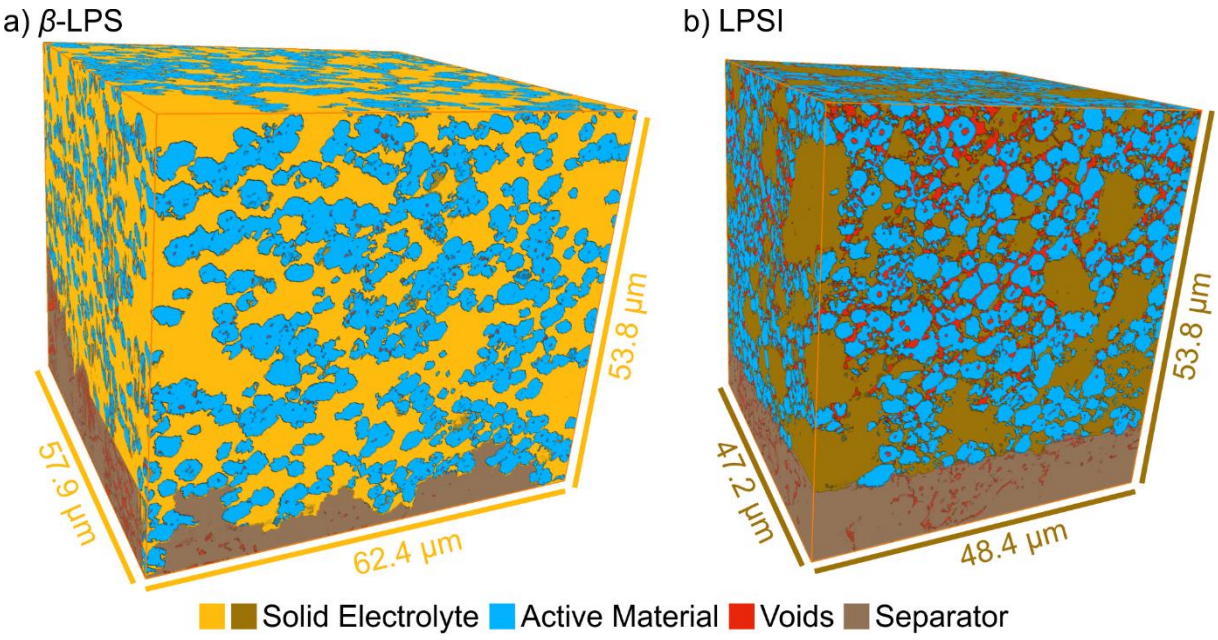

Figure 27: Overview of the two reconstructed NCM cathodes with **A**: *β*-LPS and **B**: LPSI as solid electrolyte.

However, the *β*-LPS particles are rather pervaded by a vast network of mesopores, which, unfortunately, cannot be resolved at the selected resolution of 40 nm, and hence exhibit a very

high surface area.[95] The binder is therefore likely to collect predominantly within the secondary β-LPS particles. Consequently, binder and β-LPS are perceived as a single phase, which leads to a drastic overestimation of the SE volume fraction in the reconstruction (**Table 2**). This reasoning is corroborated by the reduced mechanical stability and elasticity of the cathode film based on β-LPS. The large fraction of polymer collecting inside the mesopores does not foster the mechanical cohesion of the film, and thus does not fulfill its purpose in the first place. In the case of dense LPSI, on the other hand, the binder is presumably rather distributed equally over all interfaces between SE and CAM, enabling damage-free bending of the film.

Table 2: Comparison of the volume fractions between synthesis and reconstruction.

	β-LPS		LPSI	
	Synthesis	Reconstruction	Synthesis	Reconstruction
Active material	46.3%	44.0%	49.3%	50.8%
Solid electrolyte	46.3%	55.0%	42.7%	38.5%
Binder	7.3%	−	8.0%	−
Voids	−	1.0%	−	10.7%

The investigation of the CAM particle network showed that, in both batteries, only an insignificant fraction of particles is not connected to a single network. A loss of capacity due to the sheer isolation of CAM particles can thus be ruled out. The considerable pore space inside the LPSI-based cathode, however, significantly increases the tortuosity of the Li-ion paths within the SE phase. **Figure 28** shows values for the effective diffusion coefficient D_{eff}, which – normalized by the bulk diffusion coefficient D_{bulk} of the respective SE – corresponds to tortuosity values $\tau_{\mathrm{Li^+}}$ of 1.79 for β-LPS and 3.70 for LPSI, respectively hence differing by a factor of 2. Due to the impossible differentiation between binder and SE, especially in the case of the β-LPS-based cell, the real tortuosity is underestimated by these values. Nevertheless, it could be shown that the overestimation of the volume fraction of the SE phase in the β-LPS cell causes a downward shift of the tortuosity value by only ~0.1. Therefore, the distinct difference in tortuosity between both cathodes is predominantly caused by the less favorable morphology of the LPSI particles and thus the entire cathode.

Figure 29 depicts galvanostatic cycling curves of the two model ST cathodes at a C-rate of 0.1 C, corresponding to a theoretical capacity of the CAM of 210 mAh/g. In order to facilitate comparability, both batteries made use of two sheets of a LPSI-based separator film. It can be seen that both model ST cells (solid lines) show a lower capacity compared to the reference pellet-type (PT) cells (dashed lines), respectively, which do not incorporate any polymer. A possible explanation could be the passivation of a certain fraction of CAM particles by the

polymer. However, the differences in overvoltage between ST and PT cells, respectively, is much more pronounced. For the *β*-LPS-based cells, the overvoltage is virtually the same: 80 mV. As for the LPSI-based cells, on the other hand, a drop of overvoltage from 55 mV to 40 mV is observed when going from the ST-type cell to the PT-type cell. Obviously, for the *β*-LPS-based cells, the bottleneck is the lower ionic conductivity of the SE, whereas in the case of LPSI as SE in the cathode, the ionic conductivity is high enough so that the charge transfer at the interface becomes the decisive factor. It should also be noted that a large fraction of polymer in the ST cell based on *β*-LPS collects inside the vast pore network, which in turn has a lower impact on the charge transfer reaction.

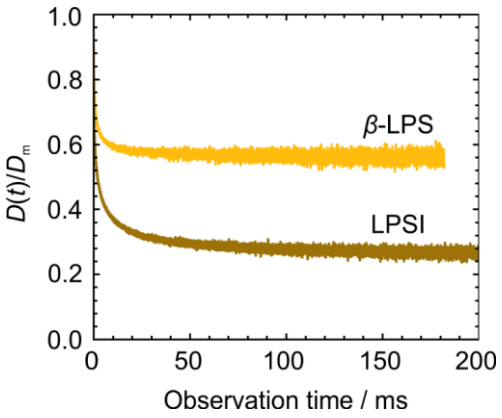

Figure 28: Evolution of transient diffusion coefficients $D(t)$ in the reconstructed SEs normalized by the bulk diffusivity D_m. Asymptotic (effective) values are reached at D_{eff}/D_m = 0.56 and 0.27 for *β*-LPS and LPSI, respectively.

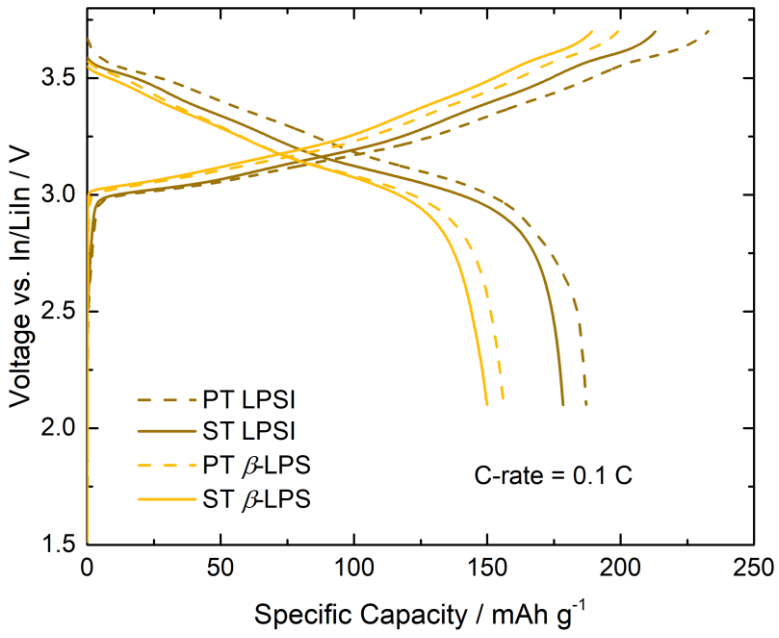

Figure 29: Initial voltage profiles of PT cells (dashed lines) and ST cells (solid lines) using either *β*-LPS or LPSI as SE inside the cathode composite at a C-rate of 0.1 C.

The better performance of the LPSI-based cell, despite their unfavorable morphology, shows that the fourfold higher conductivity overcompensates the higher tortuosity lower and better contact area between SE and CAM – even at a moderate C-rate of 0.1 C. This shows that the ionic transport within the SE phase inside the composite cathode is indeed the limitation of a better battery performance. Only if well-conducting SEs like LPSI are utilized, morphological optimizations can unfold their full potential.

Own Share of work

I came up with the initial idea for the project. *Moritz Kroll* and I designed and planned the experiments. I carried out the synthetic and analytical laboratory work and the battery testing. Furthermore, I supervised *Fabio Lange* during his work for his Bachelor thesis, which contributed to the advancement of the project. In collaboration with *Sabine Schlabach*, *Moritz Kroll* acquired the raw FIB-SEM data. In collaboration with *Sarah Karstens*, *Moritz Kroll* performed the reconstructions and the subsequent morphological investigations. *Janika Hochstrasser* carried out the transport simulations. All results were discussed with *Bernhard Roling* and *Ulrich Tallarek*. *Moritz Kroll* and I both wrote the manuscript in close consultation with *Bernhard Roling* and *Ulrich Tallarek*. All authors gave their consent to its final version. *Moritz Kroll* and *Ulrich Tallarek* took care of the submission process and the correspondence with the journal.

4 Summary

Research during my PhD studies was shared between Na-ion and Li-ion solid-state ionics and all-solid-state Li-ion batteries (ASS-LIBs). Both Na-ion and Li-ion solid-state ionics show promise as underlying chemistries of energy storage technologies, which might play a significant role in future efforts to store energy more efficiently and safely, however, with slightly different scopes. ASS-LIBs will very likely be the key to introduce renewable energies to the mass-market of lightweight electric vehicles. ASS-SIBs, being currently at a considerably earlier stage of development, might eventually contribute to cheap grid-scale energy storage causing lower costs compared to ASS-LIBs.

In the first two publications included in this cumulative thesis (sections **3.1** and **3.2**), I investigated two new Na-ion solid electrolytes (SEs): $Na_{11}Sn_2PS_{12}$ (NaSnPS) and $Na_{11.1}Sn_{2.1}P_{0.9}Se_{12}$ (NaSnPSe). In the first paper (section **3.1**), NaSnPS was reported, which exhibited an unexpected stoichiometry of $Na_{11}Sn_2PS_{12}$. This finding contradicted the previously reported theoretical works, according to which a quaternary compound NaSnPS would possess a stoichiometry of '$Na_{10}SnP_2S_{12}$', corresponding to the quaternary Li counterparts, *e.g.*, $Li_{10}SnP_2S_{12}$ or $Li_{10}GeP_2S_{12}$.[94,118,178] In addition, a hitherto unprecedented crystal structure was found, considerably deviating from the one of $Li_{10}SnP_2S_{12}$. Even though both structures constitute the same basic building blocks of alkali ions and unconnected $[SnS_4]^{4-}$ and $[PS_4]^{3-}$ tetrahedra, they are very different, with the one of NaSnPS being larger (8 formula units per unit cell instead of only 2) and more complex. Strikingly, the elemental ratio between Sn and P is also inverse, being 2:1 for NaSnPS and 1:2 for the Li analogues. Its grain conductivity amounts to a value of 3.7 mS/cm, making it, at the time, the fastest sulfide-based Na-ion conductor. Interestingly, similar results on NaSnPS were published simultaneously by the group of *Linda Nazar*.[181] Sometime later, even a third article appeared on the subject.[182]

The focus of the second paper (section **3.2**) lies on the discovery of NaSnPSe, hence the heavier analogue of NaSnPS. Whereas in the initial study, due to failed attempts at growing single crystals, the crystal structure of NaSnPS had to be solved from powder X-ray data, in the

subsequent study, single crystals from both NaSnPS and NaSnPSe were obtained. This enabled a much closer look at the occupancies of the six different crystallographic Na positions that make up the cationic lattice and thus the underlying conduction mechanism. The previously developed idea that all Na positions take part in long-range ionic motion was corroborated, and two interstitial positions (i1 and i2) were identified as playing a crucial role in creating the necessary 3D pathways. NaSnPSe is the first example of a quaternary selenium-based alkali ion conductor. Similar substitution of Se for S in the Li analogues proved impossible apart from negligible partial substitutions.[184] In contrast to the widespread belief that a softer anionic lattice necessarily leads to a higher ionic conductivity at r.t., NaSnPSe in fact exhibits a lower grain conductivity at r.t. than NaSnPS with only 3 mS/cm. This underlines not only that the activation energy of ionic motion has to be taken into account, which is indeed lower for NaSnPSe, but also the attempt frequency, which is generally lower if the lattice is softer. Interestingly, it was found that $Na_{11.1}Sn_{2.1}P_{0.9}Se_{12}$ repeatedly showed a composition slightly off from the expected stoichiometry analogous to that of NaSnPS, which indicates the tendency of forming solid solutions.

The initial outline of my PhD involved the construction of ASS-SIBs based on the self-discovered SEs, such as NaSnPS. However, it later became apparent that appropriate cathode active materials for the efficient construction of ASS-SIBs are still missing. Preliminary experiments conducted by Marvin Cronau in his Master thesis with $Na_2Ti_3O_7$[195] as anode material and $Na_2Fe_2(SO_4)_2$[196] as cathode material were extremely disappointing. Both materials significantly underperformed regarding their capacity and cycling retention compared to the reported properties described in the literature.[195,197–199] Through many iterations and preliminary cycling tests in LE cells, the materials' performance could only slightly be improved.[200] Early studies of ASS-LIBs between 1990 and 2010 could already resort to commercial $LiCoO_2$, which works well in ASS-LIBs. In the case of ASS-SIBs, however, where no commercial batteries exist, yet, selection of functioning electrode materials is much more difficult. Indeed, reports on ASS-SIB full cells are extremely limited.[197] Currently, the bottleneck for research on ASS-SIBs is thus the lack of suitable electrode materials rather than Na-ion SEs.

In the field of Li-ion SEs, research is noticeably evolving from the sheer discovery of new materials to sophisticated ways of producing them, finally enabling their cost-competitive large-scale manufacturing. In the third report (section **3.3**), an innovative synthesis strategy for the preparation of sulfide-based SEs was presented. $Li_3PS_4 \cdot 3THF$ is a readily available intermediate product that can be transformed into β-LPS or Li_6PS_5Cl.[95,194] It is generally obtained by the wet-chemical synthesis of stoichiometric amounts of Li_2S and P_2S_5 in anhydrous THF.

However, while P_2S_5 is very cheap, Li_2S, the feedstock chemical for all syntheses of sulfide-based Li-ion SEs, is extremely expensive, because the common synthesis from Li_2SO_4 as precursor involves very high temperatures above 1000 °C. Therefore, in this work, a strategy was conceived, which allows for the *in-situ* generation of Li_2S from the elements. To this end, lithium and sulfur are loaded into a flask together with THF as solvent and naphthalene (NAP) as electron transfer agent. The radical anion (NAP^-) then reduces the sulfur to S^{2-}, finally resulting in Li_2S. If high loadings of NAP are used, the reaction proceeds quickly. This preceding step is synergistically coupled to the subsequent formation of $Li_3PS_4 \cdot 3THF$ upon the addition of P_2S_5, giving rise to a one-pot synthesis or *flow-oriented synthesis of $Li_3PS_4 \cdot 3THF$*. Even though elementary Li has to be used, which is, of course, a considerable energy toll, rough calculations show the approach to be promising from a cost perspective. *β*-LPS or Li_6PS_5Cl generated from $Li_3PS_4 \cdot 3THF$ show their typical characteristics without any deterioration due to residual traces of NAP, which proves the practical applicability of the suggested strategy.

In addition to the identification of promising SEs (especially regarding their ionic conductivity, electrochemical stability and plastic properties) and their efficient synthesis, a similarly important goal is the optimal adjustment of the SE's morphology. In the fourth publication (section **3.4**), morphological aspects of ASS-LIBs were therefore investigated and correlated with their electrochemical performance. Two model cells were constructed that were based on the so-called sheet-type ASSB concept and incorporated state-of-the-art NMC-85|05|10 as CAM and either *β*-LPS or LPSI as SE. It could be demonstrated that *β*-LPS with its peculiar, microporous morphology enables a much more favorable cathode morphology than LPSI. The latter with its larger particles leads to a lower contact area between CAM and SE, more void space and thus more serious constrictions. Numerical transport simulations indicated a roughly doubled tortuosity for the cathode based on LPSI as SE component. The four times higher intrinsic ionic conductivity of LPSI, though, overcompensates this effect and enables an overall superior battery performance. This shows that the charge transfer plays only a minor role. The actual bottleneck for a better battery performance is the ionic transport within the SE phase inside the composite cathode. Even though the ionic conductivity is the most crucial prerequisite for an SE, careful attention should be paid to the morphology of the SE and thus the morphology of the resulting cathode, in order to fully benefit from the high ionic conductivities of state-of-the-art SEs.

Zusammenfassung

Die wissenschaftlichen Unternehmungen meiner Promotion lassen sich den Gebieten der Na-Ionen- und Li-Ionen-Festkörperionik sowie den Li-Ionen-Festkörperbatterien zuordnen. Sowohl Na-Ionen- als auch Li-Ionen-Festkörperionik besitzen das Potenzial, eine bedeutende Rolle bei der Entwicklung zukünftiger, kommerzieller Energiespeichertechnologien zu spielen. Die hohen angestrebten Energiedichten von Li-Ionen-Festkörperbatterien versprechen den breit angelegten Einzug von Batterien in den PKW-Markt, wohingegen Na-Ionen-Festkörperbatterien vor allem für die günstige, stationäre Speicherung von Netzstrom zum Ausgleich von Lastunterschieden von Interesse sind.

In den ersten beiden Publikationen des kumulativen Teils (Abschnitte **3.1** and **3.2)** habe ich zwei neue Na-Ionen Festelektrolyte untersucht: $Na_{11}Sn_2PS_{12}$ (NaSnPS) und $Na_{11.1}Sn_{2.1}P_{0.9}Se_{12}$ (NaSnPSe). Im ersten Artikel (Abschnitt **3.1**) wurde die Entdeckung der Verbindung NaSnPS berichtet, welche eine unerwartete Stöchiometrie aufwies: „$Na_{11}Sn_2PS_{12}$“. Diese Erkenntnis widersprach vorhergehenden, theoretischen Berichten, denen zufolge eine quaternäre Verbindung NaSnPS eine Stöchiometrie gemäß „$Na_{10}SnP_2S_{12}$“ besitzen sollte, entsprechend den verwandten quaternären Li-Verbindungen, wie z.B. $Li_{10}SnP_2S_{12}$ oder $Li_{10}GeP_2S_{12}$.[94,118,178] Darüber hinaus wurde eine bislang unbekannte Kristallstruktur entdeckt, die sich erheblich von der von $Li_{10}SnP_2S_{12}$ oder $Li_{10}GeP_2S_{12}$ unterscheidet. Obwohl beide Strukturen aus den gleichen grundlegenden Bausteinen bestehen (Alkali-Ionen und unverknüpfte $[SnS_4]^{4-}$- und $[PS_4]^{3-}$-Tetraeder), unterscheiden sie sich stark. Die Struktur von NaSnPS verfügt dabei über eine signifikant größere Elementarzelle (8 Formeleinheiten pro Elementarzelle statt lediglich 2) und ist deutlich komplexer. Markant ist, dass das Elementverhältnis zwischen Sn und P 2:1 beträgt und damit genau invers zu dem der Li-Analoga mit 1:2 ist. Die Kornleitfähigkeit von NaSnPS beträgt 3.7 mS/cm, was das Material zum Zeitpunkt der Entdeckung zum besten Sulfid-basierten Na-Ionen-Leiter machte. Interessanterweise wurden ähnliche Ergebnisse zeitgleich auch von der Forschungsgruppe um Linda Nazar publiziert.[181] Einige Zeit später erschien sogar ein dritter Artikel zum gleichen Thema.[182]

Der Fokus des zweiten Artikels (**3.2**) liegt auf der Entdeckung von NaSnPSe, welches das schwerere Analogon von NaSnPS darstellt. Während das Kristallstrukturmodell von NaSnPS in der vorangegangenen Studie noch basierend auf Röntgenpulverdaten gelöst werden musste, da die Zucht von ausreichend großen Einkristall nicht gelang, so konnten in dieser Studie nun geeignete Einkristalle erhalten werden. Dies ermöglichte einen deutlich detaillierteren Blick auf den Grad der Besetzung der sechs verschiedenen Na-Positionen innerhalb des Kristallgitters und somit auch auf den Leitmechanismus. Die zuvor entwickelte Idee, dass alle Na-Positionen am langreichweitigen Transport beteiligt sind, bestätigte sich. Des Weiteren wurden zwei Zwischengitterplätze (i1 und i2) identifiziert, die offensichtlich eine wichtige Rolle beim Aufspannen der nötigen 3D-Leitpfade spielen. NaSnPSe ist das erste Beispiel eines Selen-basierten quaternären Alkali-Ionenleiters. Ähnliche Substitutionen von S durch Se in den Lithium-Analoga stellten sich als unmöglich heraus – abgesehen von vernachlässigbar geringen Mengen.[184] Im Gegensatz zum weit verbreiteten Glauben, dass ein weicheres Anionen-Teilgitter notwendigerweise auch zu einer höheren ionischen Leitfähigkeit bei Raumtemperatur führt, weist NaSnPSe mit 3.0 mS/cm tatsächlich eine niedrigere ionische Leitfähigkeit auf als NaSnPS. Dies unterstreicht, dass nicht nur die Aktivierungsenergie der Ionenbewegung – welche erwartungsgemäß niedriger liegt bei NaSnPSe – berücksichtigt werden muss, sondern auch die Sprungfrequenz, die bei weichen Anionengittern generell geringer ausfällt. Interessanterweise wies NaSnPSe wiederholt eine Zusammensetzung auf ($Na_{11.1}Sn_{2.1}P_{0.9}Se_{12}$), die geringfügig von der Stöchiometrie $Na_{11}Sn_2PCh_{12}$ (Ch = S, Se) abwich. Es kann daher angenommen werden, dass ein gewisser Spielraum für eine Mischungsreihe mit variierendem Sn:P-Verhältnis besteht.

Der ursprüngliche Zeitplan meiner Promotion beinhaltete die anschließende Konstruktion von Festkörper-Na-Ionen-Batterien, basierend auf den selbstentdeckten Na-Ionen-Festelektrolyten, wie z.B. NaSnPS. Allerdings stellte sich erst im Rahmen der Promotion heraus, dass für Sulfid-basierte Na-Ionen-Festkörperbatterien geeignete Aktivmaterialien, insbesondere Kathodenmaterialien, noch weitestgehend unbekannt sind. Vorläufige Experimente, die von Marvin Cronau im Rahmen seiner Masterarbeit mit $Na_2Ti_3O_7$[195] als Anodenmaterial und $Na_2Fe_2(SO_4)_2$[196] als Kathodenmaterial durchgeführt wurden, verliefen äußerst enttäuschend. Beide Materialien wiesen, verglichen mit den in der Literatur berichteten Eigenschaften, signifikant niedrigere Kapazitäten sowie Zyklenstabilitäten auf.[195,197–199] Auch nach mehreren Synthese- und Zyklisierungsversuchen in Flüssigzellen konnte die Performanz des Systems lediglich geringfügig verbessert werden.[200] Frühe Studien zu Li-Ionen-Festkörperbatterien zwischen 1990 und 2010 konnten hingegen bereits auf kommerzielles

$LiCoO_2$ zurückgreifen, welches gut in eben solchen funktioniert. Im Falle von Na-Ionen-Festkörperbatterien ist die Auswahl geeigneter Elektrodenmaterialien jedoch deutlich schwieriger, was sich auch in der äußerst geringen Anzahl verfügbarer Literaturberichte zum Thema niederschlägt.[197] Der Flaschenhals bei der Erforschung von Na-Ionen-Festkörperbatterien ist derzeit daher vielmehr der Mangel an kompatiblen Elektrodenmaterialien als der an geeigneten Na-Ionen-Festelektrolyten.

Im Bereich der Li-Ionen-Festelektrolyte entwickelt sich die Forschung momentan spürbar fort von der bloßen Entdeckung neuer Materialien, hin zu raffinierten neuen Synthesewegen, was einen wichtigen Schritt auf dem Weg zur Kommerzialisierung darstellt. Im dritten Artikel (Abschnitt **3.3**) wird eine innovative Strategie zur Synthese von Sulfid-basierten Li-Ionen-Festelektrolyten vorgestellt. $Li_3PS_4 \cdot 3THF$ ist ein leicht zugängliches Zwischenprodukt, das sowohl zu β-LPS als auch Li_6PS_5Cl umgesetzt werden kann.[95,194] Es wird im Allgemeinen aus der nasschemischen Reaktion von Li_2S und P_2S_5 in wasserfreiem THF erhalten. Während jedoch P_2S_5 sehr günstig ist, so ist Li_2S – die wichtigste Chemikalie zur Synthese aller Sulfid-basierten Li-Ionen-Festelektrolyte – äußerst teuer. Der Grund dafür sind die harschen Reaktionsbedingungen, unter denen Li_2S aus Li_2SO_4 als Ausgangsstoff hergestellt wird; die benötigten Temperaturen liegen bei über 1000 °C. Daher wurde ein Synthesepfad entworfen, der die Herstellung von Li_2S aus den Elementen bei Temperaturen < 100 °C ermöglicht. Dazu werden Lithium und Schwefel zusammen mit THF und Naphthalin (NAP) als Elektronentransferreagenz in einen Kolben gegeben. Das Radikalanion von NAP (NAP^-) reduziert dabei den Schwefel bis zum Sulfid-Ion (S^{2-}). Wenn hohe Konzentrationen von NAP verwendet werden, lassen sich sehr schnelle Umsetzungen erreichen. Indem im Anschluss direkt P_2S_5 hinzugegeben wird, wird der erste Schritt der Li_2S-Herstellung synergetisch an die Herstellung von $Li_3PS_4 \cdot 3THF$ gekoppelt, die Reaktion kann folglich als eine Eintopf-Reaktion aufgefasst werden. Obschon elementares Lithium verwendet wird, was energetisch zunächst unvorteilhaft erscheint, zeigen Überschlagsrechnungen, dass die Herangehensweise attraktiv erscheint aus einer Kostenperspektive. Sowohl β-LPS als auch Li_6PS_5Cl, die ausgehend von $Li_3PS_4 \cdot 3THF$ im Folgenden synthetisiert werden, zeigen ihre typischen Eigenschaften ohne jegliche Einschränkung, beispielsweise durch Spuren von im Endprodukt verbliebenem NAP. Dies zeigt die praktische Durchführbarkeit dieses Ansatzes.

Neben der initialen Identifizierung geeigneter Festelektrolyte (insbesondere bezüglich ihrer ionischen Leitfähigkeit, elektrochemischen Stabilität und ihrer plastischen Eigenschaften) und ihrer effizienten Synthese ist vor allem auch ihre Morphologie wichtig für den effektiven Einsatz in Festkörperbatterien. Im vierten Artikel (**3.4**) wurden daher morphologische Aspekte

von Li-Ionen-Festkörperbatterien untersucht und mit jeweiligen elektrochemischen Daten korreliert. Es wurden zwei filmbasierte Modell-Zellen konstruiert, die beide auf NMC-85|10|05 als Kathodenmaterial und entweder β-LPS oder LPSI als Festelektrolytkomponente in der Kathode basierten. Es konnte gezeigt werden, dass β-LPS mit seiner besonderen, mesoporösen Morphologie eine deutlich vorteilhaftere Kathodenmorphologie bewirkt als LPSI. LPSI führt mit seinen größeren Partikeln zu einer deutlich niedrigeren Kontaktfläche zwischen Kathodenmaterial und Festelektrolyt, mehr Porenraum, und daraus folgend gravierenderen Einschnürungen. Numerische Transportsimulationen deuteten daher eine in etwa zweifach höhere Tortuosität für die LPSI-basierte Kathode an. Die vierfach höhere, ionische Leitfähigkeit von LPSI überkompensiert diesen Effekt jedoch und ermöglicht eine insgesamt überlegene Batterieleistung. Dies zeigt, dass der Ladungstransfer lediglich eine untergeordnete Rolle spielt. Der eigentliche Flaschenhals für eine überlegene Batterieleistung ist der Ionentransport innerhalb der Festelektrolytphase im Inneren der Kompositkathode. Obwohl die ionische Leitfähigkeit die wichtigste und grundlegendste Eigenschaft eines Festelektrolyten ist, sollte der Morphologie des Festelektrolyten und folglich der Morphologie der resultierenden Kathode dennoch größte Aufmerksamkeit geschenkt werden. Nur so kann die hohe ionische Leitfähigkeit eines modernen Festelektrolyten optimal in eine überlegene Batterieleistung umgemünzt werden.

5 Outlook

Both iso- and aliovalent doping/substitution are widespread strategies for the enhancement of the conductivities of solid ionic conductors.[201–203] Inspired by the Li analogues practically exhibiting a full solid solution of $Li_{10}TtP_2S_{12}$ (Tt = Si, Ge, Sn) attempting to vary the tetrel for $Na_{11}Sn_2PS_{12}$ (Tt = Si, Ge, Sn) seems obvious. Unpublished experimental work carried out in the course of my PhD work, though, showed only little possibility to substitute the tetrel. The more Si or Ge is substituted for Sn, the more impurity phases evolve and the lower are the conductivities of the resulting phases, which is in line with theoretical investigations.[204] While substitution of the tetrel seems pointless, a full solid solution exists when varying the pnictogen: $Na_{11}Sn_2PnS_{12}$ (Pn = P, Sb).[205–208] However, the highest conductivity is consistently ascribed to the initially found NaSnPS. It shall be noted that, based on unpublished results, arsenic can just as well be utilized in the solid solution. Even when considering arsenic, though, NaSnPS stays the best conductor of the structural class. Having failed to replace Sn, and upon finding that usage of higher homologues does not lead to higher conductivities – neither for the pnictogen nor for the chalcogen, the initial optimism to further tune the conductivity of NaSnPS-related compounds has dwindled. Only little room for further enhancements of the conductivity is left. Based on further unpublished results, doping of Ca^{2+} for Na^+ in NaSnPS proved equally unsuccessful. Considerably higher conductivities than $3 \cdot 10^{-3}$ mS/cm have been reached in the meantime starting out from Na_3PS_4 or Na_3SbS_4, respectively.[209] $Na_{2.9}P_{0.9}W_{0.1}S_4$ represents the current record holder for sulfide-based SEs, with a value of unrivalled $4.1 \cdot 10^{-2}$ S/cm that is also considerably higher than the highest value reported for Li-ion SEs.[210] Thus, for ASS-SIBs, identification of suitable electrode materials seems to be the decisive step for pushing ASS-SIBs forward. Since the electrochemical stability of sodium thiophosphates towards possible electrode materials is comparably low as for the lithium analogues (**Figure 14**), they equally demand efficient coating strategies. Expectedly, these are currently even to a lesser extent developed than the electrode materials themselves. Unpublished results obtained during my doctoral work indicate that $NaNbO_3$ or $NaTaO_3$, synthesized as thin-films, possess considerably

lower ionic conductivities than the intensively studied lithium analogues.[130–133,211,212] If applied to working cathode particles in a thin enough manner, they might still represent effective coating materials, though.

In the case of ASS-LIBs, research slowly leaves the stage of material development. Vast progress has been reached in the last three decades, when it comes to the identification of highly conductive Li-ion SEs as detailed in section **2.2.1**. Noteworthy, new structural classes of Li-ion SEs have not been discovered since 2011.[94] The discovery of stellar lithium-based argyrodites even dates back to 2008.[213] Doping and substitution strategies that led to higher conductivities than for Li_6PS_5Cl come at the expense of using less electrochemically stable and more expensive elements.[201,202] Interesting progress might still be gained from solution-based approaches or more efficient screening abilities by means of theoretical simulations.[8,103] However, their efficient synthesis and processing currently moves into focus of both academic and commercial research.[24] Today, material cost is already a major price driver for overall battery cost. Upon successful implementation of a lithium metal anode, graphite will no longer be needed. This will reduce the material cost for ASS-LIBs. The electrolytes used today in LE-based LIBs are a rather cheap component,[214] though, which necessitates a sophisticated manufacturing process for the cost-competitive synthesis of Li-ion SEs. The strategy shown in section **3.3** was designed as an unconventional inspiration to the community. Future efforts should elaborate on the idea of linking the solvent-mediated synthesis of Li_2S with the subsequent generation of the solid electrolyte (precursor) as it seems promising for the creation of considerable synergies.

The ideal synthesis of a highly conductive SE would directly yield the target product with the desired particle size. Generally, that means “the smaller the better”. The smaller the particle size of the SE, the less pore space will remain upon creation of the composite, and the smoother the SE will cover the CAM. This results in the reduction of both the bulk transport and the charge transfer resistivity. Whether this aim can be reached, depends mostly on the SE itself and the way it is prepared. The two strategies that are most seriously discussed are ball-milling and solvent-based syntheses. Ball mills are widely used throughout the chemical industry for grinding purposes. This usually leads only to the reduction of particle size or amorphization of the material to be ground. For the mechanical synthesis of amorphous ionic conductors in the laboratory, like LPSI, a more sophisticated type of ball mill is used, however: the planetary ball mill. It remains to be seen, whether the large impact and frictional forces needed for SEs can be efficiently realized with large-scale ball-mills at all. Particle size reduction will be critical and difficult. Solvent-based strategies seem as a very appealing alternative as they will likely lead to smoother and less agglomerated particles.

6 References

[1] P. Forster, V. Ramaswamy, *Changes in Atmospheric Constituents and in Radiative Forcing*, **2007**.

[2] R. F. Stallard, *Global Biogeochem. Cycles* **1998**, *12*, 231–257.

[3] S. O. Material, N. York, A. Nw, *Science (80-.).* **2007**, *1737*, 1737–1743.

[4] M. Eiseltová, *Restoration of Lakes, Streams, Floodplains and Bogs in Europe - Principles and Case Studies*, Springer, Heidelberg, **2010**.

[5] A. Dohong, A. A. Aziz, P. Dargusch, *Land use policy* **2017**, *69*, 349–360.

[6] R. C. Rooney, S. E. Bayley, D. W. Schindler, *Proc. Natl. Acad. Sci. U. S. A.* **2012**, *109*, 4933–4937.

[7] "If carbon dioxide hits a new high every year, why isn't every year hotter than the last? ", can be found under https://www.climate.gov/news-features/climate-qa/if-carbon-dioxide-hits-new-high-every-year-why-isn't-every-year-hotter-last, **2020**.

[8] L. Trahey, F. R. Brushett, N. P. Balsara, G. Ceder, L. Cheng, Y. M. Chiang, N. T. Hahn, B. J. Ingram, S. D. Minteer, J. S. Moore, K. T. Mueller, L. F. Nazar, K. A. Persson, D. J. Siegel, K. Xu, K. R. Zavadil, V. Srinivasan, G. W. Crabtree, *Proc. Natl. Acad. Sci. U. S. A.* **2020**, *117*, 12550–12557.

[9] U. Ratzel, O. Bayer, P. Brachat, L. Herrmann, K.-G. Krapf, C. Westerhausen, *Tieffrequente Geräusche Und Infraschall von Windkraftanlagen Und Anderen Quellen*, **2014**.

[10] R. Tonin, J. Brett, B. Colagiuri, *J. Low Freq. Noise Vib. Act. Control* **2016**, *35*, 77–90.

[11] I. van Kamp, F. van den Berg, *Acoust. Aust.* **2018**, *46*, 31–57.

[12] G. Wessel, "Wie romantisch sind Windräder?", can be found under https://www.deutschlandfunkkultur.de/klima-versus-landschaftsschutz-wie-romantisch-sind.976.de.html?dram:article_id=421958, **2018**.

[13] "SPD will finanziellen Anreiz für Windkraft schaffen", can be found under

https://www.tagesspiegel.de/politik/windbuergergeld-fuer-anwohner-spd-will-finanziellen-anreiz-fuer-windkraft-schaffen/25381368.html, **2020**.

[14] T. Armbrüster, H. Aiwanger, "„Bürger zu Beteiligten zu machen, ist der Königsweg"" can be found under https://www.deutschlandfunk.de/windradausbau-buerger-zu-beteiligten-zu-machen-ist-der.694.de.html?dram:article_id=467055, **2020**.

[15] G. Glenk, S. Reichelstein, *Nat. Energy* **2019**, *4*, 216–222.

[16] *Nat. Energy* **2016**, *1*, 1.

[17] S. Van Renssen, *Nat. Clim. Chang.* **2013**, *3*, 951–952.

[18] S. Schemme, J. L. Breuer, M. Köller, S. Meschede, F. Walman, R. C. Samsun, R. Peters, D. Stolten, *Int. J. Hydrogen Energy* **2020**, *45*, 5395–5414.

[19] B. Nykvist, M. Nilsson, *Nat. Clim. Chang.* **2015**, *5*, 329–332.

[20] W. Li, E. M. Erickson, A. Manthiram, *Nat. Energy* **2020**, *5*, 26–34.

[21] M. Armand, *Nature* **2001**, *414*, 359–367.

[22] W. G. Zeier, J. Janek, *Nat. Energy* **2016**, *1*, 1–4.

[23] T. Krauskopf, H. Hartmann, W. G. Zeier, J. Janek, *ACS Appl. Mater. Interfaces* **2019**, *11*, 14463–14477.

[24] Y. G. Lee, S. Fujiki, C. Jung, N. Suzuki, N. Yashiro, R. Omoda, D. S. Ko, T. Shiratsuchi, T. Sugimoto, S. Ryu, J. H. Ku, T. Watanabe, Y. Park, Y. Aihara, D. Im, I. T. Han, *Nat. Energy* **2020**, DOI 10.1038/s41560-020-0575-z.

[25] Z. Ding, J. Li, J. Li, C. An, *J. Electrochem. Soc.* **2020**, *167*, 070541.

[26] Cora Werwitzke, "CATL will NMC 811-Akkuzellen nächstes Jahr einführen", can be found under https://www.electrive.net/2018/08/15/catl-will-nmc-811-akkuzellen-naechstes-jahr-einfuehren/, **2019**.

[27] "Battery built like a bar of chocolate", can be found under https://www.volkswagenag.com/en/news/stories/2018/10/powerful-and-scalable-the-new-id-battery-system.html#, **2020**.

[28] H. S. Hirsh, Y. Li, D. H. S. Tan, M. Zhang, E. Zhao, Y. S. Meng, *Adv. Energy Mater.* **2020**, *10*, 2001274.

[29] M. Armand, J.-M. Tarascon, *Nature* **2008**, *451*, 652–7.

[30] J. U. Choi, J. H. Jo, Y. J. Park, K. S. Lee, S. T. Myung, *Adv. Energy Mater.* **2020**, *10*, DOI 10.1002/aenm.202001346.

[31] J. Song, K. Wang, J. Zheng, M. H. Engelhard, B. Xiao, E. Hu, Z. Zhu, C. Wang, M. Sui, Y. Lin, D. Reed, V. L. Sprenkle, P. Yan, X. Li, *ACS Energy Lett.* **2020**, *5*, 1718–1725.

[32] Y. Zheng, Y. Lu, X. Qi, Y. Wang, L. Mu, Y. Li, Q. Ma, J. Li, Y. S. Hu, *Energy Storage*

Mater. **2019**, *18*, 269–279.

[33] J.-Y. Hwang, S.-T. Myung, Y.-K. Sun, *Chem. Soc. Rev.* **2017**, *46*, 3529–3614.

[34] G. B. Appetecchi, M. Montanino, A. Balducci, S. F. Lux, M. Winterb, S. Passerini, *J. Power Sources* **2009**, *192*, 599–605.

[35] K. R. Kganyago, P. E. Ngoepe, C. R. A. Catlow, *Solid State Ionics* **2003**, *159*, 21–23.

[36] D. Guyornard, J. M. Tarascon, *Adv. Mater.* **1994**, *6*, 408.

[37] T. Kranz, S. Kranz, V. Miß, J. Schepp, B. Roling, *J. Electrochem. Soc.* **2017**, *164*, A3777–A3784.

[38] S. Kranz, T. Kranz, T. Graubner, Y. Yusim, L. Hellweg, B. Roling, *Batter. Supercaps* **2019**, *2*, 1026–1036.

[39] S. Kranz, T. Kranz, A. G. Jaegermann, B. Roling, *J. Power Sources* **2019**, *418*, 138–146.

[40] K. Xu, *Chem. Rev.* **2004**, *104*, 4303–4417.

[41] K. Xu, *Chem. Rev.* **2014**, *114*, 11503–11618.

[42] Y. Liu, Y. Zhu, Y. Cui, *Nat. Energy* **2019**, *4*, 540–550.

[43] R. Schröder, A. Glodde, M. Aydemir, G. Bach, *Appl. Mech. Mater.* **2015**, *794*, 19–26.

[44] J. Kim, J. Oh, H. Lee, *Appl. Therm. Eng.* **2019**, *149*, 192–212.

[45] A. A. Pesaran, *J. Power Sources* **2002**, *110*, 377–382.

[46] F. Leng, C. M. Tan, M. Pecht, *Sci. Rep.* **2015**, *5*, 1–12.

[47] B. Halvorson, "Here's the battery pack behind VW's global electric-vehicle push", can be found under https://www.greencarreports.com/news/1118974_heres-the-battery-pack-behind-vws-global-electric-vehicle-push, **2018**.

[48] www.akkuteile.de, "LG INR18650MJ1", can be found under https://www.akkuteile.de/lg-inr18650mj1-3500mah-3-75v-lithium-akku_100697_1297, **2019**.

[49] M. Lelie, T. Braun, M. Knips, H. Nordmann, F. Ringbeck, H. Zappen, D. U. Sauer, *Appl. Sci.* **2018**, *8*, 534–561.

[50] J. B. Quinn, T. Waldmann, K. Richter, M. Kasper, M. Wohlfahrt-Mehrens, *J. Electrochem. Soc.* **2018**, *165*, A3284–A3291.

[51] T. Waldmann, R. G. Scurtu, K. Richter, M. Wohlfahrt-Mehrens, *J. Power Sources* **2020**, *472*, 228614.

[52] "Liion-18650-AA-battery.jpg", can be found under https://de.wikipedia.org/wiki/Lithium-Ionen-Akkumulator#/media/Datei:Liion-18650-AA-battery.jpg, **2011**.

[53] R. Schröder, M. Aydemir, G. Seliger, *Procedia Manuf.* **2017**, *8*, 104–111.

[54] R. E. Ciez, J. F. Whitacre, *J. Power Sources* **2017**, *340*, 273–281.

[55] J. W. Choi, D. Aurbach *Nat. Rev. Mater.* **2016**, *1*, 16013.

[56] S. Ahmed, P. A. Nelson, K. G. Gallagher, N. Susarla, D. W. Dees, *J. Power Sources* **2017**, *342*, 733–740.

[57] N. Muralidharan, R. Essehli, R. P. Hermann, A. Parejiya, R. Amin, Y. Bai, Z. Du, I. Belharouak, *J. Power Sources* **2020**, *471*, 228389.

[58] S. T. Myung, F. Maglia, K. J. Park, C. S. Yoon, P. Lamp, S. J. Kim, Y. K. Sun, *ACS Energy Lett.* **2017**, *2*, 196–223.

[59] J. R. Dahn, U. von Sacken, C. A. Michal, *Solid State Ionics* **1990**, *44*, 87−97.

[60] J. R. Dahn, U. von Sacken, M. W. Juzkow, H. Al-Janaby, *J. Electrochem. Soc.* **1991**, *138*, 2207–2211.

[61] M. G. R. S. Thomas, W. I. F. David, J. B. Goodenough, P. Groves, *Mater. Res. Bull.* **1985**, *20*, 1137−1146.

[62] T. Ohzuku, H. Komori, M. Nagayama, K. Sawai, T. Hirai, *Chem. Express* **1991**, *6*, 161.

[63] M. Bianchini, M. Roca-Ayats, P. Hartmann, T. Brezesinski, J. Janek, *Angew. Chemie Int. Ed.* **2019**, *58*, 10434–10458.

[64] G. Assat, J. Tarascon, *Nat. Energy* **2018**, *3*, 373–386.

[65] G. Assat, A. Iadecola, C. Delacourt, R. Dedryvère, J. M. Tarascon, *Chem. Mater.* **2017**, *29*, 9714–9724.

[66] G. Assat, D. Foix, C. Delacourt, A. Iadecola, R. Dedryvère, J. M. Tarascon, *Nat. Commun.* **2017**, *8*, 1–12.

[67] P. E. Pearce, A. J. Perez, G. Rousse, M. Saubanère, D. Batuk, D. Foix, E. McCalla, A. M. Abakumov, G. Van Tendeloo, M.-L. Doublet, and J.-M. Tarascon, *Nat. Mater.* **2017**, *16*, 580–587.

[68] CATL, "CATL achieves 304 Wh/kg in new battery cells", can be found under https://pushevs.com/2019/03/30/catl-achieves-304-wh-kg-in-new-battery-cells/, **2019**.

[69] M. N. Obrovac, L. J. Krause, *J. Electrochem. Soc.* **2007**, *154*, 103–108.

[70] S. Chae, S.-H. Choi, N. Kim, J. Sung, J. Cho, *Angew. Chemie Int. Ed.* **2019**, *59*, 110–135.

[71] M. T. McDowell, S. W. Lee, J. T. Harris, B. A. Korgel, C. Wang, W. D. Nix, Y. Cui, *Nano Lett.* **2013**, *13*, 758–764.

[72] T. Yoon, C. C. Nguyen, D. M. Seo, B. L. Lucht, *J. Electrochem. Soc.* **2015**, *162*, A2325–A2330.

[73] W. Li, Z. Yang, M. Li, Y. Jiang, X. Wei, X. Zhong, L. Gu, Y. Yu, *Nano Lett.* **2016**, *16*,

1546–1553.

[74] R. Xu, X. Q. Zhang, X. B. Cheng, H. J. Peng, C. Z. Zhao, C. Yan, J. Q. Huang, *Adv. Funct. Mater.* **2018**, *28*, 1870049.

[75] S. Li, M. Jiang, Y. Xie, H. Xu, J. Jia, J. Li, *Adv. Mater.* **2018**, *30*, 1706375.

[76] A. Kushima, K. P. So, C. Su, P. Bai, N. Kuriyama, T. Maebashi, Y. Fujiwara, M. Z. Bazant, J. Li, *Nano Energy* **2017**, *32*, 271–279.

[77] J.-M. Tarascon, **2019**.

[78] R. Korthauer, *Handbuch Lithium-Ionen- Batterien*, Springer Vieweg, Berlin Heidelberg, **2013**.

[79] K. Funke, *Sci. Technol. Adv. Mater.* **2013**, *14*, DOI 10.1088/1468-6996/14/4/043502.

[80] C. Tubandt, E. Lorenz, *Zeitschrift fur Phys. Chemie B* **1914**, *87*, 513–542.

[81] Y. Wang, W. D. Richards, S. P. Ong, L. J. Miara, J. C. Kim, Y. Mo, G. Ceder, *Nat Mater* **2015**, *14*, 1–23.

[82] B. Reuter, K. Hardell, *Naturwissenschaften* **1961**, *48*, 161.

[83] T. Takahashi, O. Yamamoto, *Denki Kagaku* **1964**, *32*, 664.

[84] B. B. Owens, *J. Power Sources* **2000**, *90*, 2–8.

[85] B. B. Owens, G. R. Argue, *Science (80-.).* **1967**, *157*, 308–310.

[86] J. N. Bradley, P. D. Greene, *Trans. Faraday Soc.* **1967**, *63*, 424–430.

[87] Douglas O. Raleigh, *J. Appl. Phys.* **1970**, *41*, 1876–1877.

[88] T. Tokahashi, O. Yomomoto, S. Yamoda, S. Hoyoshi, *J. Electrochem. Soc.* **1980**, *126*, 1654–1658.

[89] B. B. Owens, P. M. Skarstad, *Solid State Ionics* **1992**, *53–56*, 665–672.

[90] K. Ozawa, *Solid State Ion.* **1994**, *69*, 212–221.

[91] E. S. Takeuchi, R. A. Leising, *MRS Bull.* **2011**, *27*, 624–627.

[92] D. C. Ginnings, T. E. Phipps, *J. Am. Chem. Soc.* **1930**, *52*, 1340–1345.

[93] "Web of Science", can be found under https://apps.webofknowledge.com/Search.do?product=WOS&SID=E5kN6d36nfWdwwwaKQh&search_mode=GeneralSearch&prID=c9e2f55c-de2d-4a50-a831-526206a6890a, **2019**.

[94] N. Kamaya, K. Homma, Y. Yamakawa, M. Hirayama, R. Kanno, M. Yonemura, T. Kamiyama, Y. Kato, S. Hama, K. Kawamoto, A. Mitsui, *Nat. Mater.* **2011**, *10*, 682–686.

[95] Z. Liu, W. Fu, E. A. Payzant, X. Yu, Z. Wu, N. J. Dudney, J. Kiggans, K. Hong, A. J. Rondinone, C. Liang, *J. Am. Chem. Soc.* **2013**, *135*, 975–978.

[96] C. A. Beevers, M. A. S. Ross, *Zeitschrift für Krist. - Cryst. Mater.* **1937**, *97*, 59–66.

[97] J. T. Kummer, *J. Inorg. Nucl. Chem.* **1967**, *29*, 2453–2475.

[98] J. L. Briant, G. C. Farrington, *J. Solid State Chem.* **1980**, *33*, 385–390.

[99] A. Hooper, *J. Physcis D Appl. Phys.* **1977**, *10*, 1487–1497.

[100] T. C. Girija, A. V. Virkar, *J. Power Sources* **2008**, *180*, 653–656.

[101] J. T. Kummer, N. Weber, *Battery Having a Molten Alkali Metal Anode and a Molten Sulfur Cathode*, **1968**, US3413150A.

[102] B. L. Ellis, L. F. Nazar, *Curr. Opin. Solid State Mater. Sci.* **2012**, *16*, 168–177.

[103] M. Ghidiu, J. Ruhl, S. P. Culver, W. G. Zeier, *J. Mater. Chem. A* **2019**, *7*, 17735–17753.

[104] A. Miura, N. C. Rosero-Navarro, A. Sakuda, K. Tadanaga, N. H. H. Phuc, A. Matsuda, N. Machida, A. Hayashi, M. Tatsumisago, *Nat. Rev. Chem.* **2019**, *3*, 189–198.

[105] R. Chen, Q. Li, X. Yu, L. Chen, H. Li, *Chem. Rev.* **2019**, DOI 10.1021/acs.chemrev.9b00268.

[106] D. H. S. Tan, A. Banerjee, Z. Chen, Y. S. Meng, *Nat. Nanotechnol.* **2020**, *15*, 170–180.

[107] T. Shi, Q. Tu, Y. Tian, Y. Xiao, L. J. Miara, O. Kononova, G. Ceder, *Adv. Energy Mater.* **2020**, *10*, 1902881.

[108] G. Homann, P. Meister, L. Stolz, J. P. Brinkmann, J. Kulisch, T. Adermann, M. Winter, J. Kasnatscheew, *ACS Appl. Energy Mater.* **2020**, *3*, 3162–3168.

[109] Q. Zhao, S. Stalin, C. Z. Zhao, L. A. Archer, *Nat. Rev. Mater.* **2020**, *5*, 229–252.

[110] K. B. Hatzell, X. C. Chen, C. L. Cobb, N. P. Dasgupta, M. B. Dixit, L. E. Marbella, M. T. McDowell, P. P. Mukherjee, A. Verma, V. Viswanathan, A. S. Westover, W. G. Zeier, *ACS Energy Lett.* **2020**, *5*, 922–934.

[111] J.-M. Doux, Y. Yang, D. H. S. Tan, H. Nguyen, E. A. Wu, X. Wang, A. Banerjee, Y. S. Meng, *J. Mater. Chem. A* **2020**, *8*, 5049–5055.

[112] R. Koerver, W. Zhang, L. De Biasi, S. Schweidler, A. O. Kondrakov, S. Kolling, T. Brezesinski, P. Hartmann, W. G. Zeier, J. Janek, *Energy Environ. Sci.* **2018**, *11*, 2142–2158.

[113] M. Keller, G. B. Appetecchi, G. T. Kim, V. Sharova, M. Schneider, J. Schuhmacher, A. Roters, S. Passerini, *J. Power Sources* **2017**, *353*, 287–297.

[114] K. H. Park, Q. Bai, D. H. Kim, D. Y. Oh, Y. Zhu, Y. Mo, Y. S. Jung, *Adv. Energy Mater.* **2018**, *8*, 1–24.

[115] M. Tachez, J. Malugani, R. Mercier, G. Robert, *Solid State Ionics* **1984**, *14*, 181–185.

[116] K. Homma, M. Yonemura, T. Kobayashi, M. Nagao, M. Hirayama, R. Kanno, *Solid State Ionics* **2011**, *182*, 53–58.

[117] S. Spannenberger, V. Miß, E. Klotz, J. Kettner, M. Cronau, A. Ramanayagam, F. di

Capua, M. Elsayed, R. Krause-Rehberg, M. Vogel, B. Roling, *Solid State Ionics* **2019**, *341*, 115040.

[118] P. Bron, S. Johansson, K. Zick, J. Schmedt auf der Günne, S. Dehnen, B. Roling, *J. Am. Chem. Soc.* **2013**, *135*, 15694–15697.

[119] N. H. H. Phuc, K. Morikawa, M. Totani, H. Muto, A. Matsuda, *Solid State Ionics* **2016**, *285*, 2–5.

[120] H. Wang, Z. D. Hood, Y. Xia, C. Liang, *J. Mater. Chem. A* **2016**, *4*, 8091–8096.

[121] A. Hayashi, S. Hama, H. Morimoto, M. Tatsumisago, T. Minami, *J. Am. Ceram. Soc.* **2001**, *79*, 477–479.

[122] R. C. Xu, X. H. Xia, Z. J. Yao, X. L. Wang, C. D. Gu, J. P. Tu, *Electrochim. Acta* **2016**, *219*, 235–240.

[123] Y. Wang, D. Lu, M. Bowden, P. Z. El Khoury, K. S. Han, Z. D. Deng, J. Xiao, J.-G. Zhang, J. Liu, *Chem. Mater.* **2018**, *30*, 990−997.

[124] L. Zhou, K. H. Park, X. Sun, F. Lalère, T. Adermann, P. Hartmann, L. F. Nazar, *ACS Energy Lett.* **2019**, *4*, 265–270.

[125] C. Yu, S. Ganapathy, J. Hageman, L. Van Eijck, E. R. H. Van Eck, L. Zhang, T. Schwietert, S. Basak, E. M. Kelder, M. Wagemaker, *ACS Appl. Mater. Interfaces* **2018**, *10*, 33296–33306.

[126] G. F. Dewald, S. Ohno, M. A. Kraft, R. Koerver, P. Till, N. M. Vargas-Barbosa, J. Janek, W. G. Zeier, *Chem. Mater.* **2019**, *31*, 8328–8337.

[127] T. K. Schwietert, V. A. Arszelewska, C. Wang, C. Yu, A. Vasileiadis, N. J. J. de Klerk, J. Hageman, T. Hupfer, I. Kerkamm, Y. Xu, E. van der Maas, E. M. Kelder, S. Ganapathy, M. Wagemaker, *Nat. Mater.* **2020**, *19*, DOI 10.1038/s41563-019-0576-0.

[128] Y. Zhu, X. He, Y. Mo, *ACS Appl. Mater. Interfaces* **2015**, *7*, 23685–23693.

[129] I. D. Scott, Y. S. Jung, A. S. Cavanagh, Y. Yan, A. C. Dillon, S. M. George, S. H. Lee, *Nano Lett.* **2011**, *11*, 414–418.

[130] N. Ohta, K. Takada, I. Sakaguchi, L. Zhang, R. Ma, K. Fukuda, M. Osada, T. Sasaki, *Electrochem. commun.* **2007**, *9*, 1486–1490.

[131] M. Gellert, K. I. Gries, J. Sann, E. Pfeifer, K. Volz, B. Roling, *Solid State Ionics* **2016**, *287*, 8–12.

[132] M. Gellert, K. I. Gries, J. Zakel, S. Kranz, S. Bradler, E. Hornberger, S. Muller, C. Yada, F. Rosciano, K. Volz, B. Roling, *J. Electrochem. Soc.* **2015**, *162*, A754–A759.

[133] M. Gellert, K. I. Gries, J. Zakel, A. Ott, S. Spannenberger, C. Yada, F. Rosciano, K. Volz, B. Roling, *Electrochim. Acta* **2014**, *133*, 146–152.

[134] R. Koerver, W. Zhang, L. de Biasi, S. Schweidler, A. O. Kondrakov, S. Kolling, T. Brezesinski, P. Hartmann, W. G. Zeier, J. Janek, *Energy Environ. Sci.* **2018**, *11*, 2142–2158.

[135] F. Strauss, T. Bartsch, L. De Biasi, A. Y. Kim, J. Janek, P. Hartmann, T. Brezesinski, *ACS Energy Lett.* **2018**, *3*, 992–996.

[136] R. Koerver, I. Aygün, T. Leichtweiß, C. Dietrich, W. Zhang, J. O. Binder, P. Hartmann, W. G. Zeier, J. Janek, *Chem. Mater.* **2017**, *29*, 5574–5582.

[137] R. Koerver, W. Zhang, L. De Biasi, S. Schweidler, A. O. Kondrakov, S. Kolling, T. Brezesinski, P. Hartmann, W. G. Zeier, J. Janek, *Energy Environ. Sci.* **2018**, *11*, 2142–2158.

[138] K. N. Wood, M. Noked, N. P. Dasgupta, *ACS Energy Lett.* **2017**, *2*, 664–672.

[139] X. Han, Y. Gong, K. (Kelvin) Fu, X. He, G. T. Hitz, J. Dai, A. Pearse, B. Liu, H. Wang, G. Rubloff, Y. Mo, V. Thangadurai, E. D. Wachsman, L. Hu, *Nat. Mater.* **2017**, *16*, 572–579.

[140] W. Zhang, F. H. Richter, S. P. Culver, T. Leichtweiss, J. G. Lozano, C. Dietrich, P. G. Bruce, W. G. Zeier, J. Janek, *ACS Appl. Mater. Interfaces* **2018**, *10*, 22226–22236.

[141] T. Krauskopf, B. Mogwitz, H. Hartmann, D. K. Singh, W. G. Zeier, J. Janek, *Adv. Energy Mater.* **2020**, *2000945*, DOI 10.1002/aenm.202000945.

[142] P. Bron, B. Roling, S. Dehnen, *J. Power Sources* **2017**, *352*, 127–134.

[143] S. Wenzel, T. Leichtweiss, D. A. Weber, J. Sann, W. G. Zeier, J. Janek, *ACS Appl. Mater. Interfaces* **2016**, *8*, 28216–28224.

[144] S. Wenzel, S. Randau, T. Leichtwei??, D. A. Weber, J. Sann, W. G. Zeier, J. Janek, *Chem. Mater.* **2016**, *28*, 2400–2407.

[145] T. Ates, M. Keller, J. Kulisch, T. Adermann, S. Passerini, *Energy Storage Mater.* **2019**, *17*, 204–210.

[146] F. Marchini, S. Saha, D. Alves Dalla Corte, J.-M. Tarascon, *ACS Appl. Mater. Interfaces* **2020**, DOI 10.1021/acsami.9b22937.

[147] J. M. Doux, H. Nguyen, D. H. S. Tan, A. Banerjee, X. Wang, E. A. Wu, C. Jo, H. Yang, Y. S. Meng, *Adv. Energy Mater.* **2020**, *10*, 1–6.

[148] T. Krauskopf, F. H. Richter, W. G. Zeier, J. Janek, *Chem. Rev.* **2020**, DOI 10.1021/acs.chemrev.0c00431.

[149] K. Lee, S. Kim, J. Park, S. H. Park, A. Coskun, D. S. Jung, W. Cho, J. W. Choi, *J. Electrochem. Soc.* **2017**, *164*, A2075–A2081.

[150] M. Yamamoto, Y. Terauchi, A. Sakuda, M. Takahashi, *Sci. Rep.* **2018**, *8*, 2–11.

[151] A. Sakuda, K. Kuratani, M. Yamamoto, M. Takahashi, *J. Electrochem. Soc.* **2017**, *164*, A2474–A2478.

[152] D. Y. Oh, D. H. Kim, S. H. Jung, J. G. Han, N. S. Choi, Y. S. Jung, *J. Mater. Chem. A* **2017**, *5*, 20771–20779.

[153] T. Ates, M. Keller, J. Kulisch, T. Adermann, S. Passerini, *Energy Storage Mater.* **2018**, *17*, 204–210.

[154] Y. J. Nam, D. Y. Oh, S. H. Jung, Y. S. Jung, *J. Power Sources* **2018**, *375*, 93–101.

[155] N. Riphaus, P. Strobl, B. Stiaszny, T. Zinkevich, M. Yavuz, J. Schnell, S. Indris, H. A. Gasteiger, S. J. Sedlmaier, *J. Electrochem. Soc.* **2018**, *165*, A3993–A3999.

[156] X. Wu, M. El Kazzi, C. Villevieille, *J. Electroceramics* **2017**, *38*, 207–214.

[157] A. S. Prakash, P. Manikandan, K. Ramesha, M. Sathiya, J. M. Tarascon, A. K. Shukla, *Chem. Mater.* **2010**, *22*, 2857–2863.

[158] Y.-S. Hu, *Nat. Energy* **2016**, *1*, 16042.

[159] X. Xia, J. R. Dahn, *Electrochem. Solid-State Lett.* **2012**, *15*, 1–4.

[160] J. Zhaoa, L. Zhaob, N. Dimovb, S. Okada, T. Nishida, *J. Electrochem. Soc.* **2013**, *160*, 3077–3081.

[161] J. Billaud, R. J. Clément, A. R. Armstrong, J. Canales-Vázquez, P. Rozier, C. P. Grey, P. G. Bruce, *J. Am. Chem. Soc.* **2014**, *136*, 17243–17248.

[162] P. Vassilaras, X. Ma, X. Li, G. Ceder, *J. Electrochem. Soc.* **2013**, *160*, 207–211.

[163] B. V. Rami Reddy, R. Ravikumar, C. Nithya, S. Gopukumar, *J. Mater. Chem. A* **2015**, *3*, 18059–18063.

[164] G. Yan, S. Mariyappan, G. Rousse, Q. Jacquet, M. Deschamps, R. David, B. Mirvaux, J. W. Freeland, J. M. Tarascon, *Nat. Commun.* **2019**, *10*, DOI 10.1038/s41467-019-08359-y.

[165] D. P. Divincenzo, E. J. Mele, *Phys. Rev. B* **1985**, *32*, 2538–2553.

[166] P. Ge, M. Fouletier, *Solid State Ionics* **1988**, *28–30*, 1172–1175.

[167] S. Komaba, W. Murata, T. Ishikawa, N. Yabuuchi, T. Ozeki, T. Nakayama, A. Ogata, K. Gotoh, K. Fujiwara, *Adv. Funct. Mater.* **2011**, *21*, 3859–3867.

[168] D. A. Stevens, J. R. Dahn, *J. Electrochem. Soc.* **2000**, *147*, 1271–1273.

[169] D. Kundu, E. Talaie, V. Duffort, L. F. Nazar, *Angew. Chemie - Int. Ed.* **2015**, *54*, 3432–3448.

[170] N. Yabuuchi, M. Kajiyama, J. Iwatate, H. Nishikawa, S. Hitomi, R. Okuyama, R. Usui, Y. Yamada, S. Komaba, *Nat. Mater.* **2012**, *11*, 512–517.

[171] P. Serras, V. Palomares, A. Goñi, I. Gil de Muro, P. Kubiak, L. Lezama, T. Rojo, *J.*

Mater. Chem. **2012**, *22*, 22301–22308.

[172] D. Wang, X. Bie, Q. Fu, D. Dixon, N. Bramnik, Y. Hu, F. Fauth, Y. Wei, H. Ehrenberg, G. Chen, F. Du, *Nat. Commun.* **2017**, *8*, 1–7.

[173] C. Zhao, L. Liu, X. Qi, Y. Lu, F. Wu, J. Zhao, Y. Yu, Y. S. Hu, L. Chen, *Adv. Energy Mater.* **2018**, *8*, 1703012.

[174] A. Hayashi, K. Noi, A. Sakuda, M. Tatsumisago, *Nat. Commun.* **2012**, *3*, 856.

[175] M. Jansen, U. Henseler, *J. Solid State Chem.* **1992**, *99*, 110–119.

[176] L. Zhang, K. Yang, J. Mi, L. Lu, L. Zhao, L. Wang, Y. Li, H. Zeng, *Adv. Energy Mater.* **2015**, *5*, 2–6.

[177] L. Zhang, D. Zhang, K. Yang, X. Yan, L. Wang, J. Mi, B. Xu, Y. Li, *Adv. Sci.* **2016**, *3*, 1600089.

[178] W. D. Richards, T. Tsujimura, L. J. Miara, Y. Wang, J. C. Kim, S. P. Ong, I. Uechi, N. Suzuki, G. Ceder, *Nat. Commun.* **2016**, *7*, 11009.

[179] V. S. Kandagal, M. D. Bharadwaj, U. V. Waghmare, *J. Mater. Chem. A* **2015**, *3*, 12992–12999.

[180] P. Bron, S. Dehnen, B. Roling, *J. Power Sources* **2016**, *329*, 530–535.

[181] Z. Zhang, E. Ramos, F. Lalère, J. Assoud, K. Kaup, P. Hartman, L. F. Nazar, *Energy Environ. Sci.* **2018**, *11*, 87–93.

[182] Z. Yu, S.-L. Shang, Y. Gao, D. Wang, X. Li, Z.-K. Liu, D. Wang, *Nano Energy* **2018**, *47*, 325–330.

[183] Y. Mo, S. P. Ong, G. Ceder, *Chem. Mater.* **2012**, *24*, 15–17.

[184] K. Yang, J. Dong, L. Zhang, Y. Li, L. Wang, *J. Am. Ceram. Soc.* **2015**, *98*, 3831–3835.

[185] S. Xiong, Z. Liu, H. Rong, H. Wang, H. Chen, *Sci. Rep.* **2018**, *8*, 9146.

[186] N. Wang, K. Yang, L. Zhang, X. Yan, L. Wang, B. Xu, *J. Mater. Sci.* **2017**, *53*, 1987–1994.

[187] T. Krauskopf, C. Pompe, M. A. Kraft, W. G. Zeier, *Chem. Mater.* **2017**, *29*, 8859 − 8869.

[188] M. A. Kraft, S. P. Culver, M. Calderon, F. Bo, T. Krauskopf, A. Senyshyn, C. Dietrich, A. Zevalkink, J. Janek, W. G. Zeier, *J. Am. Chem. Soc.* **2017**, *139*, 10909–10918.

[189] C. Luo, Y. Xu, Y. Zhu, Y. Liu, S. Zheng, Y. Liu, A. Langrock, C. Wang, *ACS Nano* **2013**, *7*, 8003–8010.

[190] Q. Li, H. Liu, Z. Yao, J. Cheng, T. Li, Y. Li, C. Wolverton, J. Wu, V. P. Dravid, *ACS Nano* **2016**, *10*, 8788–8795.

[191] J. Ding, H. Zhou, H. Zhang, T. Stephenson, Z. Li, D. Karpuzov, D. Mitlin, *Energy Environ. Sci.* **2017**, *10*, 153–165.

[192] R. P. Rao, X. Zhang, K. C. Phuah, S. Adams, *J. Mater. Chem. A* **2019**, *7*, 20790–20798.

[193] S. Yubuchi, M. Uematsu, C. Hotehama, A. Sakuda, A. Hayashi, M. Tatsumisago, *J. Mater. Chem. A* **2019**, *7*, 558–566.

[194] L. Zhou, K. H. Park, X. Sun, F. Lalère, T. Adermann, P. Hartmann, L. F. Nazar, *ACS Energy Lett.* **2019**, *4*, 265–270.

[195] P. Senguttuvan, G. Rousse, V. Seznec, J. M. Tarascon, M. R. Palacín, *Chem. Mater.* **2011**, *23*, 4109–4111.

[196] P. Barpanda, G. Oyama, S. I. Nishimura, S. C. Chung, A. Yamada, *Nat. Commun.* **2014**, *5*, 1–8.

[197] R. P. Rao, H. Chen, L. L. Wong, S. Adams, *J. Mater. Chem. A* **2017**, *5*, 3377–3388.

[198] W. Wang, C. Yu, Z. Lin, J. Hou, H. Zhu, S. Jiao, *Nanoscale* **2013**, *5*, 594–9.

[199] A. Rudola, K. Saravanan, C. W. Mason, P. Balaya, *J. Mater. Chem. A* **2013**, *1*, 2653–2662.

[200] M. Cronau, Elektrochemische Untersuchung von Interkalationsmaterialien Für Die Anwendung in Na-Ionen-Akkumulatoren, Philipps-University Marburg, **2018**.

[201] M. A. Kraft, S. Ohno, T. Zinkevich, R. Koerver, S. P. Culver, T. Fuchs, A. Senyshyn, S. Indris, B. J. Morgan, W. G. Zeier, *J. Am. Chem. Soc.* **2018**, *140*, 16330–16339.

[202] L. Zhou, A. Assoud, Q. Zhang, X. Wu, L. F. Nazar, *J. Am. Chem. Soc.* **2019**, *141*, 19002–19013.

[203] H. Yang, M. Kim, S. Hong, J. H. Lee, Y. S. Jung, *ACS Energy Lett.* **2018**, *3*, 2504–2512.

[204] K. Oh, D. Chang, I. Park, K. Yoon, K. Kang, *Chem. Mater.* **2019**, *31*, 6066–6075.

[205] M. A. Kraft, L. M. Gronych, T. Famprikis, S. Ohno, W. G. Zeier, *Chem. Mater.* **2020**, *32*, 6566–6576.

[206] E. P. Ramos, Z. Zhang, A. Assoud, K. Kaup, F. Lalere, L. F. Nazar, *Chem. Mater.* **2018**, *30*, 7413–7417.

[207] J. W. Heo, A. Banerjee, K. H. Park, Y. S. Jung, S.-T. Hong, *Adv. Energy Mater.* **2018**, *4*, 1702716.

[208] Z. Yu, S.-L. Shang, D. Wang, Y. Li, H. P. Yennawar, G. Li, H.-T. Huang, Y. Gao, T. E. Mallouk, Z.-K. Liu, D. Wang, *Energy Storage Mater.* **2018**, *17*, 70–77.

[209] T. Fuchs, S. P. Culver, P. Till, W. G. Zeier, *ACS Energy Lett.* **2020**, *5*, 146–151.

[210] Y. Kato, S. Hori, T. Saito, K. Suzuki, M. Hirayama, A. Mitsui, M. Yonemura, H. Iba, R. Kanno, *Nat. Energy* **2016**, 16030.

[211] M. Wilkening, V. Epp, A. Feldhoff, P. Heitjans, *J. Phys. Chem. C* **2008**, *112*, 9291–9300.

[212] P. Heitjans, E. Tobschall, M. Wilkening, *Eur. Phys. J. Spec. Top.* **2008**, *161*, 97–108.

[213] H. Deiseroth, S. Kong, H. Eckert, J. Vannahme, C. Reiner, T. Zaiß, M. Schlosser, *Angew. Chem. Int. Ed.* **2008**, *47*, 755–758.

[214] J. Xiang, L. Yang, L. Yuan, K. Yuan, Y. Zhang, Y. Huang, J. Lin, F. Pan, Y. Huang, *Joule* **2019**, *3*, 2334–2363.